ROLE OF HEPARAN SULFATE AND HYALURONAN IN MECHANICAL PROPERTIES OF THE LUNG MICROVASCULAR GLYCOCALYX

by

Kathleen Marie Job

A dissertation submitted to the faculty of
The University of Utah
in partial fulfillment of the requirements for the degree of

Doctor of Philosophy

Department of Bioengineering

The University of Utah

December 2015

The University of Utah Graduate School

STATEMENT OF DISSERTATION APPROVAL

The dissertation of **Kathleen Marie Job**

has been approved by the following supervisory committee members:

Vladimir Hlady	, Chair	**8/26/2013** Date Approved
Randal O. Dull	, Member	**8/26/2013** Date Approved
Kuberan Balagurunathan	, Member	**8/26/2013** Date Approved
Yan-Ting E. Shiu	, Member	**8/26/2013** Date Approved
Jeffrey A. Weiss	, Member	**9/17/2013** Date Approved

and by **Vladimir Hlady** , Chair/Dean of

the Department/College/School of **Bioengineering**

and by David B. Kieda, Dean of The Graduate School.

ABSTRACT

An intact lung capillary glycocalyx is vital to normal vascular barrier function and subsequently normal pulmonary function. Evidence suggests that the glycocalyx provides active regulatory functions, which are fundamental to normal lung fluid balance and that endothelial surface glycoproteins participate in agonist-mediated signaling. Heparan sulfates and hyaluronan glycosaminoglycans are of particular interest in mechanostimulation and subsequent mechanotransduction because of direct and indirect attachment to intracellular components involved with barrier maintenance. Also important to glycocalyx structure are associated blood serum proteins. The component contribution to the overall glycocalyx mechanical environment is integral to its transfer of extracellular mechanical signals to intracellular signals.

These components have not been characterized in terms of their mechanical contribution to the glycocalyx stiffness, which allows for endothelial mechanotransduction. Understanding these components will assist in developing a strategy to treat acute inflammation of the lungs.

In this dissertation, the mechanical contributions of glycosaminoglycans (heparan sulfate and hyaluronan) and associated macromolecules (albumin and hydroxyethyl starch) to lung glycocalyx mechanical structure are measured with novel applications of two optical micromechanical techniques: atomic force

microscopy and reflectance interference contrast microscopy. This information is combined into an inclusive mechanical model. Specifically, the biomechanical properties of the microvascular glycocalyx were acquired and analyzed by probing with physiologically relevant normal forces. The techniques and experiments described in this dissertation provided means to measure and potentially other soft biologic materials, including the local glycocalyx microenvironment.

TABLE OF CONTENTS

LIST OF FIGURES

LIST OF TABLES

LIST OF ABBREVIATIONS

Defining Term	Abbreviation
Acute lung injury	ALI
Acute respiratory distress syndrome	ARDS
Atomic force microscopy	AFM
Bovine lung microvascular endothelial cell	BLMVEC
Bovine serum albumin	BSA
Chondroitin sulfate	CS
Effective stiffness	k
Elastic modulus at 100 nanometers indentation	E_{100}
Electron microscopy	EM
Endothelial surface layer	ESL
Fluorescent correlation spectroscopy	FCS
Glycocalyx	Glyx
Heparan sulfate	HS
Heparan sulfate proteoglycan	HSPG
Heparinase III	HSIIIase
Hyaluronan	HA
Hyaluronidase	HAase
Hydraulic conductivity	Lp

Nitric oxide ..... NO

Nitric oxide synthase ..... NOS

Phosphate buffered saline ..... PBS

Rat lung microvascular endothelial cell ..... RLMVEC

Reactive oxygen species ..... ROS

Red blood cells ..... RBCs

Reflectance interference contrast microscopy ..... RICM

White blood cells ..... WBCs

ACKNOWLEDGEMENTS

I would first like to acknowledge my advisors, Dr. Vladimir Hlady and Dr. Randal Dull, without whom I would not have this project or funding. Their knowledge, experience, enthusiasm, and mentorship have helped me grow as both a scientist and an individual. I would also like to thank my committee: Drs. Jeff Weiss, Kuberan Balugurnathan, and Yin-Ting Shiu, for providing support for my research pursuits. A special thanks goes to Kristina Giantsos-Adams, Lindsey Corum, Vimal Swarup, Tony Hsiao, Nate Gooch, Colin Eichinger, Dwight, Soeren Hoehne, and all the people who have been with me during this process. I am grateful for the help of undergraduate and graduate research assistants, including Ryan O'Callaghan, Bridger Bach, and Matthew Lindsey, for assisting with experiments and data analysis. Last, definitely not least, I must thank my family and friends for their examples, support, encouragement, and patience. I love you all dearly.

CHAPTER 1

INTRODUCTION

The microvasculature is the primary control for tissue perfusion, blood delivery, and nutrient exchange. Compromised vessel function is related to both inflammatory and disease states. Blood vessels have multiple mechanisms for control function. One significant mechanism is mechanotransduction. The endothelium is continuously exposed to both pressure and shear forces. The interior microvasculature is comprised of endothelial cells lined with a specialized extracellular matrix termed the endothelial glycocalyx. The endothelial glycocalyx is integral to the discussion of overall microvascular health. During the last several decades, the role of the glycocalyx has expanded from a simple filter overlying capillary and vessel endothelium to an integrated structure capable of mechanotransduction: transmission of physical signal to chemical and physical responses both within and between cells. Until recently, the focus of understanding the mechanical characteristics of the glycocalyx has been limited to theoretical and indirect measurements. My goal with this research is to establish viable indentation and equilibrium techniques to directly measure this very soft layer.

This introduction provides an overview of the microvascular endothelial glycocalyx, mechanotransduction, and glycocalyx function. The field of

micromechanical measurements is briefly reviewed. The final section is synopses of subsequent chapters.

1.1 Microvascular Endothelial Glycocalyx

The microvascular endothelial glycocalyx is a hydrated, negatively charged, meshwork layer residing on the luminal surface of capillaries and larger blood vessels. This “fuzzy coating” layer is comprised of proteoglycans, glycoproteins, glycosaminoglycans, glycolipids, and absorbed blood serum proteins [3]. Research over the last 60+ years has attempted to characterize glycocalyx thickness, structural properties, and physiologic functions. Principally, the glycocalyx has been critically associated with leukocyte adhesion and inflammatory processes, blood flow and coagulation, and barrier function via passive filtering and active fluid shear stress transmission (reviewed in [1]).

1.1.1 Visualization of the glycocalyx

The glycocalyx was first visualized by electron microscopy (EM) in 1966 after staining with a cationic dye, ruthenium red, and fixation revealed a very thin layer covering the endothelium [4]. In 1997, Rostgaard and Qvortrup showed that a filamentous coating was present in rat capillaries by utilizing a fluorocarbon-marker, gluteraldehyde fixation technique [5]. Ultimately, in 2001, Squire et al., utilized autocorrelation functions and Fourier transforms of EM of ferritin-labeled frog mesentery to reveal a regularly spaced, quasi-periodic substructure of the glycocalyx characterized by 10-12 nm fiber diameters, 20 nm fiber spacing, and an intercluster spacing of about 100 nm with anchoring foci with potential

connection to the underlying cortical skeleton [6]. A model for these results is shown in Figure 1.1. This structural model has been used in molecular filtering and mechanotransduction models.

Glycocalyx thickness measurements vary widely depending on the endothelial source and more importantly on the methodology used. Examples of glycocalyx visualization methods are shown in Figure 1.2: EM, intravital microscopy, and 2-photon laser scanning microscopy. Initial EM measurements showed a 20 nm thick layer overlying rat intestinal mucosa [4]. This layer was much smaller than the 1.2 μm plasma layer predicted by Klitzman and Duling to explain reduced skeletal microvessel hematocrits [7] and was not able to explain observations that flow resistance in 10 μm vessels was 4 times greater than in similarly sized glass capillary tubes [8]. EM visualization techniques, summarized by Weinbaum et al. [9], likely underestimate glycocalyx thickness because methods included aqueous fixation likely comprising the glycocalyx.

Physiologically relevant measurement of in vivo glycocalyx thickness required gentler intravital procedures. Utilizing a dye-exclusion technique with a 70 kDa FITC-dextran tracer in capillaries, glycocalyx thickness measurements increased over 5 fold: 100 nm [9-11] to 400-500 nm [10]. More recently, near-wall fluorescent microparticle image velocimetry (μ-PIV) techniques have been applied to vessels [12] and immunofluorescent staining of glycosaminoglycan components of endothelial monolayers have been applied to determine thickness [13, 14]. Specifically, Stevens et al. [14] showed that the glycocalyx in lung microvascular endothelial cells was 2-3 μm via HS and HA staining. Significantly,

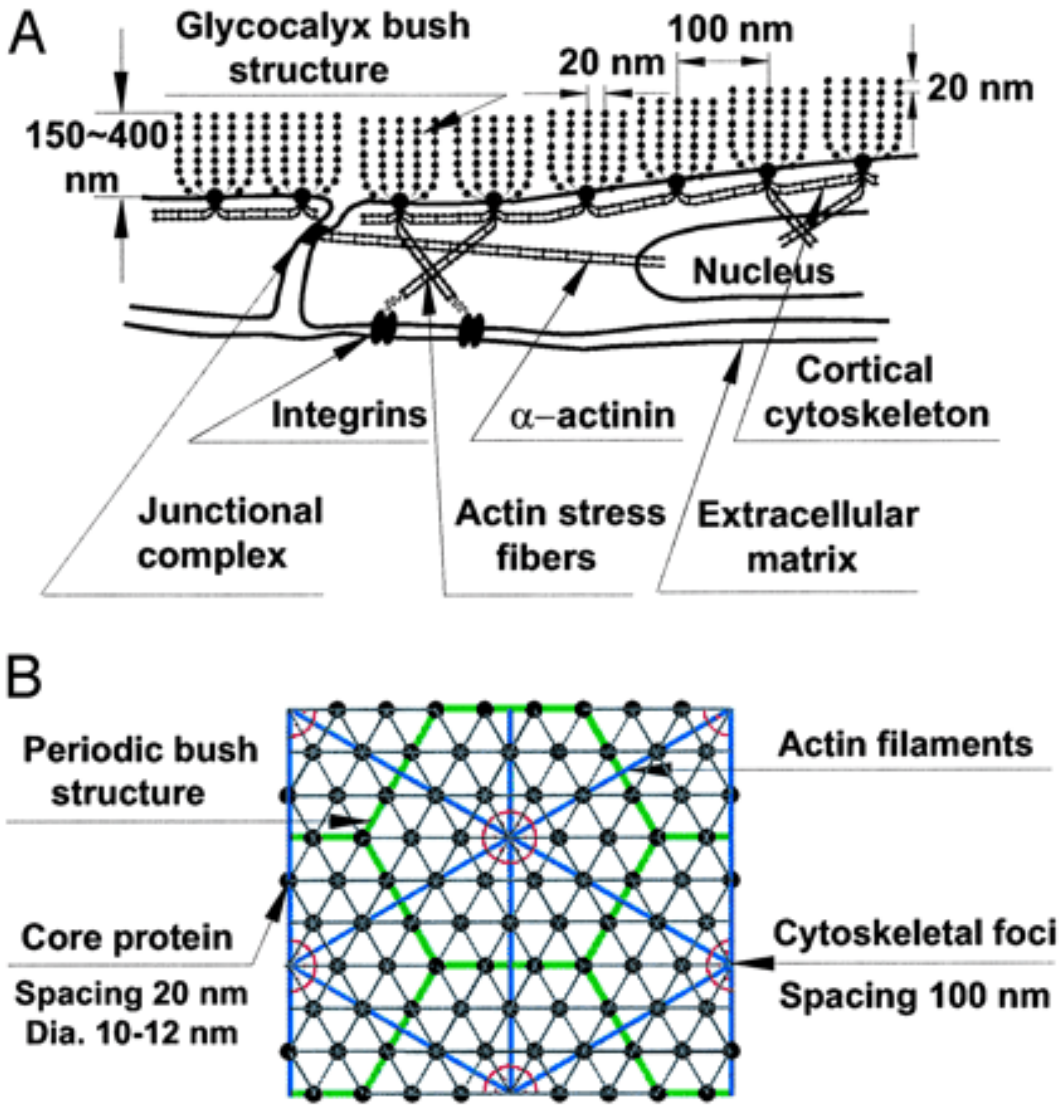

Figure 1.1 Model for quasi-periodic glycocalyx structure based on EM and freeze-fracture results. Panel a) is a diagram of the quasi-periodic structure applied to the glycocalyx, actin cytoskeleton with associated junctions and panel b) shows spacing of glycocalyx and underlying cytoskeleton components. [2] This figure was reprinted with permission from PNAS

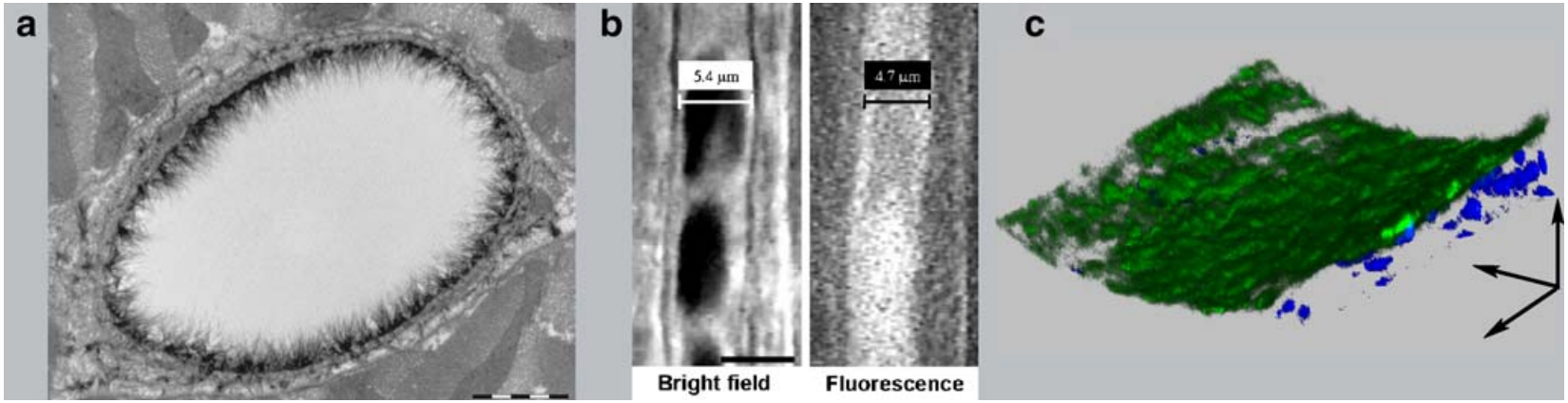

Figure 1.2 Endothelial glycocalyx visualization with three different visualization techniques as provided in the review by Reitsma et al. [1] Panel a) is an electron micrograph at left ventricular myocardial capillary stained with Alcian blue 8GX is shown (scale bar = 1 µm); panel b) is an intravital microscopic image of a hamster cremaster muscle capillary utilizing RBC passage (left) and fluorescently labeled 70 kDa dextran (right) to calculate effective glycocalyx thickness; and c) is a 3D-reconstruction of the glycocalyx (stained with FITC-labeled lectin (green)) and the cell nuclei (SYTO 41(blue)) of mouse common carotid artery where successive optical slices obtained with two-photon laser scanning microscopy. Figure was reprinted with permission from Springer.

this is a large portion (~50%) of the lumen given that capillaries are only large enough to allow red blood cells to pass single file or only 5-10 μm in diameter. Remarkably, Vink and Duling also showed that at speeds above 20 μm/s, RBCs were excluding from the ESL while stiffer WBCs were not [11]. These structural studies have established the glycocalyx as significant to flow and blood component interactions.

1.1.2 Glycocalyx Structure

The endothelial surface layer (ESL), or glycocalyx, is a three-dimensional entangled mesh of glycoproteins, glycosaminoglycans (GAGs), glycolipids and other serum factors on the surface of microvascular endothelial cells. The overall structure, and therefore function, is determined by this composition. The ultimate structure of this layer is highly dynamic and dependent upon circulating blood composition and hemodynamic conditions. Pries et al. [15] postulated a composition for this layer: the inner 100 nm is comprised of glycoproteins and proteoglycans; the outer 500 nm is comprised of soluble glycosaminoglycans and serum proteins. This structure has been found to depend on animal species, vessel location, and vessel conditions. For example, adsorbed blood proteins directly affect glycocalyx thickness. Correspondingly, recent measurement of glycocalyx thickness has spanned a significant range from 500 nm to 3 μm [14, 15]. Figure 1.3 is a diagram of this layer. The conspicuous components are the sulfated GAGs, heparan sulfate and chondroitin sulfate, and the unsulfated GAG hyaluronan, and blood serum proteins, such as albumin.

A.

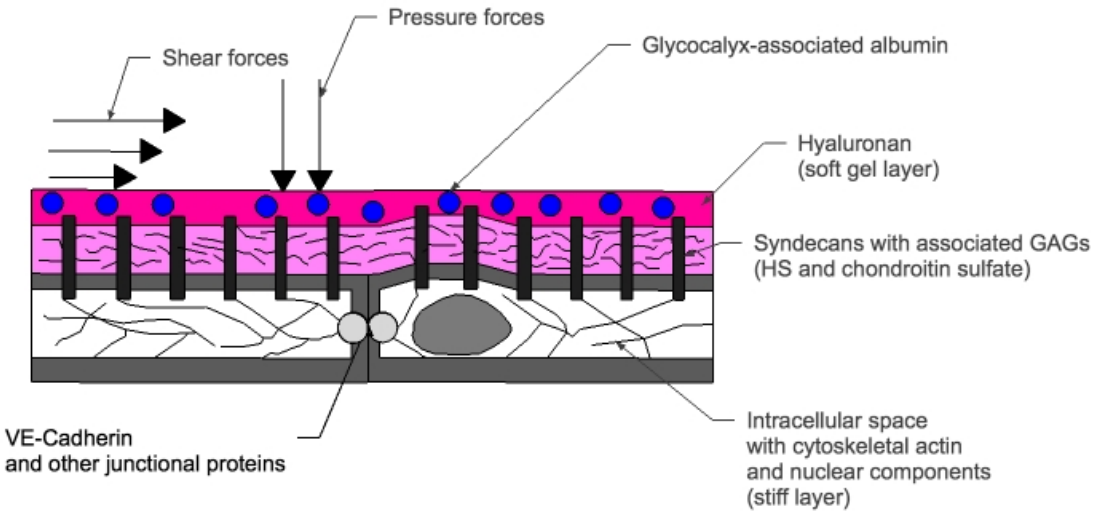

B.

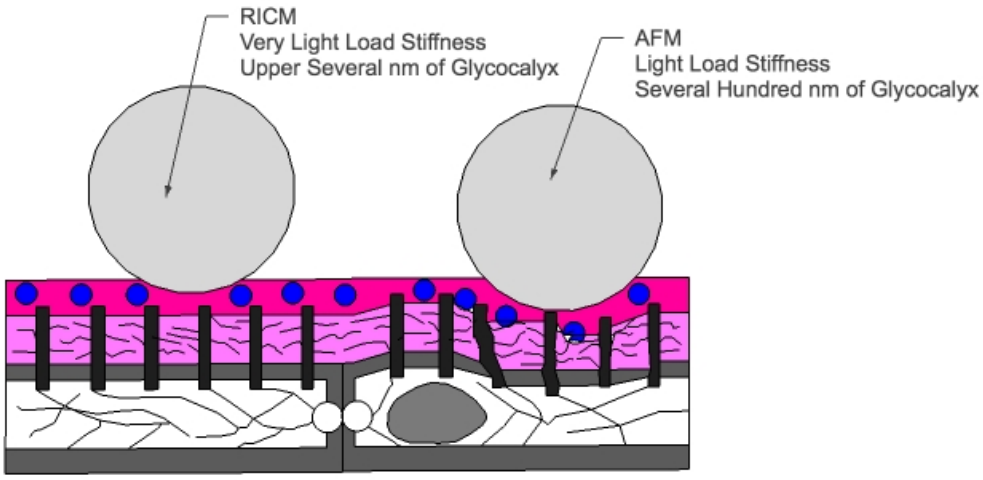

Figure 1.3 Hypothesized mechanical model of the glycocalyx with syndecan, HA and associated proteins, and underlying cell components as transducer, soft gel layer, and stiff layer, respectively. A) The luminal surfaces of endothelial cells are continuously exposed to both shear and pressure forces. B) Hypothesized deformation of glycocalyx and endothelial cells during mechanical measurement.

1.1.2.1 Sulfated Proteoglycans

A proteoglycan is comprised of polysaccharide-based glycosaminoglycan (GAG) side chains covalently attached to a protein core through a tetrasaccharide bridge [16]. GAGs associated with the glycocalyx include hyaluronan, heparan sulfate, chondroitin sulfate, dermatan sulfate, and karatan sulfate. Hyaluronan is the only GAG of this group not bound to a proteoglycan. Core protein groups include 4 subtypes of membrane-spanning syndecan, 6 subtypes of glycosylphosphatidlinositol-anchored glypican, and several other secreted groups [1, 9]. The transmembrane syndecans carry HS and CS side chains. Syndecans (1,2, and 4) are important core proteins because they are membrane-spanning and thus have the potential to directly respond to deformation and transfer signals into the cell.

HSPGs have been implicated with the endothelium for over twenty years. In 1990, Desjardins and Duling [17] showed that after HSPG-specific heparinase treatment, hematocrit values were doubled, suggesting that HSPG is a significant component of the EGL. In 2003, Florian et al. found that HSPG was present in endothelial glycocalyx [18] and Dull et al. found that the majority of the proteoglycans within the glycocalyx were HSPGs and chondroitin sulfate proteoglycans [19]. Typically, 3-5 HS chains are bound to the proteoglycan near the membrane [1]. HS is a linear polysaccharide similar to heparin; however, there is a greater proportion of glucuronic acid linked to N-acetylglucosamine disaccharide units generally found in HS [1].

Heparan sulfate proteoglycan (HSPG) is the most studied proteoglycan in

the context of endothelial mechanotransduction. Heparan sulfate is a GAG that is bound to a core protein group (syndecan, glypican, or perlecan) and is a major component of the glycocalyx that has been associated with mechanotransduction [18-21]. HSPG syndecans have direct connections through or anchored association with the cell membrane that could allow for communication. HSPGs have been associated with changes in cell growth, division, and other cellular functions. Specifically, HSPG sulfation pattern has been associated with targeted ligand binding, including ECM components, morphogens, cytokines, cell adhesion molecules, and growth factors [22]. Structural changes in heparan sulfate and other proteoglycan associated GAGs (chondroitin sulfate) may affect glycocalyx mechanics by interactions with other endothelial components or based upon other physical characteristics. As discussed previously in section 1.1.1, it appears that there are contacts of the glycocalyx with underlying components. When either HS is degraded with heparinase or the actin cytoskeleton is degraded with cytochalasin, flow sensitivity, as measured by nitric oxide (NO) production, hydraulic conductivity, and protein extravasation, is reduced or attenuated, suggesting a mechanosensitive connection of HS with the underlying cytoskeleton and/or inflammatory machinery.

1.1.2.2 Hyaluronan

Hyaluronan (HA) is a highly hydrated, unbranched GAG that is ubiquitous in mammalian physiology and shown to be abundant within the glycocalyx. The basic disaccharide HA unit is D-glucuronic acid and D-N-acetylglucosamine with alternating β-1,4 and β-1,3 glycosidic linkages. HA molecular weight is highly

variable (2.5 to 1,000 kDa) (Reviewed in [23]). Unlike HS and chondroitin sulfate, HA is nonsulfated.

HA is known to form networks that are dependent on pH and particle concentration in solution. This viscoelastic network is potentially capable of barrier and sieve functions [24], but also force transmission. Like HSPGs, HA has been associated with cell growth, migration, wound healing, inflammation, tumor growth, and angiogenesis [25]. HA is not attached to a core protein, but believed to be directly associated with the cellular membrane, via the CD44 receptor that controls a calcium pathway to NO production [26], or allowed to self-associate and intercalate with the glycocalyx [15, 27-29] and associated albumin [14].

1.1.2.3 Albumin

The interaction of serum proteins with the glycocalyx is important to the structural and functional properties [30-33]. Serum albumin (67 kDa), which is the most abundant protein in the blood, has been shown to interact with the glycocalyx, to be involved in proper regulation of fluid balance, and to be critical to hydraulic conductivity [14, 32, 34-36]. It has been shown that albumin interacts with the both hyaluronan and heparan sulfate in the glycocalyx [14] [22]. Furthermore, albumin supplementation has shown protective effects within the vasculature [37]. Additionally, while protein-free perfusate results in collapse of the glycocalyx [38], there is also partial restoration of the glycocalyx with plasma-based resuscitation [39].

1.2 Mechanotransduction

The connections between mechanical forces and cellular changes have been broadly investigated during the last three decades for multiple cell types. While our knowledge is increasing, the relationships between mechanosensing, mechanotransduction, and mechanotransmission are complex. In the endothelium, the glycocalyx has been identified as a mechanosensing structure.

1.2.1 Endothelial Response to Fluid Forces

Endothelial cells and the endothelial surface layer (ESL) are continuously exposed to fluid forces: pressure forces (perpendicular) and shear forces (tangential forces). Linear and turbulent blood flows exert complex forces on the endothelium that ultimately affect vascular tone and health. These forces are associated with changes in endothelial morphology, cell-cycle entry, intracellular signaling, intercellular signaling, cytoskeletal reorganization, protein synthesis, and intracellular calcium levels. Within the glycocalyx, syndecan core proteins [2, 29] and associated GAGs [18, 40, 41] have been implicated in shear stress transmission.

When shear forces are applied to endothelial cells, there is an initial spike increase in intracellular calcium, an integral marker for inflammatory processes, and an increase in actin polymer turnover and reorganization [42]. After 24 hours, GAGs relocate near cell-cell junctions [43] and endothelial monolayers realigned in the direction of flow. Recently, Giantsos-Adams et al. showed that bovine aortic endothelial cells not only realign when exposed to shear, but the regrowth of glycocalyx HSPGs are dependent upon shear rate [44]. Hyaluronan removal

has also been found to significantly reduce shear-induced nitric oxide production in endothelial cells [41, 45].

Like shear force, pressure changes applied across intact endothelium initiate increases in nitric oxide/ROS production [41] and hydraulic conductivity [40]. When HS was removed, endothelial cells no longer showed time-dependent increases in permeability in response to pressure changes and showed a decrease in ROS production in response to shear.

1.2.2 Inflammation and Mechanotransduction

The capillary endothelial glycocalyx serves as an interface between endothelial cells and capillary blood flow [9] and is vital to microvascular functions including fluid filtration. This interface has the dual roles of excluding red blood cells, albumin, anionic biomacromolecules, and other large proteins from vascular tissues [46] and of transmitting vascular mechanical forces via cytoplasmic signaling pathways [18] affecting junction opening, inflammation, and coagulation. Examples of glycocalyx associated inflammatory responses to stress include the release of mitochondrial-produced reactive oxygen species [47], including NO via the endothelial nitric oxide synthase (eNOS) [29, 41, 48], and vasodilators such as prostacyclin [41, 49] as well as initiation of cell proliferation and motility [50], actin and vinculin reorganization [51], nonlinear, agonist-mediated increases in hydraulic conductivity [40], and calcium oscillation amplitudes upon exposure to physiologic pressure changes [52]. ROS production and cytosolic calcium influx has been associated with elevated P-selectin expression [53], which results in leukocyte margination [54]. Moreover,

glycocalyx shedding and degradation in inflammatory models attenuates these responses [18, 21, 45, 51, 55-57]. These results mechanistically connect increased pressure with enhanced permeability and suggest that the capillary glycocalyx is biomechanically involved in modulating vascular barrier function and inflammation [58].

1.2.3 Clinical Significance of Mechanotransduction

Capillary endothelial cells found in the walls of the alveoli experience fluctuating mechanical forces with each cycle of inspiration and expiration. During critical illness and mechanical ventilation, however, excessive forces result in increased capillary permeability and in increased edema. Elevated capillary pressure and permeability has been mechanistically associated with disease states such as congestive heart failure [59] and acute conditions such as neurogenic pulmonary edema [60], high altitude pulmonary edema [61], and acute respiratory distress syndrome associated with ventilator induced lung injury [62]. It has been shown that pressure-induced permeability increases occur at pressures that do not result in capillary wall rupture [63, 64]. This suggests that there is a mechanism besides capillary wall failure that mediates barrier function.

An intact lung capillary glycocalyx is vital to normal vascular barrier function and subsequently normal pulmonary function. Evidence suggests that the glycocalyx provides active regulatory functions, which are fundamental to normal lung fluid balance. Specifically, endothelial surface glycoproteins participate in agonist-mediated signaling [40]. As previously discussed, HS and HA have been implicated in mechanotransduction. Also important to glycocalyx

structure are associated blood serum proteins. The component contribution to the overall glycocalyx mechanical environment is integral to its transfer of extracellular mechanical signals to intracellular signals.

Figure 1.3A shows a plausible mechanical model relating HA, HS, syndecan, albumin, and other cellular structures. Drag on these glycocalyx components strains these elements; these strains lead to intracellular transmission and initiation of inflammatory signaling pathways. Heparan sulfate proteoglycans are postulated to be the transducer of glycocalyx signal transduction [51, 65].

1.3 Micromechanical Measurements of Cellular Components

The deformability of any material describes its ability to transmit physical signals. Measuring the stiffness and strain of biologic tissues and particularly cells requires techniques that are capable of very sensitive measurements of very soft materials. Most cellular mechanics models describe the mechanics of cytoskeletal environment without reference to the glycocalyx [66]. Interestingly, Satcher and Dewey concluded that while the endothelial cell has been shown to respond to surface stress and elastically deform upon 10^4 Pa pressure, the elastic modulus of the cell can be 2-10 times higher due to underlying cytoskeletal components [67]. Weinbaum et al., constructed a mathematic model of the flexural rigidity of core proteins that coupled dynamic surface layer responses with mechanical loading stresses and deformations in the underlying cytoskeleton [2]. This model describes evidence for core proteins acting as transducers of fluid shear stress. They predicted that a 10 dyne/cm^2 shear force

would produce an insufficient drag force (7.0×10^{-4} pN) on a single core protein; however, if shear was applied across the entire core structure, there would be sufficient drag (1.9×10^{-2} pN) to displace the actin cytoskeleton by 6 nm. These findings highlight the mechanical role of the glycocalyx: glycocalyx components, such as GAGs, serve to sense stresses due to fluid flow and transmit them to the anchored transmembrane proteins, thus facilitating cellular mechano-sensing [18, 68]. The glycocalyx is largely modeled as viscoelastic structure with both elastic and viscous characteristics. The glycocalyx is essentially a very soft layer overlying another slightly stiffer layer. Direct measurement of the mechanical properties of this structure requires the use and development of these techniques.

1.3.1 Soft Tissue Measurement

Measurement of cellular or tissue mechanics requires extremely sensitive techniques that have spatial resolutions of <1 μm [69]. The most common optical techniques used to measure mechanical properties of living cells have been cell poking, atomic force microscopy (AFM), magnetic tweezers, micropipette aspiration, magnetic twisting bead cytometry, and flow chambers [3, 66, 70], which utilize loading forces varying from 10 pN to 5 μN [70]. Typical cell indentation techniques such as AFM use sharp cantilevers that apply finite loading rates that progressively stress the cellular surface, cell membrane, and underlying cytoskeletal elements, which may result in measuring nonequilibrium mechanical properties of cells [71-73]. Magnetic tweezers are able to exert small magnetic forces or torques on small, magnetized molecules or polymers.

Twisting cytometry is a similar technique that utilizes ligand-coated microspheres to twist and measure separation forces between a receptor-ligand pair. Flow chambers are able to apply shear forces across monolayers to measure changes in thickness and other associated properties. These techniques have yet to be developed to a point where they can differentiate between subtle changes in the glycocalyx.

1.3.2 Complementary Measurement Techniques

AFM has been a method of choice to measure mechanical properties of endothelial cells using indentation techniques [73-77]. Typical AFM indentation experiments involve the use of a sharp AFM tip that indents the cell membrane and exerts pressure on cell membrane and cytoskeleton. Sharp tips apply the force of a small area that does not measure the average mechanical environment and has the potential to poke through the soft layer being measured. AFM provides stress and strain information; however, it is a nonequilibrium technique that is limited here by glycocalyx thickness (measured to be between 0.2 and 3 μm [reviewed in [78]]), contact point determination, and noise in the contact region. A more comprehensive picture of the mechanical properties of the glycocalyx could be obtained if AFM was supplemented with a nonindenting, equilibrium-based technique.

Reflectance interference contrast microscopy (RICM), an interferometric technique initially described by Curtis [79], has been quantitatively used to characterize local bending elastic modulus of red blood cells [80], measure absolute distances from a surface [81], perform contour analysis on giant

vesicles [82], measure the bending modulus, membrane tension, and adhesion energy of single cells [83], and describe the dynamics of wetting by partially wetting fluids on a solid surface [84]. RICM is estimated to have a spatial resolution of approximately 300 nm [85] and a sub-nanometer vertical resolution [86, 87]. Rädler and Sackmann utilized polystyrene microspheres hovering over surfaces as force probes to determine weak repulsive interaction with RICM [88]. The balance of the forces (i.e., weight of the particle minus its buoyancy vs. electrostatic repulsion) relied on the stochastic fluctuations of the particle's vertical position around the equilibrium to find how the interaction energy depended on distance. In a similar manner, RICM was used to characterize the effective stiffness of the endothelial glycocalyx layer. A simple model comparing hypothesized indentation effects of AFM and RICM on the endothelial surface is shown in Figure 1.3b.

1.4 Dissertation Overview

The central objective of the work described in this dissertation was to develop techniques capable of measuring and describing the mechanics of the glycocalyx microenvironment. Individual components have not been characterized in terms of their mechanical contribution to the glycocalyx stiffness. Specifically, two techniques were used to characterize the contributions of major glycosaminoglycans and macromolecules in lung glycocalyx mechanics and endothelial permeability: atomic force microscopy and reflectance interference contrast microscopy. In Chapter 2 and Chapter 3, these techniques were developed to measure the glycocalyx micromechanical microenvironments.

These studies comprised initial measurements of the mechanical contributions of glycosaminoglycans, heparan sulfate and hyaluronan, to the lung glycocalyx. In Chapter 4, the mechanical role of clinically relevant macromolecules in the glycocalyx was investigated. The rationale for each chapter is briefly discussed in the following sections.

1.4.1 Stiffness of the Pulmonary Endothelial Glycocalyx Measured with Atomic Force Microscopy

The mechanics of the glycocalyx in live cells have not been widely investigated. The endothelial cell has been shown to respond to surface stress of 0.1 Pa, yet the elastic modulus of the cell is on the order of 1000 Pa [67]. Protruding glycocalyx components, as well as cilia, amplify stress signals and provides a mechanism for mechanosensing [68]. Existing models, however, broadly describe the cytoskeletal environment without reference to the glycocalyx in the mechanical environment [66]. If the glycocalyx and the underlying layers are modeled where the underlying layers are stiffer, information regarding this layer and can be obtained and applied to developing more complete and accurate models. Well-characterized techniques can be modified and utilized to make these measurements. AFM is a regularly used technique that can easily be modified to distribute cantilever contact area with the glycocalyx.

1.4.2 Use of Reflectance Interference Contrast Microscopy to Characterize the Endothelial Glycocalyx Stiffness

Currently, there are several techniques commonly used to measure mechanical properties of living cells: cell poking, atomic force microscopy (AFM),

magnetic tweezers, micropipette aspiration, magnetic twisting cytometry, flow chambers, and others [3, 66, 70]. Typical cell indentation techniques such as AFM use finite loading rates that progressively stress the cellular surface, cell membrane, and underlying cytoskeletal elements, which may result in measuring nonequilibrium mechanical properties of cells [71-73].

Mechanical measurement of biologic materials at submicron levels requires sensitive techniques. More recently, AFM tip modification has allowed for the forces to be applied over a larger area, thus minimizing poking through cellular layers; however, AFM still applies progressive forces. The development of RICM, described in Chapter 3, has allowed for measurement of equilibrium glycocalyx mechanical properties. These techniques allow for differentiation between subtle changes in the constitution of the glycocalyx.

1.4.3 Mechanical Effects of Macromolecule Addition to the Glycocalyx

The glycocalyx is a proteoglycan/glycosaminoglycan covering, which resides on the luminal surface of blood vessels and the microvasculature. This gel-like coating has been found to act as a macromolecular filter and to function in both chemical and physical signal transduction. Evidence suggests that the glycosaminoglycan heparan sulfate is integral to pressure induced increases in hydraulic conductivity [18]. The same has been shown for shear forces in regards to both heparan sulfate and hyaluronan [41]. The importance of macromolecules to glycocalyx function has also been established; albumin is integral to endothelial health and function [89] and has shown that albumin interacts with the glycocalyx [14]. Macromolecule addition has previously been thought to act

by plugging of the capillary layer, but there is evidence to suggest that other macromolecules interact with the glycocalyx [90-93]. While there have been efforts to determine the glycocalyx interactions with albumin, there is less known about the effect of macromolecules such as HES on the glycocalyx and overall tissue compliance [94]. In Chapter 3, compliance measurements were acquired as function of macromolecule titration.

The mechanical characteristics of hyaluronan and the clinically relevant macromolecules in the glycocalyx that allow for endothelial mechanotransduction were investigated separately in Chapter 2 and Chapter 3. Understanding these components in conjunction with associated proteins ultimately can assist in developing a strategy to treat acute inflammation of the lungs. In Chapter 4, glycocalyx mechanics were probed in a combination of HA removal and macromolecule reconstitution. Composite results from these studies describe the mechanical contributions of glycosaminoglycans (heparan sulfate and hyaluronan) and macromolecules (albumin and hydroxyethyl starch) to lung glycocalyx structure.

1.4.4 Hydraulic Conductivity of Microvascular Endothelial Monolayers

The significance of glycocalyx mechanical properties is ultimately demonstrated by endothelial changes in permeability in response to mechanical stimuli. The majority of inflammatory methods include application of shear or pressure with subsequent measurement of fluid, protein, and/or inflammatory molecule flux. Endothelial cells have previously been shown to respond to both

shear and pressure forces [18, 40, 89]. Furthermore, changes in fluid flux have been shown to a function of albumin concentration [89]. In Appendix A, hydraulic conductivity, which measures the fluid flux across the vascular wall, was used as an indicator of mechanotransduction. Specifically, the effects of albumin and the clinically relevant hetastarch were investigated.

1.4.5 Glycosaminoglycan Characterization of Microvascular Endothelial Cells

The mechanosensing functions of the mesh-like glycocalyx are determined by its structure. This structure is determined by glycocalyx composition, which is a function of cell surface GAG presentation. In Appendix B, GAG content of rat lung microvascular endothelial cells was measured and reported. The specific disaccharide contents are included for both heparan and chondroitin sulfates.

CHAPTER 2

STIFFNESS OF THE PULMONARY ENDOTHELIAL GLYCOCALYX MEASURED WITH ATOMICFORCE MICROSCOPY AND REFLECTANCE INTERFERENCE CONTRAST MICROSCOPY[1]

Ryan O'Callaghan[2], Kathleen Marie Job[2], Randal O. Dull, Vladimir Hlady

2.1 Abstract

The mechanical properties of endothelial glycocalyx were studied using atomic force microscopy with a silica bead (diameter ~18 μm) serving as an indenter. Even at indentations of several hundred nanometers, the bead exerted very low compressive pressures on the bovine lung microvascular endothelial cell (BLMVEC) glycocalyx and allowed for an averaging of stiffness in the bead-cell contact area. The elastic modulus of BLMVEC glycocalyx was determined as a pointwise function of the indentation depth before and after enzymatic degradation of specific glycocalyx components. The modulus-indentation depth profiles showed the cells becoming progressively stiffer with increased indentation. Three different enzymes were used: heparinases III and I and

[1] Reprinted with permission from AJP Lung, [95] O'Callaghan R, Job KM, Dull

[2] Both others contributed equally to work

hyaluronidase. The main effects of heparinase III and hyaluronidase enzymes were that the elastic modulus in the cell junction regions increased more rapidly with the indentation than in BLMVEC controls, and that the effective thickness of glycocalyx was reduced. Cytochalasin D abolished the modulus increase with the indentation. The confocal profiling of heparan sulfate and hyaluronan with atomic force microscopy indentation data demonstrated marked heterogeneity of the glycocalyx composition between cell junctions and nuclear regions.

2.2 Introduction

The endothelial glycocalyx is a polysaccharide-protein coating on the luminal surface of the vascular endothelium and forms a negatively charged, complex meshwork. The primary glycosaminoglycan constituents of glycocalyx are heparan sulfates (HS), chondroitin sulfates and hyaluronan (HA). The syndecan family of transmembrane proteoglycans and membrane-bound glypicans both carry HS and chondroitin sulfate side chains, [15, 29], while HA is a nonsulfated GAG that is secreted into the pericellular space and is associated with other components of glycocalyx. In vivo, the glycocalyx is known to associate with blood proteins such as fibrinogen [96] and albumin [97] that contribute to the permeability barrier of the vessel wall. Several important functions are assigned to the in vivo glycocalyx [9]: 1) a molecular sieve and hydrodynamic barrier for transvascular exchange of macromolecules; 2) an exclusion layer preventing interactions of blood proteins and cell with the endothelial membrane, per se; 3) a modulator of leukocyte binding and rolling;

and 4) a transducer of mechanical impulses to the intercellular cytoskeleton and associated signaling pathways.

Glycocalyx shedding and degradation in models of inflammation lead to impaired endothelial mechano-transduction of fluid shear stress [18, 45, 51], adhesion of platelets [98] and leukocytes [55, 99, 100] to the endothelial surfaces, and leakage of plasma proteins and fluid from the vascular space [56, 99]. The activation of inflammation pathways [99], edema [48], loss of capillary density [101] and deregulation of organ blood flow [21] can all be related to the loss of glycocalyx function; however the mechanism(s) that trigger the shedding of glycocalyx have yet to be established.

The highly complex, multifunctional and multicomponent structure of the endothelial glycocalyx poses a question: which approach is the most appropriate to study its multifaceted features? A reductionist approach used by many groups, including ours, is to elucidate the roles and functions of its constituent parts using enzyme digestions [17, 41, 102-104]. We have used specific enzymes to degrade glycocalyx HS and HA components and measure diffusion and the dynamics of albumin association within the glycocalyx expressed by bovine lung microvascular endothelial cells (BLMVECs) in vitro [14]. Here, atomic force microscopy (AFM) was used to quantify the elastic properties of BLMVEC glycocalyx before and after enzymatic degradations of these components.

AFM has been a method of choice to measure mechanical stiffness of endothelial cells using indentation techniques [73-77]. Typical AFM indentation experiments involve the use of a sharp tip that indents the cell membrane and

exerts pressure on the membrane and cytoskeleton. Using AFM, Mathur et al. [73] have found fivefold differences in elastic moduli measured over the nucleus vs. the peripheral cell body of human umbilical vein endothelial cells. Ohashi et al. [74] have used AFM and finite-element analysis to show the increase in elastic moduli for bovine endothelial cells exposed to shear stress. Costa et al. [77] used non-Hertzian pointwise approach to analyze how the elastic moduli of human aortic endothelial cells changes with indentation depth (δ).

We approached the measurement of glycocalyx stiffness using the same pointwise approach with one major difference: because the sharp AFM tip (typical r = 10 nm) could easily exert high local pressure on glycocalyx elements, or poke through the glycocalyx layer with little resistance, we substituted this sharp AFM tip with a larger silica bead (diameter ~18 μm). Thus we traded the high resolution of sharp tip AFM for low compressive pressures and spatial averaging of mechanical properties in the bead-cell contact region. These lower compressive pressures and spatial averaging in the bead-cell contact area allowed us to determine the elastic modulus of BLMVEC in a pointwise fashion, as a function of the δ, before and after enzymatic degradation of specific glycocalyx components. Three enzymes were used: heparinase III (HSase III) or heparinase I (HSase I), both at the concentrations of 15 mU/ml, or hyaluronidase (HAase) at 1.2, 12, and 50 U/ml concentrations. In addition, cytochalasin D was used to disrupt the cell cytoskeleton and differentiate between the elastic contributions of glycocalyx and underlying cellular structures.

2.3 Methods

2.2.1 Cell Culture

BLMVECs (Vec Technologies, Rensselaer, NY) were cultured onto glass coverslips (1 in. round, 0.17 mm thick, Fisher Scientific, Pittsburgh, PA) precoated with 0.4% bovine gelatin (SigmaAldrich, St. Louis, MO) for 1 h, followed by 100 μg/ml bovine fibronectin (Sigma-Aldrich, St. Louis, MO) for 1 h at 37°C and 5% CO_2. BLMVECs were plated at a density of 2.5×10^5 cells/cm^2 and cultured for 7–10 days.

2.3.2 Enzymatic Degradation of the Glycocalyx

Glycocalyx components were selectively digested by incubating cells with HAase (from strep. hyalurolyticus, Sigma-Aldrich, St. Louis, MO; EC 4.2.2.1; concentrations 1.2, 12, or 50 U/ml), HSase I (Sigma-Aldrich; EC 4.2.2.7; 15 mU/ml), or HSase III (Sigma-Aldrich; EC 4.2.2.8; 15 mU/ml) in MCDB-131 medium supplemented with 25 mM HEPES, pH 7.4, 0.01% penicillin/streptomycin, and 1% BSA (Fraction V, Sigma) at 37°C and 5% CO_2 for 1 h. Cells were then rinsed with the same medium and used in AFM experiments.

2.3.3 Cytochalasin Disruption of Cytoskeleton

The effect of cytoskeleton disruption on elastic modulus was determined by incubating confluent monolayers of BLMVECs with 100 nM cytochalasin D (Sigma-Aldrich; EC 244–804-1) for 30 min at 37°C and performing subsequent AFM indentation as described below. Cytochalasin D was initially solubilized in DMSO, then diluted in cell medium to 100 nM (~300 μM DMSO or 0.02%).

Identical cytochalasin treatment was conducted with BLMVEC monolayers pretreated for 1 h with 50 U/ml HAase.

2.3.4 AFM Indentation

A borosilicate glass microsphere (diameter = 17.3 ± 1.4 μm; catalog no. 9020, Duke Scientific, Palo Alto, CA) was glued to the tip of a rectangular AFM cantilever (nominal spring constant = 0.03 N/m) and mounted to the z-piezo on an Explorer AFM head (Topometrix, Santa Clara, CA). The AFM scanner was placed above the BLMVEC monolayer covered with medium, and the bead was brought into contact with cells. The loading force was minimized to prevent any cell damage. In the indentation measurement, the cantilever deflection was measured by a position-sensitive diode (PSD) as a function of z-piezo displacement producing raw AFM data. The measurements were taken at multiple ($n > 80$) locations on the BLMVEC monolayer surface. The loading rate was 10 μm/s, and the maximal loading force varied between 5 and 10 nN. The typical δ was up to ~500 nm. After the indentation measurements were completed, the sample topography was mapped by scanning the same AFM bead over the BLMVEC monolayer over a $(100\ \mu m)^2$ region. From the topological scans, the specific loci of cell-cell junctions and cell nuclei were judiciously assigned to each indentation run (Figure 2.1). The indentation runs that did not localize exactly to either of the two locations were excluded from the analysis. The contribution of individual glycocalyx components to the overall stiffness was assessed by the enzymatic digestions, followed by subsequent AFM indentation measurements.

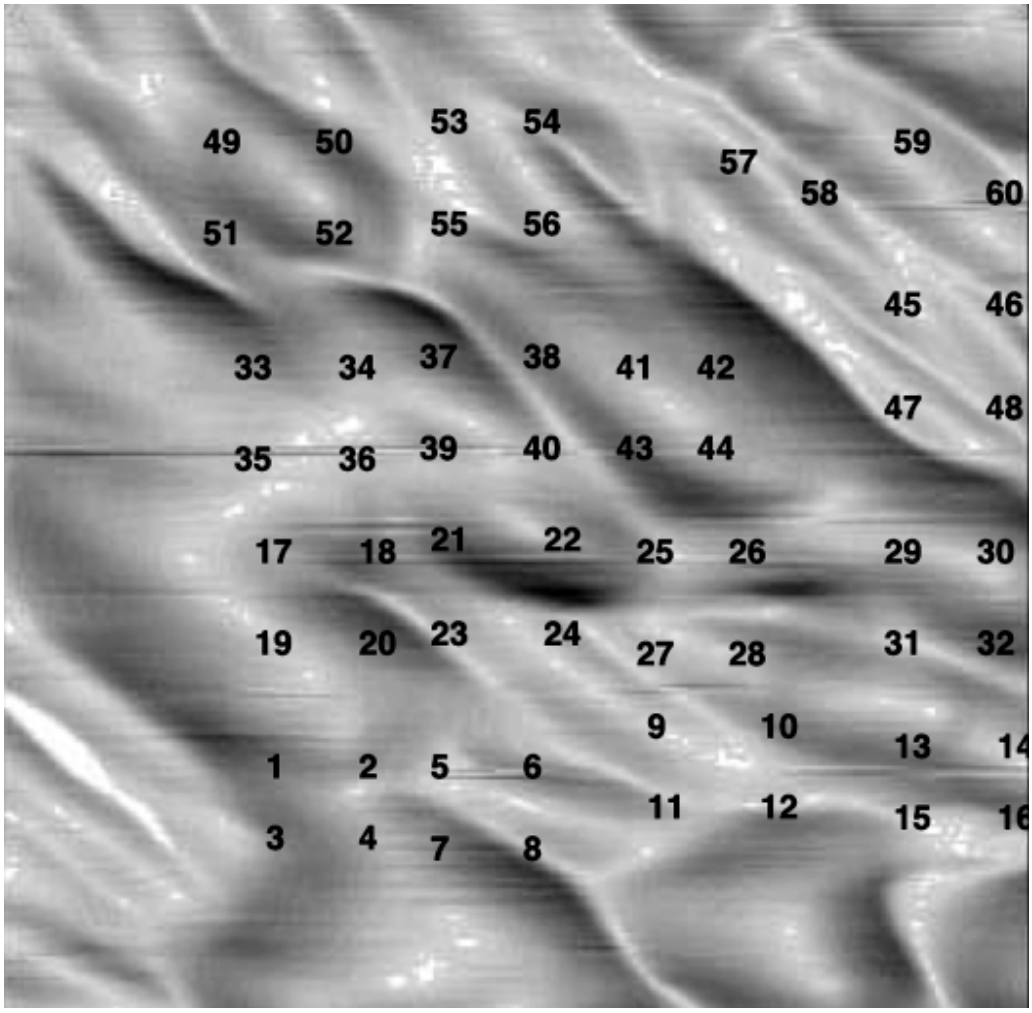

Figure 2.1 Atomic force microscopy (AFM) topography scan of a 100 × 100 μm^2 area of the bovine lung microvascular endothelial cell (BLMVEC) monolayer using a spherical bead as an AFM tip. The numbers indicate the locations at which force-indentation measurements were taken. These were assigned to cell junction or cell nucleus locations.

2.3.5 AFM Data Analysis

The AFM indentation data were analyzed by finding the point of contact between the bead and the cell surface layer in raw AFM data and then performing a pointwise analysis to determine the stiffness of the glycocalyx as a function of the δ. The stiffness of the cantilever (in N/m) was calibrated using the AFM instrument built-in software function, which also provided the conversion factor between the cantilever deflection signal (in nA) and cantilever force (nN). Once the stiffness of the cantilever was known, a hypothetical rigid substrate deflection–displacement line with the slope equal to the negative cantilever stiffness was plotted through the contact point as shown in Figure 2.2A. The indentation into the glycocalyx, δ, was the found by subtracting the displacement value of each data point from the displacement value on the rigid substrate line at the identical force, F. This procedure produced the force-indentation F(δ) curve shown in Figure 2.2B. To account for spherical geometry of the AFM probe, the indenter geometry function for a sphere of radius R was used [105]:

$$\Phi(\delta) = \frac{4}{3\pi}\sqrt{R\delta^3} \tag{2.1}$$

where R is that of the bead indentor. This indenter geometry function was then used to find the pointwise elastic modulus, E, for every data point on the F(δ) curve [77]:

$$E(\delta) = \frac{F(\delta)}{2\pi\Phi(\delta)} \tag{2.2.}$$

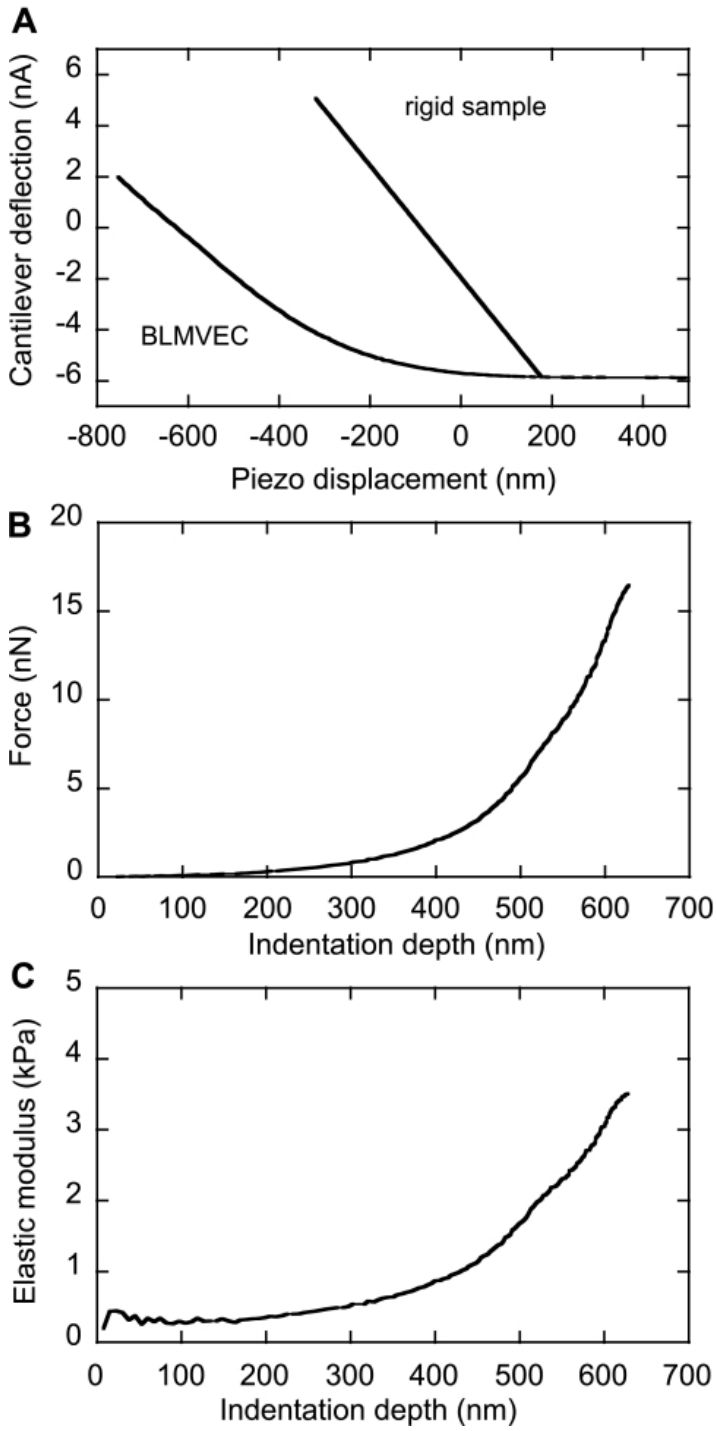

Figure 2.2 Conversion of raw AFM data into the pointwise elastic modulus E. A: typical raw AFM data for untreated BLMVEC and rigid samples. B: BLMVEC force vs. indentation data. C: the pointwise E calculated from the force-indentation data plotted as a function of indentation depth δ.

The E of a cell (in kPa), plotted as a function of indentation, δ (Figure 2.2C), showed that the E of control BLMVECs glycocalyx was constant up to the δ values of ~200 nm. The depth of indentation, where the E(δ) curve shows an inflection, was used as an estimate of the effective thickness of the glycocalyx, δ_g. Statistical analysis of BLMVEC moduli recorded before and after enzymatic treatments was performed using a Wilcoxon-Mann-Whitney rank-sum test.

2.3.6 Confocal Imaging

BLMVEC monolayers were treated with enzymes, washed with phosphate-buffered saline, and fixed with 4% paraformaldehyde at room temperature. HS was immunostained with anti-HS (HepSS-1, US Biologicals, Swampscott, MA) and incubated with Alexa Fluor 596 labeled anti-IgM-k (BD Biosciences, San Jose, CA). HA was localized using biotinylated HA-binding protein (US Biologicals; H7980–35) and then labeled with avidin-Alexa Fluor 488 conjugate (Invitrogen, Carlsbad, CA; A-21370). A FV1000-XY, Olympus IX81 confocal microscope and a 60 × NA 1.45 oil immersion lens were utilized for imaging (Core Facilities, University of Utah). Images of (200 μm)^2 area were taken with vertical separation distance of 0.2 μm. The fluorescence intensity profiles through the confocal images stack were extracted using ImageJ software (W. Rasband, National Institutes of Health) at 6 μm^2 areas at junction and nucleus locations.

2.4 Results

Analysis of AFM spherical bead indentation experiments yielded two dependent variables: E and δ. Figure 2.3 shows how average modulus changes with the δ, <E>(δ) at cell junctions (Figure 2.3A) and nuclei (Figure 2.3B), before and after enzymatic digestions with HSase III (15 mU/ml) and HAase (50 U/ml). The difference between BLMVEC controls and the enzyme-treated cells was remarkable; in the case of the controls, the E initially rose slowly with indentation and reached ~1 kPa at δ = 600 nm at the junctions. After the enzyme digestion, the modulus increased more rapidly at smaller indentations for both enzymes and also showed signs of leveling at large indentations. The modulus of control BLMVECs had a low value of ~0.25 kPa and was approximately constant up to the δ values of ~200 nm. Upon further indentation, the modulus increased, which indicated that the loading forces compressing the glycocalyx were progressively transmitted to the less compliant cell membrane and underlying cytoskeleton. The finding that the enzymatic treatment increased stiffness in the region between 0 < δ < 600 nm relative to controls indicated that the glycocalyx, which resided in this region, was being degraded. For nuclear locations, however, the difference between <E>(δ) data for controls and enzyme-treated BLMVECs was indistinguishable. The average modulus diverged only at larger δ values, and HSase III action made the cells stiffer, while HAase made them a bit softer (Figure 2.3B). One way to analyze the <E>(δ) data is by using two-layer composite compliance model [106]:

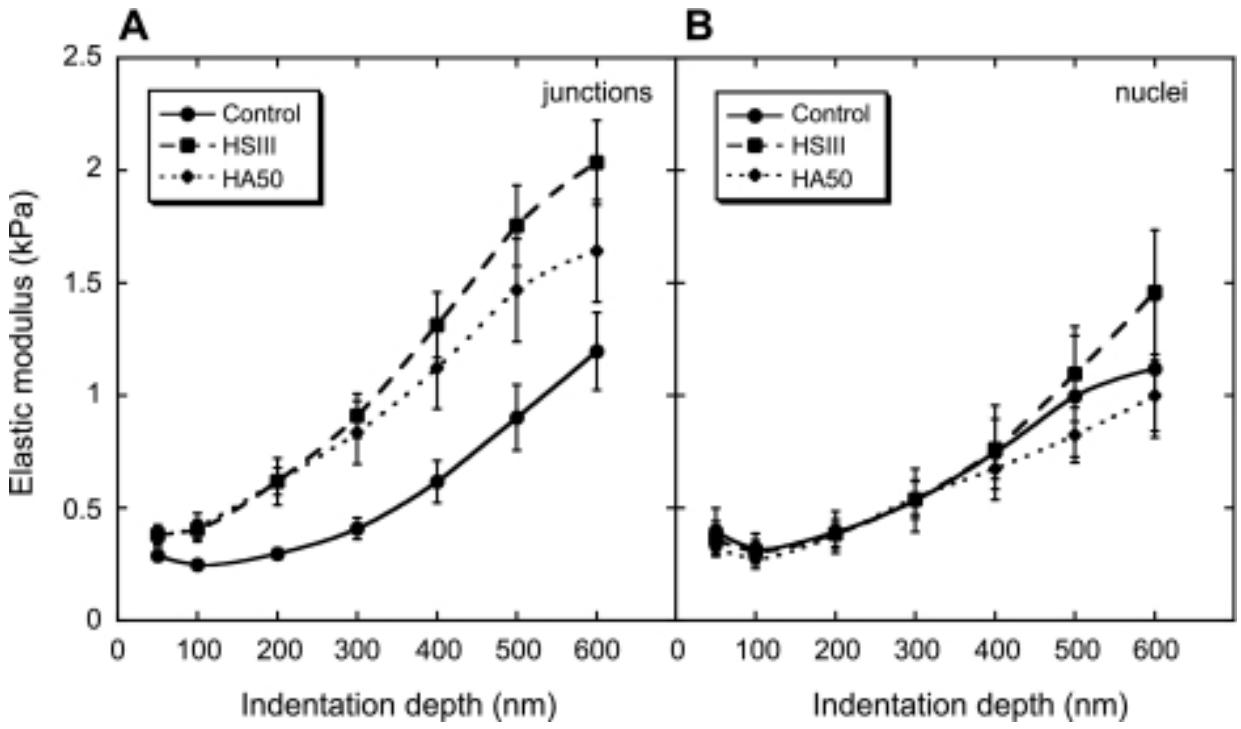

Figure 2.3 Average E shown as a function of the δ, E(δ), at cell junction (A) and nuclear (B) locations for untreated BLMVECs (junctions: n = 43, nuclei: n = 11), and after enzymatic digestions of glycocalyx with heparinase (HSase) III (HS III; 15 mU/ml) (junctions: n = 43, nuclei: n = 11), and hyaluronidase (HAase) (50 U/ml; HA50) (junctions: n = 33, nuclei: n = 9). The vertical bars represent the SE of the mean.

$$\frac{1}{E(\delta)} = \frac{1}{E_{glycocalyx}}(e^{-\frac{\alpha\delta}{\delta_g}}) + \frac{1}{E_{cell}}(1 - e^{-\frac{\alpha\delta}{\delta_g}}) \quad (2.3)$$

where $E_{glycocalyx}$ and E_{cell} are the mean elastic moduli of the glycocalyx and the cell, respectively, and α is a parameter defining the mechanical interlayer interactions. The compliance of the spherical bead indenter was assumed to be much smaller compared with the other two right-hand side terms and was omitted from analysis. The model accounts for the transfer of mechanical deformation between the two layers, i.e., the glycocalyx and the cell, by the term $\exp(-\alpha\delta/\delta_g)$ [107]. This transfer function is dependent on the δ, the δ_g, and the extent of interlayer interactions, which are dependent on the local composition of glycocalyx. A fit to the two-layer composite compliance model for BLMVECs treated by HSase III and HAase yielded the best fitted parameters as follows: E_{cell} = 2.93 ± 0.38 kPa and $E_{glycocalyx}$ = 0.26 ± 0.03 for HSase III, and E_{cell} = 2.35 ± 0.31 kPa and $E_{glycocalyx}$ = 0.28 ± 0.03 kPa for HAase (50 U/ml). The δ_g was estimated to be 420 nm (HSase III) and 450 nm (HSase 50). The fitted α parameter was ~2.2; however, because it appears in the exponent ratio α/δ_g, its effect on the fit was strongly affected by estimate of the δ_g. The <E>(δ) results for untreated BLMVECs did not display a sigmoidal shape, so the fitted results were inconclusive. The biomechanical role of cellular structures below the glycocalyx was investigated by treating the cells with cytochalasin D. Cytochalasin D is known to inhibit actin polymerization within the cell, thus causing softening of the cell [108]. Figure 2.4 compares the <E>(δ) data at the cell junctions for untreated BLMVECs, cells treated with cytochalasin D, and cells treated first with enzyme

HAase (50 U/ml) and then with cytochalasin D. The E of cytochalasin D-treated BLMVECs remained <0.5 kPa for the whole range of δ values (δ < 500 nm). The pretreatment of cells with enzyme HAase followed by cytochalasin D treatment resulted in an E profile that was almost indistinguishable from the cell treatment with cytochalasin D alone. A similar trend of cytochalasin D cell softening was found at the nuclear locations (data not shown). The results of the cytochalasin D experiments confirmed that the observed increases in elastic moduli at intermediate indentations (100 < δ < 500 nm), for control and enzyme-treated BLMVECs (Figure 2.3 and Figure 2.4), were due to the progressive transmission of the compressive loads from the glycocalyx to the underlying cytoskeletal structure. Consequently, the effective stiffness of glycocalyx was represented by the modulus at 100-nm δ, E_{100}. Figure 2.5 shows the actual E_{100} data for each indentation run and for all enzyme treatments measured at cell junctions. Figure 2.5A compares the digestion of BLMVEC glycocalyx with HSase III (15 mU/ml) or HAase (50 U/ml) to the control. For both enzymes, the mean elastic moduli $\langle E_{100} \rangle$ (shown by the horizontal lines), as well as the spread of E_{100} data, increased upon the enzyme digestion (HSase III, P = 0.003, HAase, P = 0.035, each compared with the controls). Clearly, the enzymatic digestion made the BLMVECs appear a bit stiffer compared with controls. The majority of the E_{100} data, however, remained <0.4 kPa, indicating the enzymes might not have completely digested the glycocalyx. Figure 2.5B compares the effect of HAase concentrations on E_{100}. Similar findings, such as larger spread of moduli and Increases in $\langle E_{100} \rangle$, were observed for BLMVECs treated with HAase at low (1.2

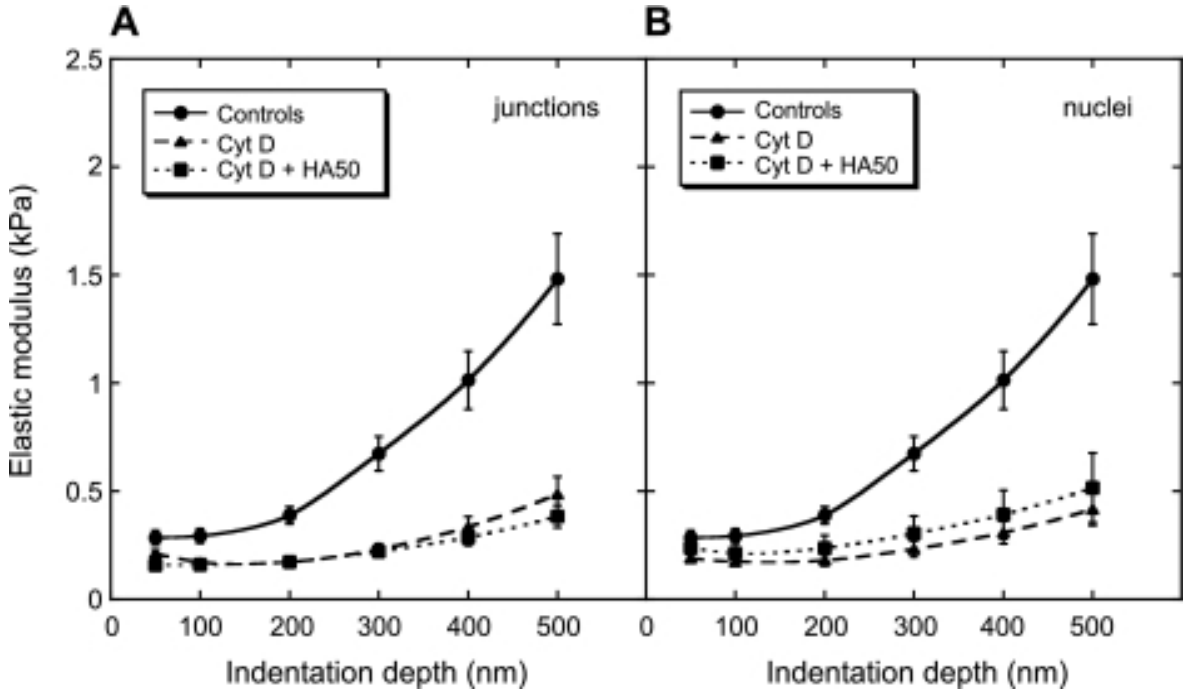

Figure 2.4 E(δ) for the cell junctions of untreated BLMVECs (n = 27), cells treated with cytochalasin D (Cyt D; n = 32), and cells treated first with HA50 and then with Cyt D (n = 23). The vertical bars represent the SE of the mean.

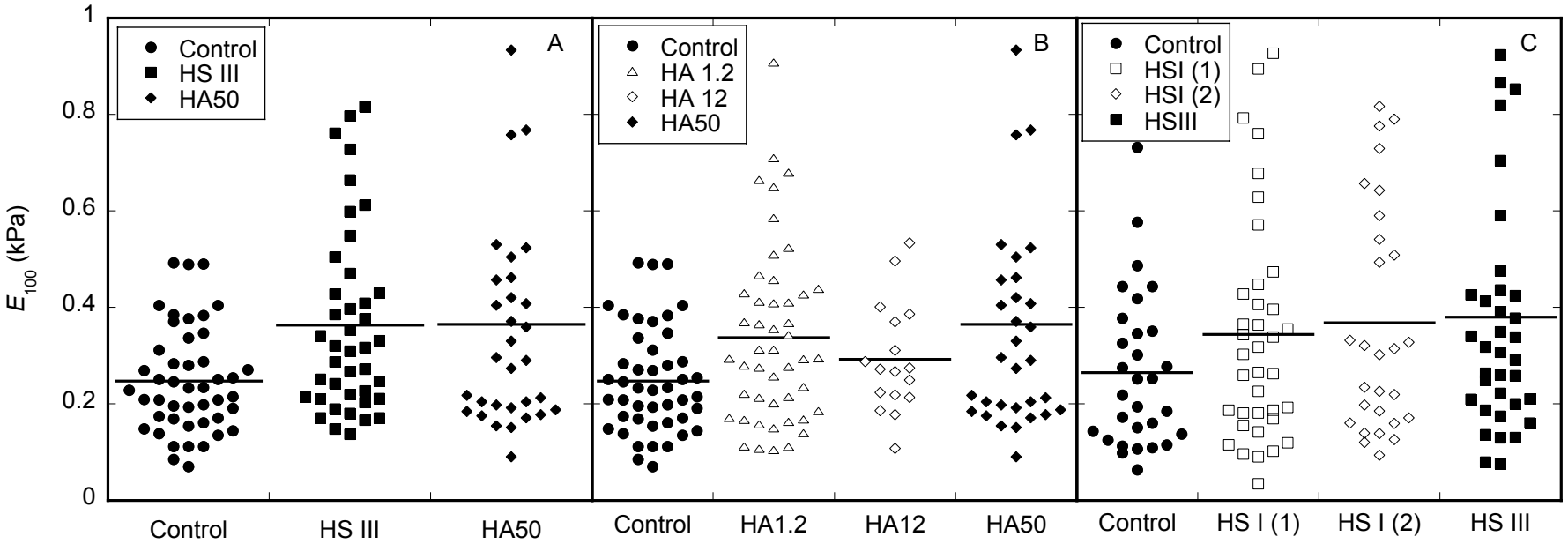

Figure 2.5 Elastic moduli at the 100-nm δ (E_{100}) before and after enzymatic digestions. A: the comparison between the BLMVEC controls and the cells treated with enzymes [HS III, P = 0.003, HA50, P = 0.035]. B: the effect of the HAase concentrations [HAase 1.2 U/ml (HA 1.2), P = 0.017, HAase 12 U/ml (HA 12), P = 0.128, HA50, P = 0.035]. C: the comparison between BLMVEC controls and duplicate run of HSase I (HS I) [(1) P = 0.192, (2) P = 0.100] and HS III (P = 0.051). The mean modulus for each data set is shown by horizontal line. Each data set is compared with untreated BLMVEC controls (*P < 0.05).

U/ml, P = 0.017) and high (50 U/ml, P = 0.035) concentration compared with controls. HSase III. While the repeated treatment of BLMVECs with HSase showed very similar $<E_{100}>$, only the treatment with HSase III showed significant difference from the controls [HSase I (first run) P = 0.192, HSase I (second run) P = 0.100, HSase III, P = 0.050].

Confocal imaging of enzyme-treated and control BLMVECs was used to create the concentration profiles for HS (Figure 2.6) and HA (Figure 2.7) at both cell junction and nuclear locations. For untreated BLMVECs, a higher concentration of HS was found at the cell junctions compared with nuclear locations (Figure 2.6, A vs. B). The action of HSase III (15 mU/ml) reduced the integrated fluorescence intensity at both locations (junctions: a 65% decrease, nuclei: a 54% decrease) and shifted the fluorescence maxima to smaller distances from the basal side of the cells. This indicated the enzyme was more effective at the upper cell surface, as expected.

The confocal imaging also revealed that the spatial distribution of hyaluronan was different from that of heparan sulfate: the stain fluorescence intensity was much larger above the nuclei than at the cell junctions (Figure 2.7A vs. Figure 2.7B). The HAase (50 U/ml) digestion of hyaluronan was more effective at the nuclear locations reducing the integrated fluorescence intensity by ~4/5, than at the cell junctions (a mere 1/4 reduction). Similarly to the case of heparan sulfate digestion, the maxima of the HA stain fluorescence intensity shifted to the smaller distances from the basal side of the cells upon the treatment with HAase.

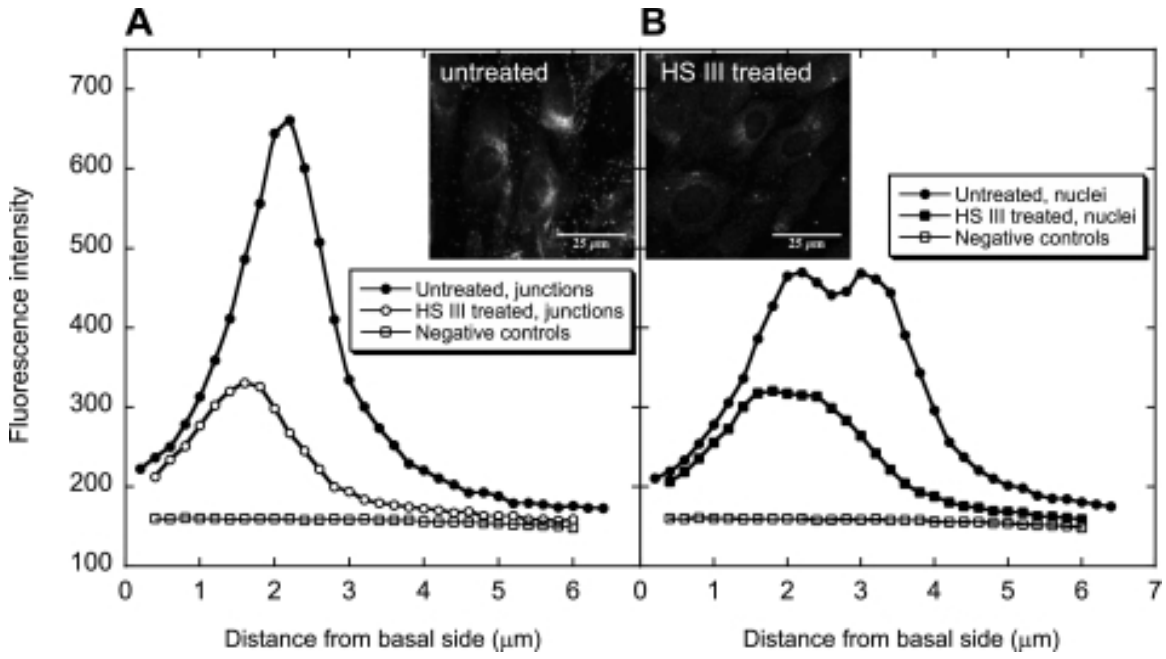

Figure 2.6 Confocal vertical profiles of HS before and after enzyme digestion with HS III (15 mU/ml) (n = 3). A: cell junction location. B: nuclear location. Negative controls were not treated with the enzyme or anti-HS, but only stained with the secondary anti-IgM-k antibody. The insets show confocal images of untreated and HS III-treated BLMVECs.

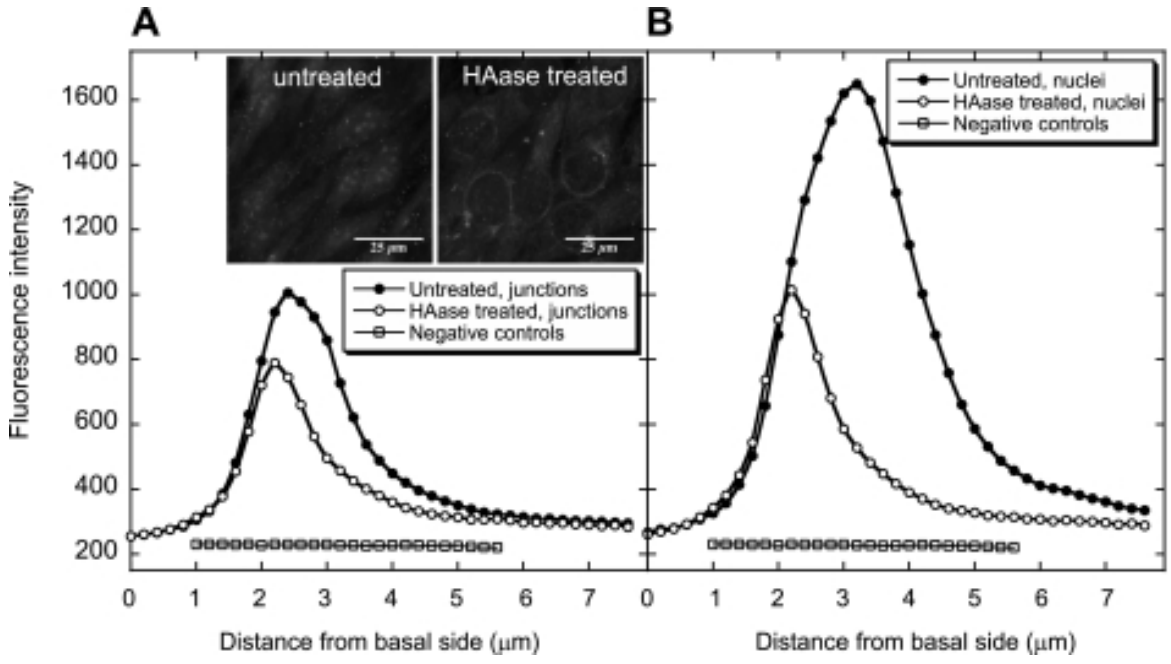

Figure 2.7 Confocal vertical profiles of HA before and after enzyme digestion with HA50 (n = 3). A: cell junction location. B: nuclear location. Negative controls were not treated with the enzyme or HA binding protein, but only stained with avidin-Alexa Fluor 488 conjugate. The insets show confocal images of untreated and HAase-treated BLMVECs.

2.5 Discussion

The goal of the present study was to characterize the effect of glycocalyx components on stiffness of BLMVEC glycocalyx and to elucidate the contributions of HS and HA. The technique selected was spherical probe AFM, because the probe exerted smaller loading forces over larger contact area than in the case of typical indentation with a sharp AFM tip. For example, the contact area of a spherical bead (d = 18 μm) at 50 nm indentation was ~2.8 μm^2, or a circular area with r = 0.94 μm, and the bead exerted only 180-Pa pressure at 0.5 nN load. The same spherical bead used to indent the cells was used to scan the topography of BLMVEC monolayers and to develop coordinates that allowed precise assignment of indentation locations at cell junctions, which are believed to be the loci of mechanotransduction (37). For comparison, indentation measurements were also carried out at the nuclear locations.

The force-indentation data, F(δ), were used in a pointwise calculation of the E as a function of the δ, E(δ) [9]. A large number of E(δ) curves (typical n > 30) were averaged to analyze the difference between BLMVEC controls and cells treated with enzymes. In the case of controls, the <E>(δ) measured at the cell junctions was essentially flat up to 200-nm indentation and then reverted to an increasing function up to an indentation of 600 nm. After enzymatic digestion with HSase III (15 mU/ml) or HAase (50 U/ml), the average modulus <E>(δ) increased more rapidly at smaller indentations at ~100-nm δ (Figure 2.3A). The effective δ_g was estimated from the inflection of <E>(δ) curves where possible, or from the model described by Equation 2.3. As previously reported, the δ_g

determined by in vivo fluorescence imaging of mesenteric vessels (or hamster cheek pouches) [109], by in vitro measurements on BLMVECs utilizing fluorescence correlation spectroscopy, and by confocal immunohistochemistry [14] was found to be larger than 500 nm. This thickness agrees with the estimates from individual E(δ) curves (for example, see (Figure 2.2 C). The average <E>(δ) data after HSase III or HAase digestion showed that the enzymes decreased this value to ~420–450 nm. The two-layer composite compliance model [106] was used to assess the biomechanical properties of glycocalyx and underlying cell membrane and cytoskeleton. The fit to the model yielded reasonable E estimates for glycocalyx and underlying cellular structures, but was less sensitive to the δ_g and the parameter α. Such simple models do not represent the physical properties of cellular structures well; neither glycocalyx nor underlying cytoskeleton is a uniform homogeneous layer, but is instead a mesh of interconnected stiffer and softer elements [110]. Hence, the usefulness of such model might be rather limited. In addition, not all <E>(δ) data could be fitted well with the model, because some E(δ) curves did not display sigmoidal shape, which was a prerequisite for a good fit. This was especially noticeable for BLMVEC controls that required larger δ values to show the leveling of the E (Figure 2.3). One may infer in such cases that the δ_g was larger than the δ used. The estimates for the δ_g from the inflection of <E>(δ) confirm such an inference. The change of the glycocalyx composition, for example, by enzymatic digestion, has the potential to affect the way by which loading forces are transmitted to the underlying membrane and cytoskeleton. In terms of the two-layer composite

compliance model (Equation 2.3), the mechanical coupling effect was described by the empirical term $\exp(-\alpha\delta/\delta_g)$. However, no firm conclusion about the coupling factor α could be made, as its influence on the fit was heavily affected by the δ_g.

The <E>(δ) results indicated that increase of loading transmits the compressive forces to the underlying cellular structures (Figure 2.3 and Figure 2.4). This agrees with the accepted physical picture in which mechanical perturbations of the glycocalyx are transduced to a chemical signal within the cell cytoplasm [9]. The matching of mechanical compliances is expected for proper mechanochemical transduction; a very soft glycocalyx would not be sensitive enough to small perturbations due to circumferential stretch and pressure changes within the vasculature. Similarly, a rigid glycocalyx imbedded in a compliant matrix could be too sensitive to weak force perturbations. Disrupting the underlying cytoskeleton with cytochalasin D largely eliminated the increase of <E>(δ) in the range of $0 < \delta < 500$ nm (Figure 2.4), confirming that modulus increases observed in BLMVECs were due to progressive compression of underlying cytoskeleton. It was not possible to estimate how much of the <E>(δ) increase was due to the bending stiffness of the cell membrane; however, membrane contribution was expected to be small [110].

Based on the appearance of <E>(δ) curves, the pointwise modulus at 100-nm indentation was assigned as an effective measure of glycocalyx stiffness. At a smaller δ of 50 nm, the modulus was determined to be too noisy due to AFM raw data noise and the accuracy of determining the contact zero indentation

point (Figure 2.2). Larger variations of E at very small indentations have been reported in the literature due to the sharp AFM tip used when human aortic endothelial cells [77], osteoblasts [111], bovine pulmonary artery endothelial cells [76], and human umbilical vein endothelial cells [73] were indented. The distribution of E_{100} was narrow for BLMVEC controls ($0.1 < E_{100} < 0.5$ kPa), but the range increased after enzymatic digestion of the glycocalyx ($0.1 < E_{100} < 1.0$ kPa, Figure 2.5A). This demonstrated structural heterogeneity of the glycocalyx layer. Lectin-binding studies have confirmed that there is both macro- and microheterogeneity of the glycocalyx structure over the length scale of a single cell [112, 113]. Our own confocal images of BLMVEC glycocalyx also demonstrated significant heterogeneity [14, 114]. Experimentally, it was possible that, at some of the cell junctions, the spherical bead probe indented a larger area than predicted due to the concave shape of these regions.

Insight into heterogeneous distribution of glycocalyx components is provided by the confocal depth profiles of HA and HS before and after enzymatic digestion (Figure 2.6 and Figure 2.7). There was a significant difference between $\langle E \rangle(\delta)$ at cell junctions and at nuclear locations. One can speculate that the mechanical coupling between glycocalyx and the underlying cytoskeleton at the cell junctions is different than at the nuclear locations. Confocal profiling showed that nuclear locations of BLMVECs were predominantly decorated with HA polymer chains (Figure 2.7, A vs. B), known to be noncovalently attached to cell membrane receptors and to HS proteoglycans. In contrast, the cell junctions appeared to be richer in HS than the nuclear regions (Figure 2.6, A vs. B).

Admittedly, confocal vertical profiling does not have the same resolution as lateral confocal imaging. However, it was possible to resolve the vertical distribution of HS above the nuclei where the stain showed two peaks, indicating that HS is present at both the basal and upper cell surfaces (Figure 2.6B). No such resolution was possible for the HA stain. In general, the fluorescence was not eliminated by the enzyme treatments; the enzymes predominantly digested HA and HS polymers from the upper cell surface, which was exposed to enzyme solution. We conclude that the enzymes did not completely digest each glycocalyx component, as indicated by depth profiles (Figure 2.6 and 2.7).

Two forms of HSases (HSase I and HSase III) have been tested for their effects on glycocalyx stiffness. HSase I cleaves disaccharide substrates that have a higher sulfate content, whereas HSase III cleaves unsulfated disaccharides. It has been reported that endothelial HS participate in both flow [18, 41] and pressure-induced [40] mechanotransduction that subsequently activates nitric oxide synthase. Increased levels of nitric oxide are associated with barrier dysfunction, as assessed by increased hydraulic conductivity [18, 40, 115]. It has been reported that selective removal of cell-surface HS with HSase III abolished pressure and flow-mediated nitric oxide production and the associated barrier dysfunction, establishing a direct link between the glycocalyx and barrier-dependent mechanotransduction [18, 40, 41]. According to the present results, only HSase III had a significant effect on increasing the glycocalyx modulus (Figure 2.5C, $P = 0.050$), thus supporting the previous findings. HAase degradation of the glycocalyx at higher enzyme concentrations

also resulted in a significant increase in E_{100} compared with untreated cells (Figure 2.5, A and B, P = 0.035). It is, therefore, possible that HA acted as a softer, multiattachment cross-linker within the glycocalyx structure, and that its removal exposed stiffer elements of the glycocalyx.

One major conclusion from the present study is that enzymatic digestion of a single GAG in the glycocalyx leaves the other components in place so that they are able to maintain a similar stiffness in the probe-cell contact area. For example, it is likely that digestion of HA, which was found more concentrated above nuclear regions, leaves HS and associated transmembrane proteins, such as syndecan core protein, to transmit the compressive forces exerted by the AFM probe. Similarly, digestion of HS, which was found more concentrated in the cell junction areas as well, leaves syndecans in place and possibly also associated HA polymer. Yet these spatial differences in the composition of vascular glycocalyx must exist for functional reasons, which have yet to be fully elucidated.

2.6 Summary

AFM was used to assess the mechanical properties of BLMVEC glycocalyx: its modulus and thickness. The AFM indenter was a silica bead (diameter ~18 μm) used instead of sharp AFM cantilever tip. This resulted in low compressive pressures on the glycocalyx, allowing determination of the E in a pointwise fashion as a function of the δ. The modulus-δ profiles showed cells becoming progressively stiffer with the indentation. Three different enzymes were used to digest glycocalyx components: HSases III and I and HAase. For HSase

and HAase treatments, the E in the cell junction increased more rapidly at lower indentations than in controls. These enzymes also reduced the δg. Cytochalasin D abolished the modulus increases with the indentation. It was found that the digestion of a single glycocalyx component leaves the other components in place so that they were able to maintain a similar stiffness in the probe-cell contact area. More importantly, the combined confocal profiling and AFM results demonstrated marked heterogeneity of the glycocalyx spatial composition between cell junctions and nuclear regions.

CHAPTER 3

USE OF REFLECTANCE INTERFERENCE CONTRAST MICROSCOPY TO CHARACTERIZE THE ENDOTHELIAL GLYCOCALYX[3]

Kathleen M. Job, Randal O. Dull, and Vladimir Hlady

3.1 Abstract

Reflectance interference contrast microscopy (RICM) was used to study the mechanics of the endothelial glycocalyx. This technique tracks the vertical position of a glass microsphere probe that applies very light fluctuating loads to the outermost layer of the bovine lung microvascular endothelial cell (BLMVEC) glycocalyx. Fluctuations in probe vertical position are used to estimate the effective stiffness of the underlying layer. Stiffness was measured before and after removal of specific glycocalyx components. The mean stiffness of BLMVEC glycocalyx was found to be ~7.5 kT/nm^2 (or ~31 pN/nm). Enzymatic digestion of the glycocalyx with pronase or hyaluronan with hyaluronidase increased the mean effective stiffness of the glycocalyx; however, the increase of the mean stiffness on digestion of heparan sulfate with heparinase III was not significant.

[3] Reprinted with permission from AJP Lung, [116] Job KM, Dull RO, Hlady V. Use of reflectance interference contrast microscopy to characterize the endothelial glycocalyx stiffness. American journal of physiology Lung cellular and molecular physiology. 2012;302:L1242-9.

The results imply that hyaluronan chains act as a cushioning layer to distribute applied forces to the glycocalyx structure. Effective stiffness was also measured for the glycocalyx exposed to 0.1%, 1.0% and 4.0% BSA; compliance increased at two extreme BSA concentrations. The RICM images indicated that glycocalyx thickness increases with BSA concentrations. Results demonstrate that RICM is sensitive to detect the subtle changes of glycocalyx compliance at the fluid-fiber interface.

3.2 Introduction

In addition to responding to chemical signals, mammalian cells also respond to mechanical stresses [66, 68, 117, 118]. For example, mechanical forces alter cell migration [119], cell growth [120], inflammation [121], and disease state regulation [122]. The endothelial glycocalyx is of particular interest as it has been implicated in mechano-transduction [9]. The endothelial glycocalyx is a negatively charged, protein and polysaccharide, brush-like layer that resides on the luminal surface of endothelial cells. In the lung vasculature this multi-functional layer responds to fluid shear [18, 45, 123], fluid pressure [40], and oncotic pressure [48] to regulate inflammation and ultimately the fluid balance [29, 51]. The glycosaminoglycan (GAG) heparan sulfate (HS), with associated transmembrane protein syndecan, and the unsulfated GAG hyaluronan (HA) have been implicated in biomechanical activation [40, 45]. Additionally, albumin, the dominant protein in blood plasma, has been shown to interact with the glycocalyx and be involved in proper regulation of fluid balance [14, 34-36].

Currently there are several techniques commonly used to measure

mechanical properties of living cells: cell poking, atomic force microscopy (AFM), magnetic tweezers, micropipette aspiration, magnetic twisting cytometry, flow chambers, and others [3, 66, 70]. The loading forces used in these techniques vary from 10 pN to 5 μN [70]. Typical cell indentation techniques such as AFM use finite loading rates that progressively stress the cellular surface, cell membrane, and underlying cytoskeletal elements, which may result in measuring nonequilibrium mechanical properties of cells [71-73]. Most cellular mechanics models describe the mechanics of cytoskeletal environment without reference to the glycocalyx [66]. Interestingly, Satcher and Dewey concluded that while the endothelial cell has been shown to respond to surface stress and elastically deform upon 10^4 Pa pressure, the elastic modulus of the cell can be 2-10 times higher attributable to underlying cytoskeletal components [67]. This points to the mechanical role of the glycocalyx: glycocalyx components, such as GAGs, serve to sense stresses attributable to fluid flow and transmit them to the anchored transmembrane proteins thus facilitating cellular mechano-sensing [18, 68].

Recently, we have used AFM with a silica bead serving as an indenter (diameter ~18 μm) to measure the elastic response of bovine lung microvascular endothelial cells (BLMVEC) [95]. We found that the glycocalyx stiffness and thickness changed after removal of GAGs by specific enzymes, which agreed with the literature reports [78, 124, 125]. In the present report, we describe how a microinterferometric technique based on reflectance interference contrast microscopy (RICM) can provide information about the outermost cellular layer mechanics, e.g. at the fluid-fiber interface, that is complementary to the bead-

AFM study.

RICM, an interferometric technique initially described by Curtis [79], has been quantitatively used to characterize local bending elastic modulus of red blood cells [80], measure absolute distances from a surface [81], perform contour analysis on giant vesicles [82], measure the bending modulus, membrane tension, and adhesion energy of single cells [83], and describe the dynamics of wetting by partially wetting fluids on a solid surface [84]. RICM is estimated to have a spatial resolution of ~300 nm [85] and a sub-nanometer vertical resolution [86, 87]. Rädler and Sackmann utilized polystyrene microspheres hovering over surfaces as force probes to determine weak repulsive interaction with RICM [88]. The balance of the forces (i.e. weight of the particle minus its buoyancy vs. electrostatic repulsion) relied on the stochastic fluctuations of the particle's vertical position around the equilibrium to find how the interaction energy depended on distance. In a similar manner, RICM could be used to characterize the effective stiffness of the endothelial glycocalyx layer.

The work described herein uses RICM to mechanically interrogate the glycocalyx with a glass bead serving as a force probe that exerts very small loads fluctuating around ~50 pN and indents the glycocalyx only several nanometers. In contrast to microrheology techniques, the RICM thus measures the mechanical properties resulting from normal loading forces (i.e, pressure). Specifically, we used RICM to study how effective glycocalyx stiffness changes when HS or HA are removed by specific enzymes digestion and when albumin concentration in the media is changed. The results demonstrate the potential of

using RICM micro-interferometry as a sensitive research tool in cellular biomechanics.

3.3 Methods

3.3.1 Cell Culture

BLMVECs (Vec Technologies) were grown in MCDB-131 Complete (Vec Technologies) and in MCDB 131 (M853, Sigma) supplemented with 15 mM sodium bicarbonate, pH 7.4, 1% penicillin/streptomycin, and 10% FBS. BLMVECs were subcultured (1.25 x 10^5 cells/cm^2) on ethanol-dried, autoclaved coverslips (17 mm thick), which were treated with 0.4% gelatin (Sigma-Aldrich) and 100 μg/cm^2 fibronectin (Sigma-Aldrich) each for 1 h. Passage 5-7 BLMVECs were maintained at 37°C and 5% CO_2 until usage 9-11 days after subculture. The testing medium used during experiments was MCDB-131 (Sigma-Aldrich), pH 7.4, supplemented with 25 mM HEPES and 1% penicillin/streptomycin designated as medium II (MII).

3.3.2 Enzymatic Digestion

Enzymes (Sigma-Aldrich) were used to selectively degrade HA and/or HS from the BLMVEC glycocalyx: hyaluronidase (from Streptomyces hyalurolyticus; no. 4.2.2.1; 50 U/ml) and heparinase III (from Flavobacterium heparinum; Sigma, no. 4.2.2.8; 15 mU/ml; Sigma) in MII + 1% BSA for 1 h at 37°C and 5% CO_2. Pronase (from Streptomyces griseus; Sigma, no. 2.4.24.31; 0.01 mg/ml in MII + 1% BSA for 5 min at 37°C and 5% CO_2), a broad-spectrum protease, was used to nonspecifically degrade the glycocalyx. The RICM experiments were

performed at room temperature in media not containing the enzyme.

3.3.3 Actin Disruption

The actin cytoskeleton was disrupted with 100 nM cytochalasin D (from Zygosporium mansonii; Sigma, EC # 244-804-1; Sigma) for 30 min in MII + 1% BSA for 5 min at 37°C and 5% CO_2. Cytochalasin D is known to inhibit actin polymerization [95, 126, 127]. The RICM experiments were performed at room temperature in media not containing the enzyme. Treated and untreated samples were stained for actin after 1 h. BLMVEC monolayers were fixed with 4% paraformaldehyde for 10 min, rinsed with PBS for 5 min, incubated with 0.165 μM Alexa Fluor® 594 phalloidin (Invitrogen) for 40 min, rinsed with PBS, air dried, and then mounted with ProLong® Gold AntiFade Reagent (Invitrogen). Samples were imaged using a Nikon Diaphot inverted microscope equipped with a x54 oil immersion objective (NA 0.99, 170/0.17 Leitz) and TRITC filters.

3.3.4 Albumin Treatment

After the preincubation of BLMVEC monolayers for 5 min with MII, experiments were performed in MII + 0.1%, 1.0% or 4.0% of highly purified BSA (Fraction V, Proliant,).

3.3.5 RICM Micro-interferometry

Figure 3.1 shows a schematic for a spherical glass bead separated from a flat glass coverslip by a cell monolayer. Incident monochromatic light is partially transmitted and reflected at each interface resulting in an interference pattern attributable to the recombination of reflected light. This interference pattern is

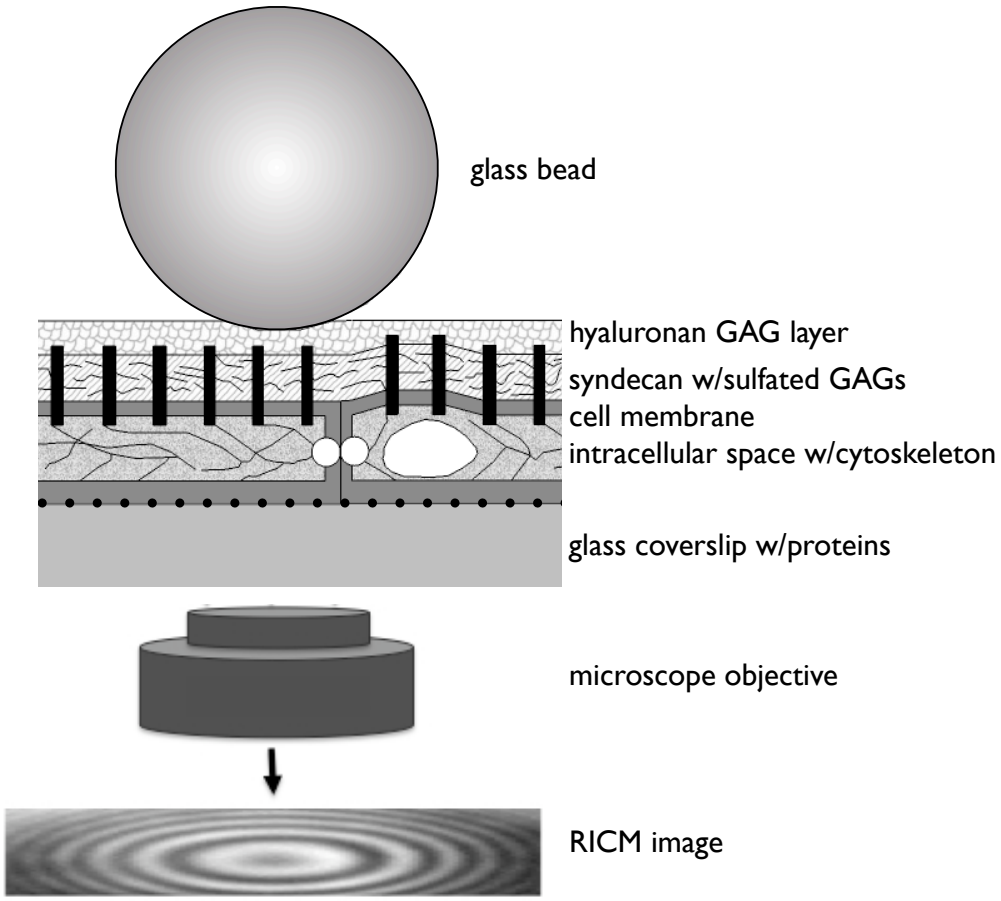

Figure 3.1 Schematic of RICM bead probe placed on the top of BLMVEC glycocalyx (not drawn to scale). Monochromatic light reflected from bead and coverslip surface constructively interferes to create an interference pattern in the RICM image that is captured by microscope objective and CCD camera. The interference pattern changes when the distance between the bead and the coverslip change.

used to determine the how the vertical separation distance between a probe bead and an underlying reflective glass surface changes as a function of time. For a bead compressing an elastic layer, the system can be modeled as a particle in a potential energy minimum where gravitational and elastic forces balance each other [88]. The vertical position of the particle fluctuates around the minimum as described by the Langevin equation [88, 128]:

$$m\left(\frac{d^2h}{dt^2}\right)+\gamma(h)\left(\frac{dh}{dt}\right)+\frac{dU(h)}{dh}=f_{stoch} \tag{3.1}$$

where h is the vertical separation distance between the bead probe and the coverslip; m is mass; d^2h/dt^2 acceleration; g(h) is the hydrodynamic drag coefficient; dh/dt velocity; U(h) describes the interaction potential; and f_{stoch} represents the stochastic thermal force. Assuming the vertical separation distance to be much smaller than the bead size indicates a strongly overdamped system so that the first l.h.s. term can be disregarded. The hydrodynamic drag coefficient is given by the Stokes formula:

$$\gamma(h)=6\pi\eta R\Gamma(h) \tag{3.2}$$

where h is the medium viscosity, R is the probe radius and the dimensionless correction factor G(h) is approximately equal to R/h if h << R. Under these two assumptions, the bead-underlying layer system is in thermal equilibrium and the bead fluctuations in h follow the Boltzmann law:

$$p(h)=Ae^{-U(h)/kT} \tag{3.3}$$

where p(h) is the probability of finding the bead at separation distance, h, A is the probability normalization constant, U(h) is the interaction potential, k is the Boltzmann constant, and T is temperature.

Measuring the fluctuations of bead vertical position. The interference pattern for a spherical bead on the flat shows fringes similar to Newton rings (Figure 3.2). Several methods for fitting the fringe profile have been described in the literature including the simple, finite aperture [129, 130], and nonlocal theories [86]. At small illumination numerical aperture and for the observation of thick objects, an assumption of normal incidence is justified [88, 130] and the vertical separation distance, h, between the bead and the substrate can be obtained by fitting the fringe intensity profile to the following equation:

$$I(x,h) = A_0 + A_1 e^{-gx^2} + A_2 e^{-lx^2} \cos\left(\left(\frac{4\pi n_2}{\lambda}\right)\left(R - \sqrt{R^2 - x^2}\right) + h + \delta\right) \tag{3.4}$$

where I(x,h) is the fringe intensity as a function of both vertical separation distance, h, and the distance from fringe center, x, and R is the bead radius. The constants A_2 and l describe the diminishing contrast of the fringes, A_1 and g account for the nonlinear background resulting from diffuse reflection away from the bead center; A_0 is the intensity offset; n_2 is the refractive index of the medium between the bead and the coverslip; and δ is the phase shift at the probe surface. As can be seen from Figure 3.2A, the RICM image also shows intensity variations attributable to the cellular layer. These variations arise from the refractive indices of cellular components such as the nucleus and actin cytoskeleton. To average over these intracellular variations, the intensity profile

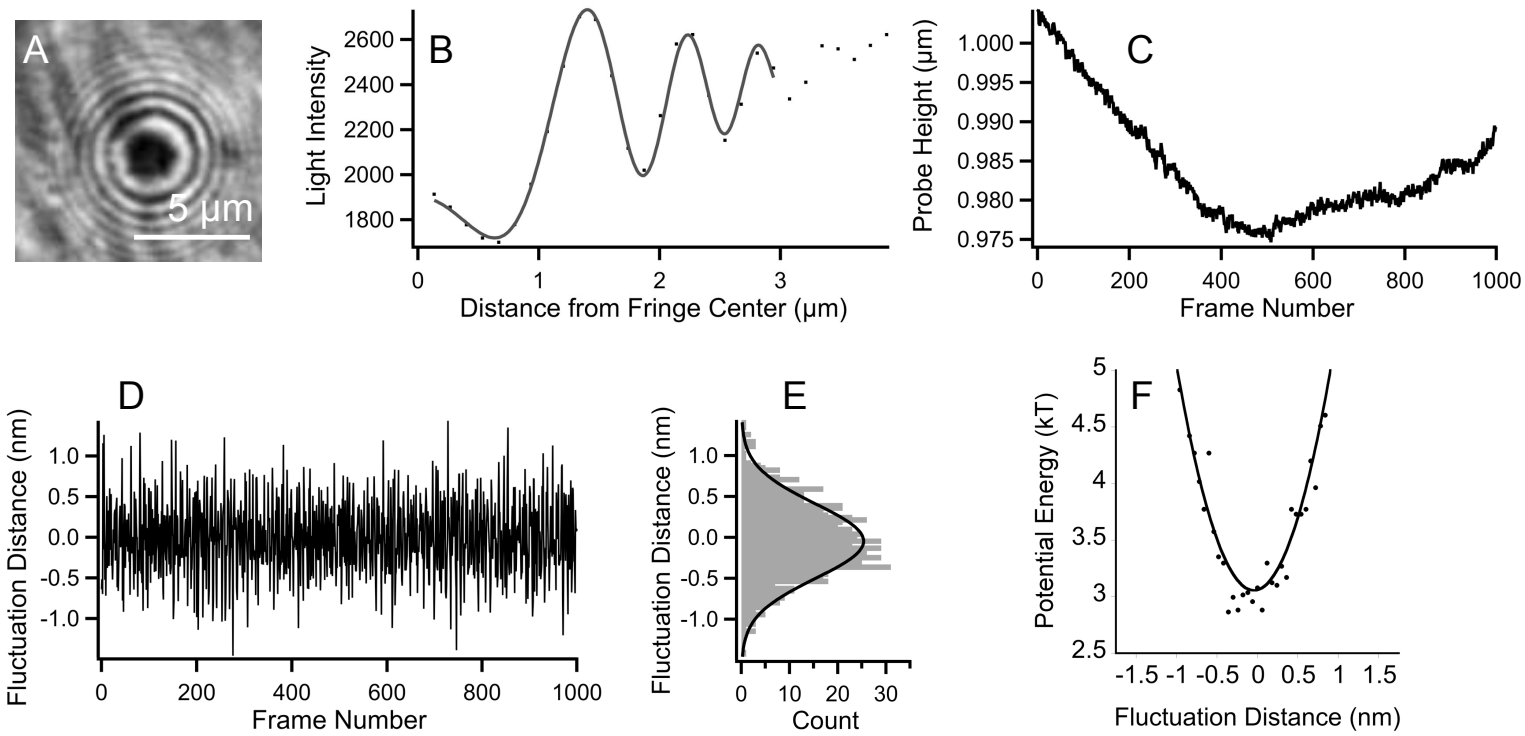

Figure 3.2 RICM image of a glass probe on a BLMVEC monolayer (A); Radial intensity profile of a single RICM image frame: the first few fringes were fitted for each frame (B); Changes in probe height during an RICM experiment shown as a function of the frame number (C); Vertical distance fluctuations obtained from data in (C) after high pass Hanning filtering (D); p(h), shown as solid line, calculated from the histogram of distance fluctuations (E); the potential energy profile U(h) calculated from p(h) (F).

of interference fringes was radially integrated (Figure 3.2B) and then fit to Equation 3.4 using n_2 = 1.33 (water). As a result of incoherent monochromatic light focused with small aperture, the intensity distortions increased with the distance from the fringe center and therefore only the intensity of the first few fringes was used in fitting. Note that the absolute vertical separation distance between the bead and the coverslip is not known because the actual fringe number was unknown, however, the changes in the vertical separation distance from one RICM image to the next are obtainable. In RICM experiments a sequence of ~1000 images was acquired at 15 to 20 Hz, with an exposure time of 30 ms, and the changes in vertical separation distance were calculated by fitting each successive RICM fringe image.

Vertical separation distance changes in time, h(t), were not only due to the stochastic force, f_{stoch}, but also to physiological movements of the cell and its cytoskeleton, including flickering [131], and bead movements resulting from various external causes (Figure 3.2C). To separate the fluctuations in h attributable to stochastic thermal force from other causes, the RICM-derived h(t) data were filtered with a high pass Hanning filter with a frequency cutoff at 2-3 Hz (Igor Pro 5.02; Wavemetrics) (Figure 3.2D).[4]

With sufficient sample size, the probability of finding the bead at the separation distance h, p(h) (Figure 3.2E), was used to find the interaction potential, U(h), using the Equation 3.3 (Figure 3.2F). The second derivative of

[4] It was assumed that slower vertical separation distance changes were due to causes other than thermal motion of the bead. Slower cell movements were thus eliminated.

U(h)/kT provided a measure of the effective stiffness for bead-cell interactions. Because the bead was rigid compared with the viscoelastic structure below it and the loading forces were very small, the computed effective stiffness, U''(h) was assigned to the underlying glycocalyx.

3.3.6 RICM Experiments

Borosilicate glass beads (diameter 17.3 μm ± 1.4 μm; Duke Scientific) were dispersed in MII + 1% BSA and then randomly placed on confluent BLMVEC monolayers. Contact area was projected to be less than ~2.8 μm^2 based on calculations using AFM with identical probes [95]. A coverslip covered with gelatin and fibronectin (no BLMVECs) was used as negative control. Images of interference fringes were recorded utilizing a Zeiss inverted microscope (IM35, Zeiss) equipped with an HBO 50W light source, a 54x oil immersion objective (NA 0.99, 170/0.17 Leitz), a monochromatic filter (λ = 546.1 nm) and a digital CCD Camera (C4742-80-12AG, Hamamatsu). The microscope was on an antivibration table and each RICM experiment was conducted in a closed chamber to reduce noise resulting from the movement of air over the sample. Each BLMVEC monolayer experiment lasted approximately 1.5 h. During this period, up to 15 RICM image sequences were acquired from beads located at cell-cell junctions. Statistical outliers were thrown out. Effective stiffness results were compared using an unpaired Wilcoxon-Mann-Whitney rank sum test with significant differences assigned when $p < 0.05$.

3.4 Results

Figure 3.3 shows the examples of phase contrast images for untreated (A) and heparinase-treated (B) BLMVEC monolayers with a bead probe. Although the placement of each bead was random, the majority of the beads settled in the cell-cell junction regions because of the cell topography. Neither the enzyme treatments nor the albumin concentration change disrupted the confluence and the "cobblestone" appearance of BLMVEC monolayers.

Figure 3.4 compares the effective stiffness of glass coverslips treated with 0.4% gelatin and 100 μg/cm^2 fibronectin against glass coverslips seeded with BLMVECs grown to confluence. Figure 3.4A shows the typical interaction potential profiles and Figure 3.4B shows the effective stiffness for each sample. The mean effective stiffness of 303.5 ± 120.4 kT/nm^2 was found for coverslips without BLMVECs (n = 10) and 12.6 ± 8.4 kT/nm^2 for BLMVECs seeded coverslips (n = 10), respectively. The results indicated the upper limit of the stiffness measurable for protein-covered coverslip and suggested a vertical resolution of <1 nm. BLMVEC monolayers were significantly more compliant than unseeded coverslips ($p < 0.0001$). In other words, the softer the sample is, the better the RICM resolution is for reconstructing U(h) profiles.

The contributions of HS and HA to the stiffness of BLMVEC glycocalyx were investigated before and after the treatment of BLMVEC monolayers with the medium containing hyaluronidase (HAase), heparinase III (HSIIIase), or pronase. As seen in Figure 3.5, with the use of ~17.3 μm diameter probes the RICM experiments yielded the mean effective stiffness 7.53 +/- 6.08 (control, n = 17),

A

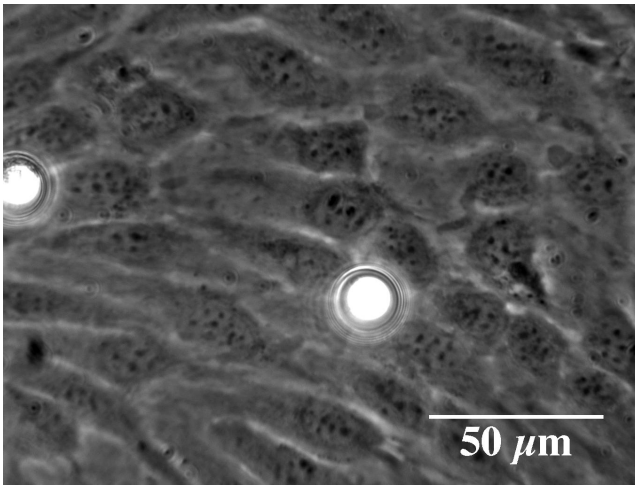

B

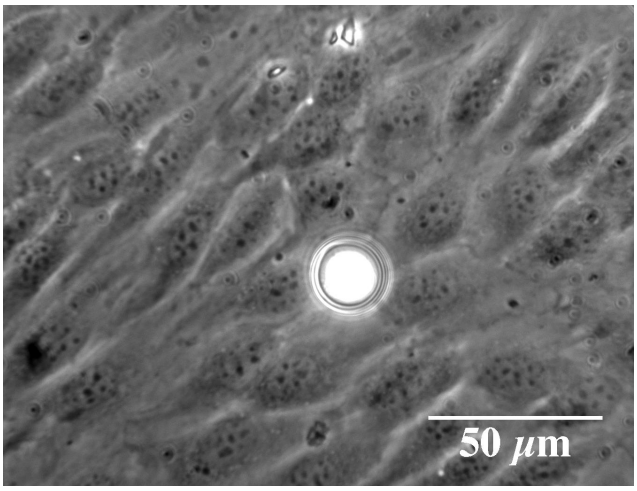

Figure 3.3 Phase contrast images of BLMVEC monolayers with borosilicate glass probes (diameter ≈ 17.3 μm): untreated (A) and heparinase III treated (B).

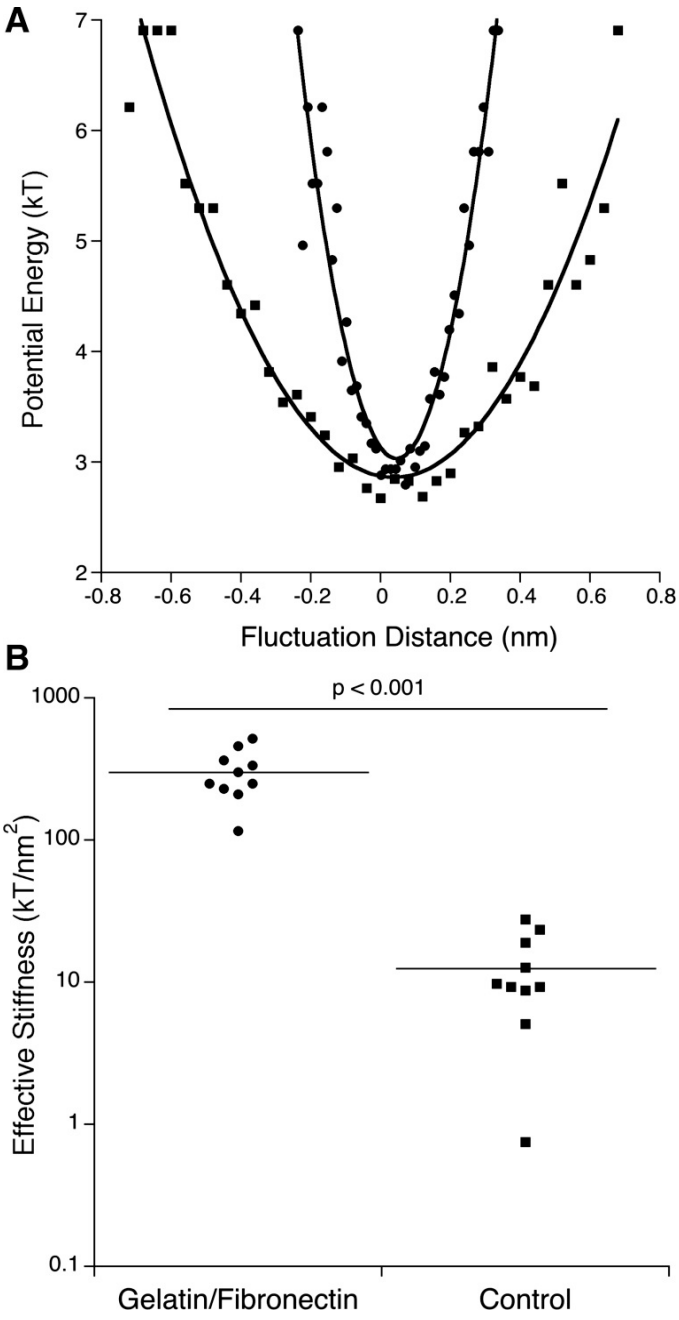

Figure 3.4 Potential energy profiles acquired from RICM data utilizing borosilicate glass probes (diameter ≈ 17.3 μm) for gelatin/fibronectin incubated glass coverslip (●) and BLMVEC monolayer (■) (A). Calculated effective stiffness for gelatin/fibronectin incubated glass coverslips (n = 10) and BLMVEC monolayers (n = 10) (B). BLMVEC monolayers samples were significantly more compliant than protein covered coverslips ($p < 0.001$).

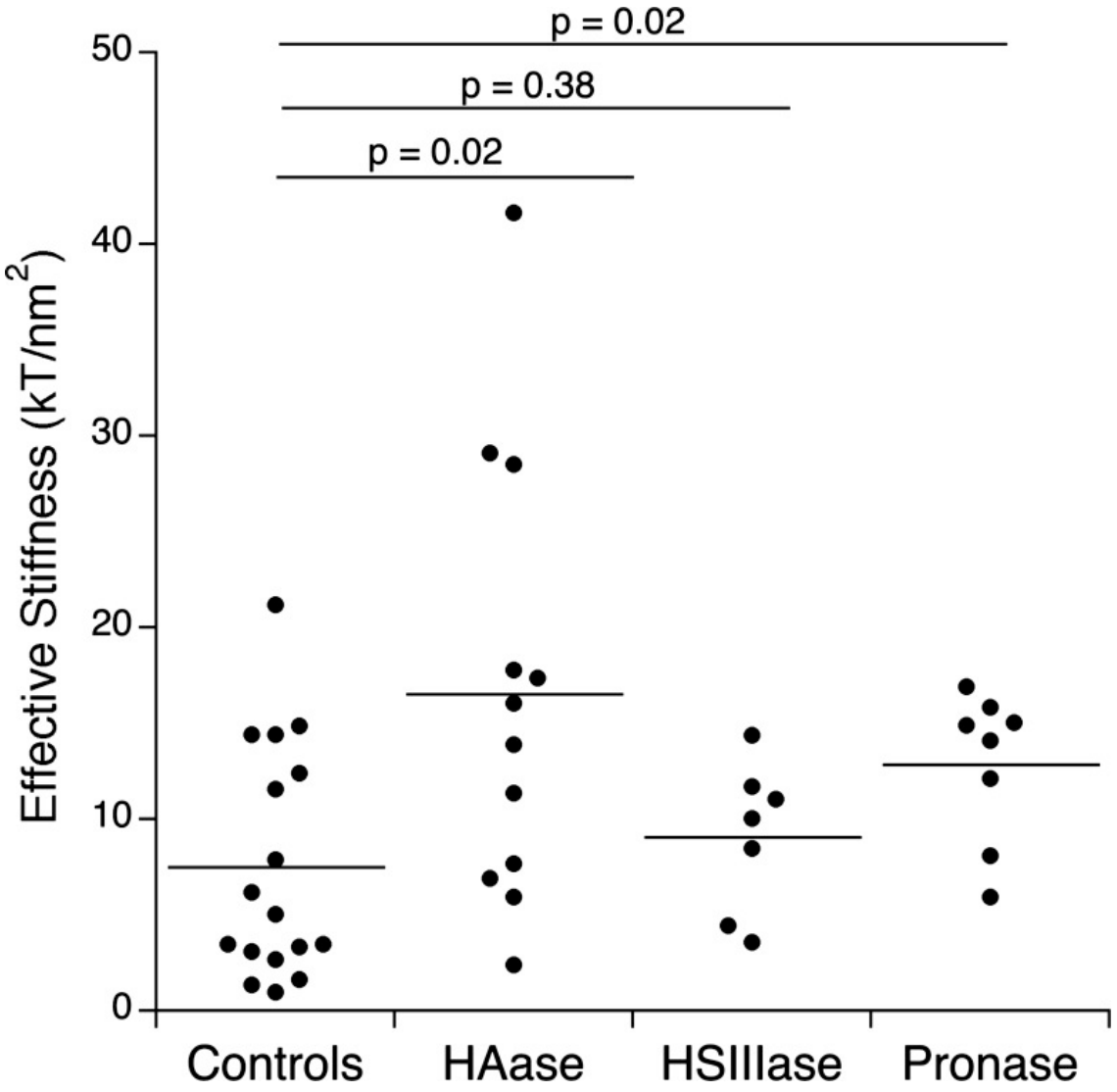

Figure 3.5 Effective stiffness of BLMEC glycocalyx measured by RICM utilizing borosilicate glass probes (diameter ≈ 17.3 μm) after hyaluronidase, heparinase III, and pronase treatments. Hyaluronidase treated BLMVEC glycocalyx (n = 12) and pronase treated BLMVEC monolayers (n = 8) showed significant changes in effective stiffness ($p < 0.05$) when compared to the controls (n = 17); heparinase III treated BLMVEC glycocalyx (n = 7) was not statistically different from controls.

16.56 +/- 11.48 (HAase treated cells, n = 12; p = 0.02), 9.10 +/- 3.91 (HSIIIase treated cells, n = 7; p = 0.38), and 12.87 +/- 3.90 kT/nm^2 (pronase treated cells, n = 8; p = 0.02). At a significance level of $p < 0.05$, enzymatic digestion with hyaluronidase or pronase resulted in a significant increase of mean effective stiffness. The spread of measured stiffness values was large indicating heterogeneity of the BLMVEC glycocalyx and/or uneven enzyme action. Based on immunohistochemistry of HS and HA, the heterogeneous distribution of GAGs both before and after enzymatic degradation is the most likely explanation for the observed variations in effective stiffness [95].

Contributions of underlying cytoskeletal actin components are shown in Figure 3.6. Treatment with cytochalasin D increased ($p < 0.001$) BLMVEC monolayer effective stiffness to 33.12 +/- 20.8 kT/nm^2 (n = 23) from untreated effective stiffness of 15.27 +/- 9.18 kT/nm^2 (n = 22).

The effect of albumin concentration to the glycocalyx stiffness is shown in Figure 3.7. The bottom three images show representative RICM interference images of 17.3-μm diameter glass bead for 0.1%, 1.0%, and 4.0% BSA concentrations in MII. The increase of the innermost dark fringe size indicated that the addition of albumin swelled the glycocalyx by ~100 nm. The glycocalyx mean stiffness was significantly softer in MII with 0.1 and 4% BSA compared with results in MII + 1.0% BSA: 4.55 +/- 2.07 kT/nm^2 (0.1% BSA, n = 7), 13.72 +/- 11.07 kT/nm^2 (1% BSA, n = 9), and 2.83 +/- 1.20 kT/nm^2 (4.0% BSA, n = 10).

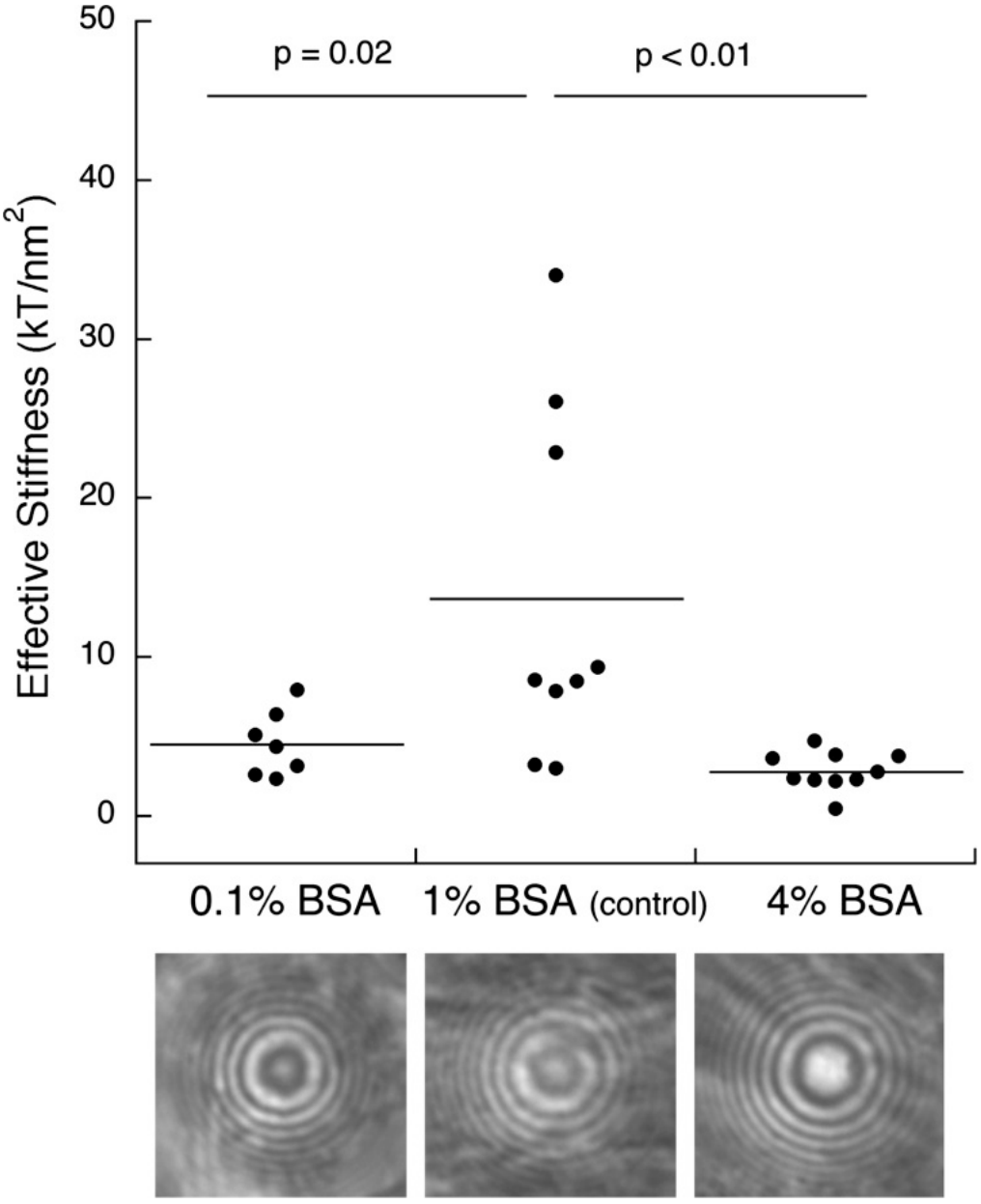

Figure 3.6 Effective stiffness of BLMVEC glycocalyx measured by RICM utilizing borosilicate glass probes (diameter ≈ 17.3 μm) in presence of 0.1%, 1%, and 4% BSA in the medium. Equilibrium glycocalyx stiffness was highest with 1% BSA ($p < 0.05$) when compared with 0.1 and 4% BSA samples. The representative RICM images (bottom) show that the glycocalyx thickness increases with the addition of BSA.

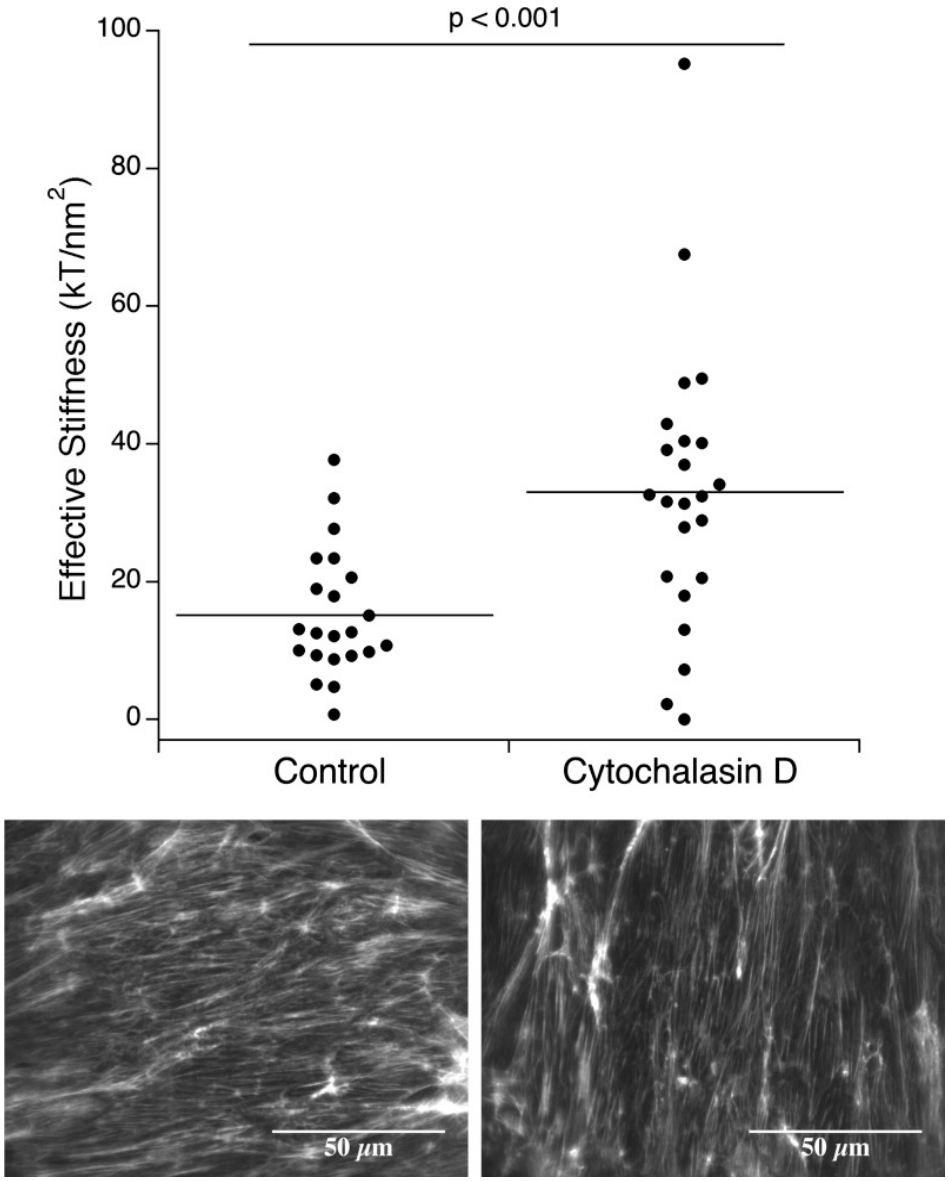

Figure 3.7 Effective stiffness of BLMEC glycocalyx measured by RICM utilizing borosilicate glass probes (diameter ≈ 17.3 μm) after actin disruption with 100 nM cytochalasin D treatment (30 minutes). Cytochalasin D treatment of confluent monolayers resulted in increased stiffness. The confocal images (bottom) show the staining of the actin cytoskeleton for control and 100 nM cytochalasin D treated monolayers.

3.5 Discussion

The study described here explored the feasibility of a novel application for the RICM technique and its potential to provide insight into the biomechanical property of the endothelial glycocalyx. As utilized here, RICM measured the fluctuations of the glass bead vertical position, h(t), at equilibrium where the gravitational pull on the bead and the viscoelastic response of the underlying cellular structures balanced each other. These vertical bead position changes occurred very fast; the instantaneous velocities of the bead are expected to follow the Maxwell-Boltzmann distribution. The positional changes were then translated into a potential energy profile, U(h), from which the estimation of the effective stiffness, U''(h), was made. The main premise for the interpretation of RICM results is illustrated in Figure 3.1; the bead probe pushes into the outermost layer of glycocalyx and indents it only a few nanometers at a light load depending on the bead size, density, and buoyancy. With very light loads at equilibrium, the RICM technique is complementary to AFM and can report on the outermost glycocalyx layer with nanometer indentation resolution. In RICM experiments each bead applies its load (weight minus the buoyancy) to the underlying structure: the loads were ~50 pN for the 17.3 μm diameter bead probe. The vertical position fluctuations were on the order of +/-1 nm (Figure 3.2) indicating that the expected stiffness will be on the order of 50 pN/nm, or 12 kT/nm2.

As illustrated by Figure 3.4, RICM captured the difference between the potential energy profiles for protein-covered glass and softer BLMVEC

monolayers. The width of potential energy profile is directly related to the magnitude of vertical position fluctuations (Figure 3.4A); these were greater on the BLMVEC seeded coverslip compared to the gelatin/fibronectin-coated coverslip. The limit of RICM technique thus lies in the measurements of stiffer systems where the CCD camera readout noise may be too large [132]. The majority of the potential energy profiles used to calculate the effective stiffness, U”(h), were symmetric and only a few cases of asymmetry in the probability function, p(h), were observed (Figure 3.2E). Prieve [133] described similar asymmetry while using total internal reflection microscopy to measure equilibrium potential energy profiles between spherical polystyrene probes and glass surface. Such asymmetry was accounted for by the probe being unattached to the underlying surface. Comparison analysis was performed on both halves of the energy profile curves showing slight asymmetry; differences were insignificant.

Comparison between controls and enzyme-treated BLMVECs showed that hyaluronidase and pronase treatments resulted in mean effective stiffness that was statistically different from control monolayers at a 95% confidence interval ($p < 0.05$); however, HSIIIase treatment did not significantly alter the stiffness (Figure 3.5). The finding that the enzymatic digestion of HA increased the glycocalyx stiffness could be interpreted that HA acted as a cushioning layer to distribute applied forces over glycocalyx structure. HA GAGs are long polymer chains that interpenetrate the glycocalyx and bind to CD44 and other glycocalyx components. This implies different roles for glycocalyx components in mechano-

transduction: receptor-anchored HA chains are designed to capture flow shear forces and transmit them to transmembrane syndecans decorated with HS GAGs. Based on that physical picture, the enzymatic removal of HS GAGs would have affected the glycocalyx stiffness to a lesser extent, which was indeed found (Figure 3.5). When HS linkages are disrupted, HA linkages may remain and therefore could maintain similar effective stiffness. At 10-fold higher loading forces (~1 nN), O'Callaghan et al. saw a decrease in BLMVEC elastic modulus upon heparinase treatment, which supports the proposed glycocalyx structure-function relationship [95].

Recently, Oberleithner et al. used a bead-AFM technique to measure glycocalyx stiffness of vascular endothelial cells [134]. Under similar loads, they found glycocalyx to be significantly softer than reported her. The discrepancy is most likely due to the viscoelasticity of glycocalyx and the differences in AFM and RICM loading rates. Oberleithner et al. [134] used slow loading rate with AFM tip velocity of 400 nm/s. Their AFM results, when corrected for the size of the spherical indenter and converted into elastic modulus, were in excellent agreement with our previously reported BLMVEC glycocalyx modulus, E ~0.3 kPa [95]. In contrast to the slow loading rate of AFM, the RICM bead fluctuates very fast; the rms velocity can be predicted by the energy equipartition theorem. These vertical fluctuations thus exert small but fast changing compressive forces to glycocalyx. Even when such velocities are corrected for the viscous drag of water [135], the RICM loading velocities are still faster by an order of magnitude than in typical AFM indentation experiments. Because of the viscoelastic

behavior of glycocalyx, such fast changing indentations will make the glycocalyx appear stiffer than what is measured under a slow indenting AFM tip. On the basis of the differences between AFM and RICM measured stiffness, we postulate that the endothelial glycocalyx, like many other cross-linked polymeric networks, undergoes stiffening at faster applied loads.

By indenting several hundred nanometers using AFM, we have showed significant softening of BLMVEC monolayers after treatment with 100 nM cytochalasin D [95]. RICM results, however, showed doubling of the effective stiffness of the outer several nanometers of BLMVEC glycocalyx (Figure 3.7) after 100 nM cytochalasin D treatment. It is plausible that cytochalasin D treatment collapses the glycocalyx and/or causes the cell to shed it; or the cell junction regions become much thinner thus causing RICM sampling of the stiffer underlying glass surface. The effects of cytochalasin D treatment on glycocalyx structure are unclear in the literature; however, support for junctional thinning is provided by the actin-stained images in Figure 3.7 (bottom) wherein actin distribution is less uniform. Complete glycocalyx degradation with pronase (Figure 3.5) showed that nonglycocalyx components were stiffer than the overlying glycocalyx, thus supporting the assignment of the RICM-measured stiffness to the glycocalyx layer. To determine membrane effects, membrane RICM intensity fluctuations were analyzed based on a linear contrast approximation described by Gönnenwein [132] and the results indicated that the membrane fluctuations and its stiffness (>> 10 kT/nm^2) do not significantly contribute to RICM measurement of glycocalyx stiffness.

Within the glycocalyx, syndecan core protein, HS, and HA have all been associated with shear stress transmission [18, 29, 40, 41, 127]. Transmembrane syndecans together with HS GAGs are of particular interest because they span the membrane and have the potential for direct interaction with intracellular components [29]. HA, unlike HS, is not attached to proteoglycans and is believed to bind directly to the cellular membrane through the CD44 receptor [26] and associate with other glycocalyx components [27, 28]. Previous study has shown that removal of HS or HA reduces the endothelial cell shear-induced response [104]. Thi et al. labeled HS proteoglycan with an anti-HS proteoglycan antibody and found relatively uniform staining with increased fluorescence at cell junctions [51]. Banerjee and Toole used HA protein in cultured pulmonary aortic endothelial cells and found that when cells were permeabilized there was greater fluorescence within the cytoplasm as well as perinuclear staining [136]. Confocal imaging of HS and HA distribution on BLMVECs showed that HA was more concentrated above the nuclear regions whereas HS was more concentrated at junctions [95]. In the present study the RICM technique was used to find how the effective stiffness changed when these two GAGs were digested with specific enzymes. One limitation of this approach was that the RICM data acquisition for dozen of bead probes took approximately ~1-h period during which the cells could have expressed additional GAGs.[5] The RICM measurements were made after the enzymes were removed from the medium. Another limitation was that the bead placements were random. Measurement locations were therefore

[5] The RICM measurements were made after the enzymes were removed from the cell medium.

carefully selected to the probe sites associated with the cell junction regions.

Although the RICM results suggest that the main role of HA is maintaining and cushioning the glycocalyx, it is also known that albumin in circulation associates with HA [14]. In the present study increasing albumin concentrations above BLMVEC monolayers to 4% did significantly soften the mean glycocalyx stiffness. This softening with additional albumin supports the implications of glycocalyx structure and the role of HA within the glycocalyx. Increased stiffness at 1% BSA indicates an ideal albumin concentration for glycocalyx structure and signal transmission capability. Progressive swelling of glycocalyx thickness has been observed upon BSA addition (Figure 3.6). It remains to be seen whether the combined action of adding albumin and removing HA and/or HS with specific enzymes will be able to further differentiate the role of these two glycocalyx GAGs.

3.6 Summary

Very light loads and small indentations by bead probes allowed the RICM technique to be used for the measurement of the effective stiffness of endothelial glycocalyx. The mean stiffness of BLMVEC glycocalyx in enzymatic studies was found to be ~7.5 kT/nm^2 (or ~31 pN/nm). Enzymatic digestion of HA and nonspecific glycocalyx digestion with pronase increased the mean effective stiffness of the glycocalyx; however, the effect of HS digestion was not significant. The results imply that HA chains act as a cushioning layer to distribute applied forces to the glycocalyx structure. Effective stiffness was also measured for the glycocalyx exposed to 0.1%, 1.0%, and 4.0% BSA. The RICM

images indicated that glycocalyx thickness and its compliance increases at higher BSA concentrations. Generally, these results demonstrate that RICM is sensitive enough to detect the subtle changes in glycocalyx stiffness attributable to removal of GAG components in a manner that is complementary to bead-AFM indentation technique.

CHAPTER 4

MECHANICAL EFFECTS OF MACROMOLECULE ADDITION ON THE COMPROMISED GLYCOCALYX

4.1 Introduction

Proper fluid balance across the lung endothelium is particularly important in the operating room where acute changes in patient heart rate, blood pressure, and fluid administration apply pathologic forces that can activate mechanotransduction pathways associated with inflammation and increased endothelial permeability, leading to increased extravascular lung water. Mechanical ventilation is often required to treat pulmonary edema; however, this supportive modality can be associated with further complications, including pneumonia and ventilator-induced lung injury (VILI). In the operating room, acute pathological forces on the lung endothelium, including increases in heart rate, blood pressure, and fluid administration, provide stimuli to activate inflammatory mechanotransduction pathways. VILI can exacerbate underlying acute lung injury (ALI) and acute respiratory distress syndrome (ARDS) described for trauma patients. Patients presenting with ALI ultimately have a 10% mortality rate [137] and a 50% mortality rate when presenting with the severe form of ALI, acute respiratory distress syndrome (ARDS) [138, 139]. In VILI and ALI/ARDS scenarios, a complex set of inflammatory mediators initiate cascading local and

systemic inflammatory responses, including increased capillary permeability and inflammatory cell migration into tissue and airspaces [137, 140]. Research aimed at preventing and/or ameliorating lung injury symptoms clinically includes controlled ventilation measures, appropriate volume replacement strategies, and glycocalyx maintenance [114] with the ultimate focus on regulating vascular permeability and inflammation.

Circulating volume maintenance is critical for hypervolemic patients. Both crystalloid and colloidal administration are commonly used to increase the circulating volume in hypovolemic patients, [137, 141]. The volume expanding and protective effects of colloids have been found to persist longer than crystalloid reperfusion [37, 137, 142, 143]. High molecular weight colloids are retained longer within the vascular space than crystalloids [144]; however, the efficacy of specific colloids widely varies [145]. For example, while both albumin, a natural protein, and neutral hydroxyethyl starch (HES), a synthetic colloid, lead to less fluid extravasation, only albumin was found to clinically prevent extravasation after ischemia [142, 146]. HES pretreatment has also been found to attenuate microvascular perfusion failure [147]. These results may be explained by passive and/or active interactions with the glycocalyx. Current hypotheses suggest that while negatively charged albumin can support the glycocalyx and its functions [13], neutrally charged HES is not expected to support glycocalyx-mediated permeability [148]. Over the last two decades, the capillary glycocalyx has been implicated in mediating inflammation and vascular permeability is currently affecting the way that fluid resuscitation is administered

[141].

The glycocalyx is a mesh of proteoglycans and glycosaminoglycan covering the luminal surface of blood vessels and the microvasculature. This gel-like coating has been found to act as a macromolecular filter [149] and to function in both chemical and physical signal transduction [40, 41, 149]. Experimental evidence suggests that the heparan sulfate in glycocalyx is integral to pressure induced increases in hydraulic conductivity [18]. Similar increases in hydraulic conductivity have been shown for shear forces applied to glycocalyx in regard to both heparan sulfate and hyaluronan [41]. The importance of macromolecules to glycocalyx function has also been established; albumin is integral to endothelial health and function [89] and has been shown to interact and accumulate within the glycocalyx [14]. Macromolecule addition has previously been thought to act by plugging the intercellular capillary junction, but there is evidence to suggest that macromolecules might also interact with the glycocalyx [90-93]. While albumin interactions with the glycocalyx has been investigated, much less known about the effect of hydroxyethyl starch on the endothelial glycocalyx and on the overall microvascular tissue compliance [94].

Our lab has established two complementary techniques to probe the micromechanics of the endothelial glycocalyx: reflectance interference contrast microscopy (RICM) and atomic force microscopy (AFM). Both RICM and AFM utilized the same size glass sphere as a probe to deliver small loading forces to the glycocalyx. The resulting indentations were used to find elastic modulus (AFM) or effective stiffness of the underlying molecular glycocalyx structures

(RICM). Because both albumin and HES have been used to decrease fluid extravasation in lungs, we investigated how their presence of the lung endothelial glycocalyx affected mechanics. To further differentiate their interactions with the glycocalyx components, glycocalyx was subjected to enzymatic degradation using hyaluronidase.

4.2 Methods

4.2.1 Cell Culture

Bovine lung microvascular endothelial cells (BLMVEC; VEC Technologies; passage 5-13) were subcultured (1.25 x 10^5 cells/cm^2) and grown to confluence on ethanol dried, autoclaved 25 mm round, glass coverslips pretreated with 0.4% gelatin (Sigma-Aldrich) and 100 μg/cm^2 fibronectin (Sigma-Aldrich) each for 1 hour. Growth media was MCDB-131 Complete Medium (VEC Technologies) or a 50/50 mixture of this media and MCDB 131 Medium (Sigma, M8537) supplemented with penicillin/streptomycin, 10% FBS, and 15 mM sodium bicarbonate at pH 7.4. BLMVEC monolayers were maintained at 37 °C and 5% CO_2 until use on days 7-12 in RICM and AFM experiments. [116]

4.2.2 Enzymatic Treatment

Monolayers were incubated with 50 U/mL hyaluronidase (EC 4.2.2.1; hyaluronidase from Streptomyces hyaluroliticus, Sigma) for 1 hour prior to experiments in MCDB-131 supplemented with 1% BSA and 25 mM HEPES at pH 7.4. Incubation was done at 37 °C and 5% CO_2.

4.2.3 Macromolecule Treatment

Prior to experiments, monolayers were briefly rinsed with in unsupplemented MIII (1/3 mixture of MCDB-131 supplemented with 25 mM HEPES at pH 7.4) and Ringer's Lactate (pH 7.4). Stiffness measurements were performed in MIII supplemented with 0.1%, 1%, or 4% weight volume of either Fraction V bovine serum albumin (Proliant Biologicals; MW = 66.5 kDa) or an artificial, high molecular weight hetastarch (HES) routinely used as a plasma expansion (HEXTEND; Wt Avg MW = 450-800 kDa, 0.75 degree of substitution) (see Figure 4.1).

4.2.4 Reflectance Interference Contrast Microscopy (RICM)

Effective stiffness of the glycocalyx was measured using RICM as previously described [116]. Briefly, RICM is an interferometric technique that measures the fluctuations in the vertical position of glass spheres placed on a confluent monolayer of BLMVECs. The glass sphere (~17.3 μm diameter) served

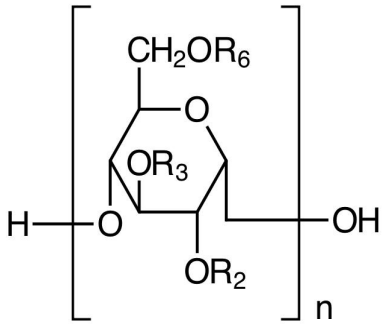

Figure 4.1 Structure of HEXTEND. This synthetic hetastarch is provided as a 6% colloidal solution in lactated electrolyte injection.

as a force probe that exerts very small loads fluctuating around ~50 pN and indents the glycocalyx only several nanometers. The sphere-cell equilibrium is modeled as a particle at a potential energy minimum where gravitational and restoring elastic forces balance each other [88].

The vertical position fluctuations are known to follow the Boltzmann law [88, 116], so that the profile of the potential energy, U, around the minimum can be calculated as a function of the vertical position, h. The second derivative of U(h) thus provides a measure of effective stiffness for sphere-cell interactions. Such effective stiffness is assigned to the underlying glycocalyx because loading forces were small and the bead was rigid compared with the underlying structure. Sphere locations have been selected to represent cell-cell junction positions. RICM is estimated to have a spatial resolution of approximately 300 nm [85] and a sub-nanometer vertical resolution [116].

4.2.5 Atomic Force Microscopy (AFM)

The spherical tip AFM experiments used to measure the elastic modulus of BLMVECs have been previously described [95]. Briefly, an AFM cantilever tip was modified with a borosilicate glass sphere with a diameter of ~18 μm, which was then used to indent into BLMVEC monolayers. An increasing loading force, from 0 to 5-10 nN, was applied at a rate of 10 μm/s. Indentation locations were assigned based on the topography map obtained at the end of the indentation experiments cell-cell junctions or cell-nuclei locations. The AFM indentation data was analyzed point-wise to obtain the elastic modulus, E, as a function of the indentation depth, δ. The resulting E(δ) curves were analyzed using a two-layer

composite compliance model to obtain the mean elastic moduli of the glycocalyx and the underlying cellular structures [95, 106]. Specifically,

$$\frac{1}{E(\delta)} = \frac{1}{E_{glycocalyx}}(e^{-\frac{\alpha\delta}{\delta_g}}) + \frac{1}{E_{cell}}(1 - e^{-\frac{\alpha\delta}{\delta_g}}) \quad 4.1$$

which includes the mean elastic moduli of the glycocalyx and the cell ($E_{glycocalyx}$ and E_{cell}, respectively), mechanical interlayer interactions (the parameter α), and glycocalyx-specific indentation (δ_g). For such analysis to be conclusive, the E(δ) curves should display a sigmoidal shape. In the absence of such shape, the glycocalyx modulus was estimated from a point-wise modulus at 100 nm indentation depth, E_{100}.

4.2.6 Statistical Analyses

Statistical analysis of BLMVEC effective stiffnesses and elastic moduli were performed using a Wilcoxon-Mann-Whitney Rank sum test. Differences were considered significant at a 95% confidence interval ($p < 0.05$).

4.3 Results

The effects of macromolecule administration to BLMVEC monolayer biomechanics before or after glycocalyx degradation were investigated utilizing two complementary techniques: AFM and RICM. AFM measures the indentation forces as a function of depth into the glycocalyx/cell structure; RICM measures the equilibrium forces associated with the outer several nanometers the glycocalyx/cell structure. The physiologically relevant macromolecule BSA and

the clinically relevant macromolecule HES were selected for analysis.

For moduli measurements, junctional locations were assigned based on the associated AFM topography scan, which was acquired after initial AFM location selection and measurements. Macromolecule addition increased compliance with increasing indentation depth for monolayer samples not enzymatically compromised. For HAase compromised monolayers, BSA addition decreased compliance and HES addition slightly increased compliance. Sample size was between 19 and 40: 0.1% BSA, n = 40; 1% BSA, n = 40; and 4% BSA, n = 35; 0% HES, n = 33; 1% HES, n = 20; and 4% HES, n = 19. Figure 4.2 shows average elastic moduli measurements as a function of indentation depth at BLMVEC monolayer cell junctions MIII supplemented with 1% (■) BSA and 1% (●) HES. The vertical bars represent the standard error of the mean. 1% BSA addition resulted in the lowest compliance as well as larger changes in moduli with depth at junctions. 1% BSA and 1% HES suggested a multilayer compliance model and were fit to a double-layer model [95]. Fitting parameters are shown in the table in Figure 4.2. Elastic moduli for the deeper cell layer were between 0.9 and 2.5 kPa. Elastic moduli for the glycocalyx layer was 0.12 and 0.8 kPa for 1% BSA and 1% HES samples, respectively. Differences between the control group indentation profiles and the respective BSA and HES samples are shown in Figure 4.3 and Figure 4.4. Figure 4.3A and Figure 4.3B show comparisons for BSA and HES titrations, respectively; Figure 4.4A and Figure 4.4B show comparisons for BSA and HES, respectively, addition after HAase pretreatment.

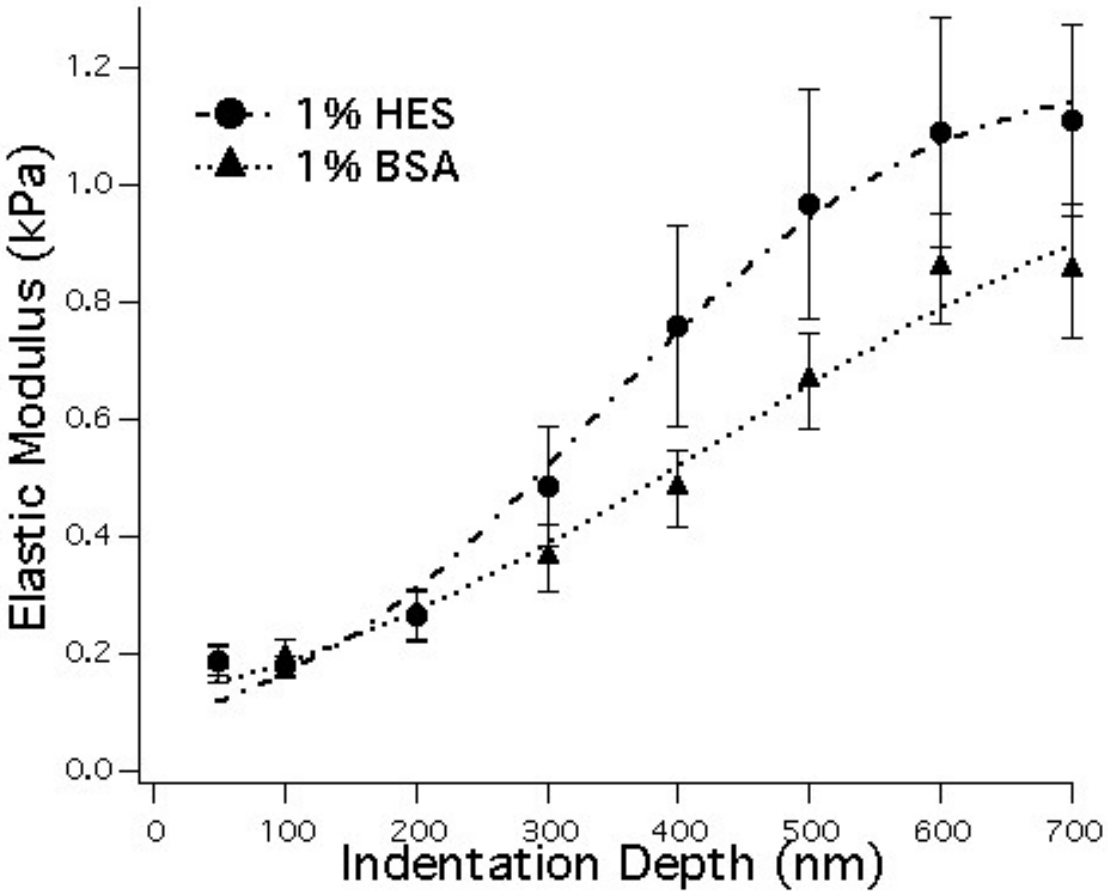

Parameter	1% HES	1% BSA
Eglycocalyx (kPa)	0.08 ± 0.02	0.12 ± 0.03
Ecell (kPa)	1.21 ± 0.07	1.15 ± 0.23
α	2.46	2.59
Glycocalyx Thickness (nm)	317.21	531.39
chi-square	0.0106	0.0097

Figure 4.2 Average elastic moduli at cell junctions of BLMVEC monolayers as a function of indentation depth for samples with 1% HES (●, n = 20) and 1% BSA (▲, n = 40) supplementation. The vertical bars represent the standard error of the mean. Data were fit to a double-layer model; parameters are shown in the table below.

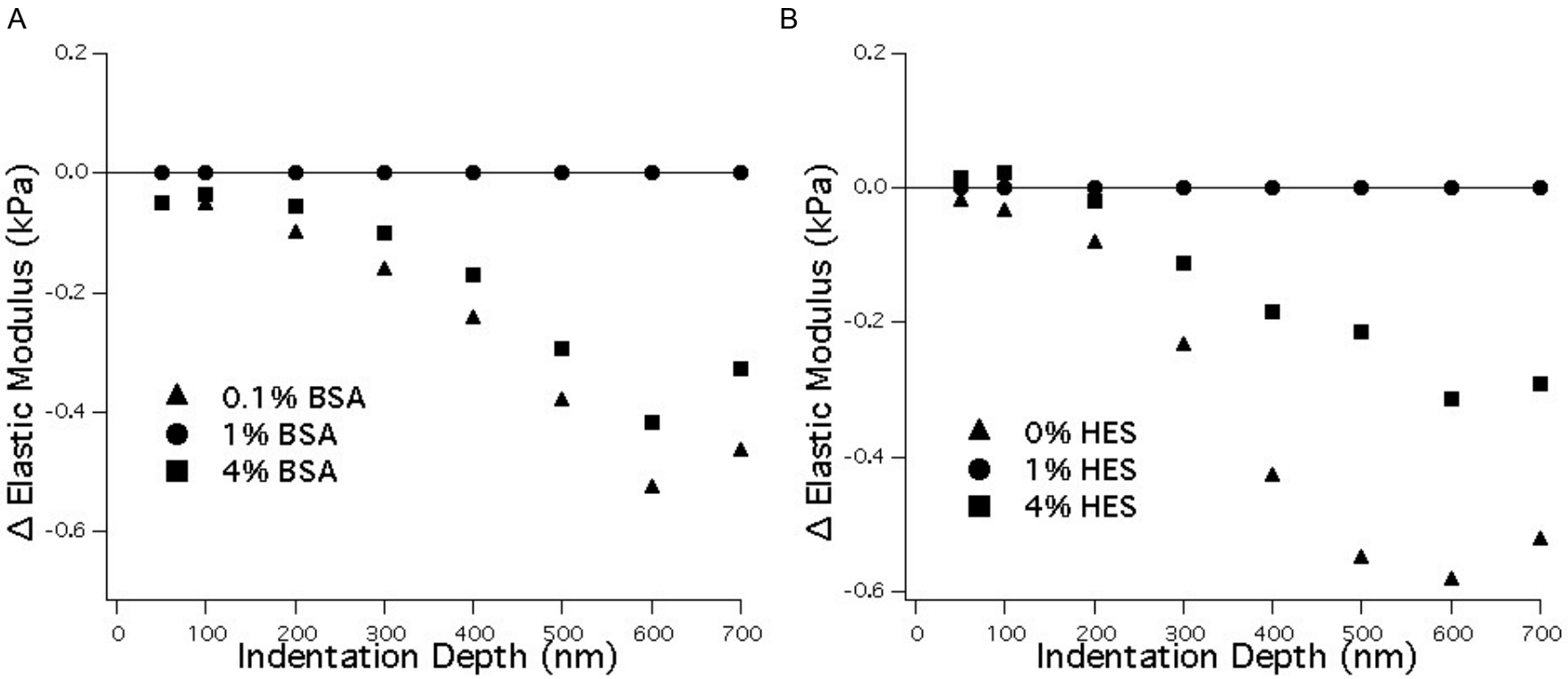

Figure 4.3 Change in mean BLMVEC elastic moduli shown as a function of indentation depth. Sample E(δ) data were compared to the respective 1% experiment controls. BSA supplementation is indicated in panel A (BSA 0.1% (■), 1% (●), and 4% (▲)); HES supplementation is indicated in panel B (HES, 0% (■), 1% (●), and 4% (▲)).

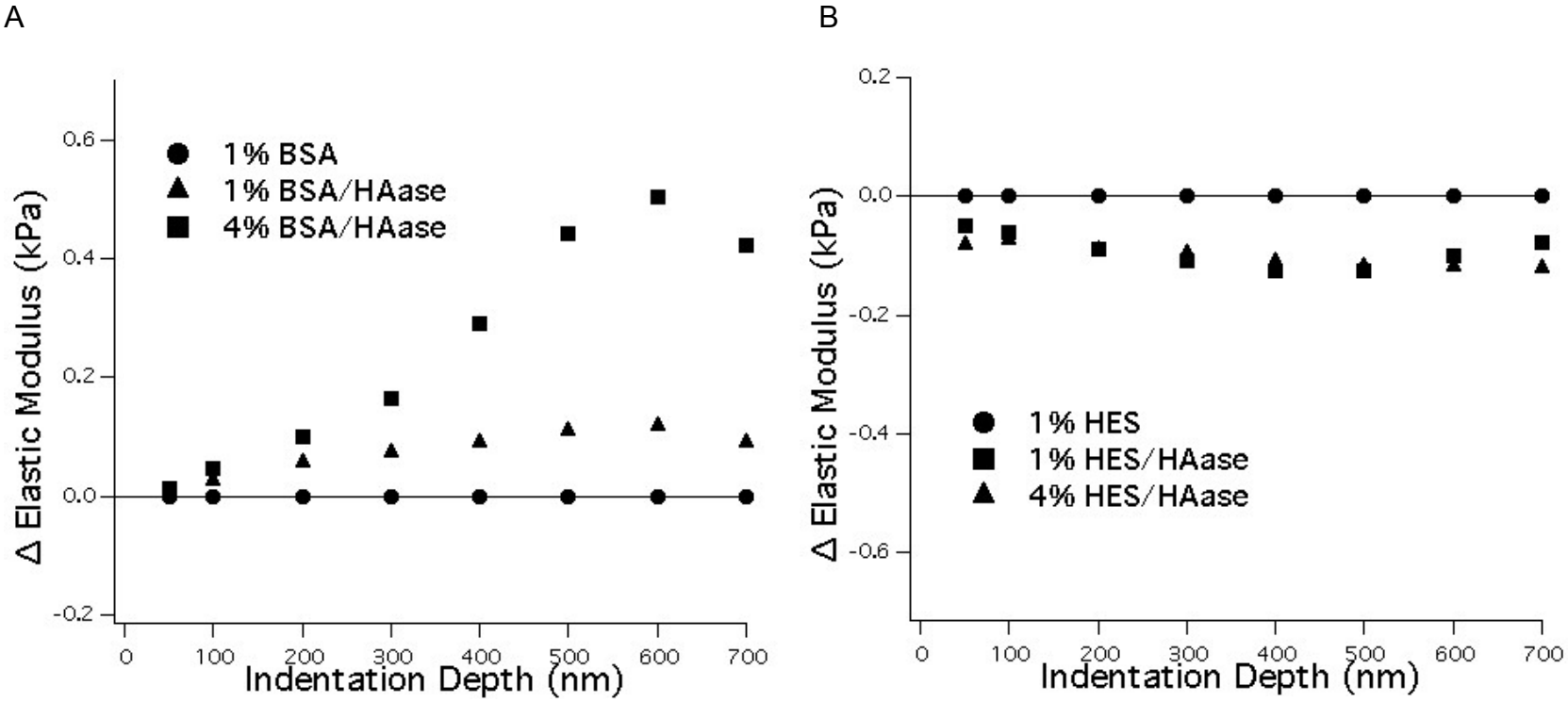

Figure 4.4 Change in mean elastic moduli after enzymatic digestion of glycocalyx hyaluronan (using 50 U/mL hyaluronidase) shown as a function of indentation depth obtained by subtracting the respective the E(δ) data from 1% experiment controls. A: BSA, 1% control (●, n = 51), 1% after HAase (▲, n = 47) 4% after HAase (■, n = 46); B: HES, 1% control (●, n = 41), 1% after HAase (▲, n = 42), 4% after HAase (■, n = 40).

Double-layer fitting was not feasible for all samples since not all samples showed discernible, multilayer compliance. Therefore, the elastic moduli at junctions at the relatively shallow indentation depth of 100 nm (E_{100}) were compared in subsequent figures. Figure 4.5, Figure 4.6, Figure 4.7, and Figure 4.8 show average elastic modulus at an indentation depth of 100 nm (E_{100}) and effective stiffness of BLMVEC monolayers as a function of macromolecule addition and enzymatic treatment. Figure 4.5 and Figure 4.6 show results of BSA or HES addition, respectively. Figure 4.7 and Figure 4.8 show results of BSA or HES addition after pretreatment with 50 U/mL hylaluronidase, respectively.

Figure 4.5A shows E_{100} results for BSA addition (0.1% (■), 1% (●), or 4% (▲) BSA). Statistical differences were found between 1% BSA and both 0.1% BSA ($p < 0.01$) and 4% BSA groups ($p < 0.02$; Wilcoxon-Mann-Whitney) (see Figure 4.5A). Statistical outliers were thrown out prior to statistical analysis. Effective stiffnesses as measured by RICM are shown in Figure 4.5B (average ± standard error): 0.1% BSA, 12.9 kT/nm^2 ± 2.1, n = 14; 1% BSA, 10.2 kT/nm^2 ± 1.2, n = 35; and 4% BSA, 3.4 kT/nm^2 ± 0.6, n = 24. Statistical differences were found between 4% BSA and both 0.1% BSA ($p < 0.001$) and 1% BSA groups ($p < 0.001$; Wilcoxon-Mann-Whitney) with the greatest compliance shown for 4% BSA.

Figure 4.6A shows E_{100} results for HES titration (0.1% (■), 1% (●) or 4% (▲) HES). Differences were significant between the no added macromolecule and 1% HES groups at junctions ($p < 0.001$). E_{100} peaked at reconstitution with 1% HES. Correlating fluctuation analysis of RICM images showed similar

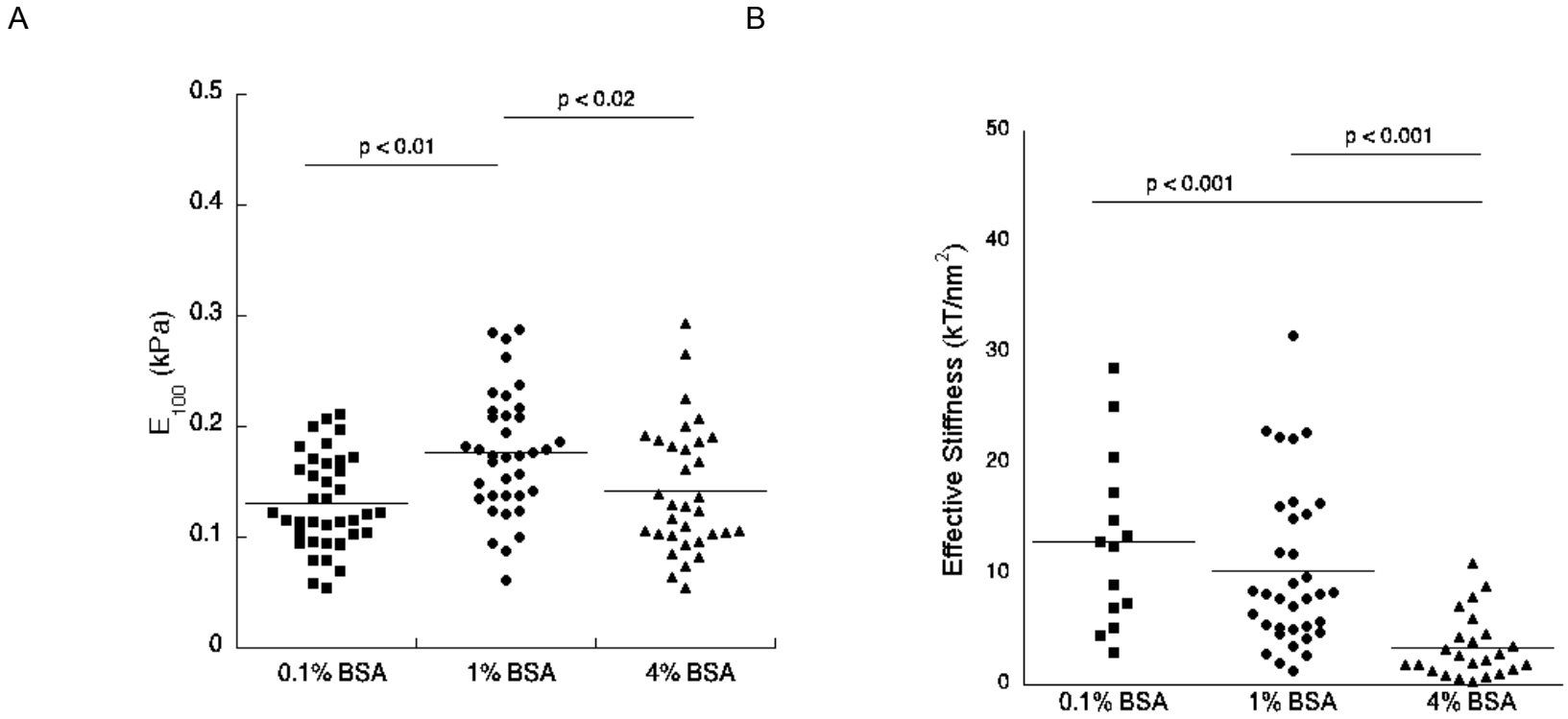

Figure 4.5 Elastic moduli at 100 nm indentation depth (panel A; AFM) and equilibrium constants of the outermost layer (panel B; RICM) for BSA supplemented monolayers. Samples were acquired in media III and labeled according to supplements concentration: 0.1% (■), 1% (●), or 4% (▲) BSA. BSA titration samples 0.1% and 4% BSA showed a significant decrease in E_{100} compared to the 1% BSA sample ($p < 0.01$ and $p < 0.02$, respectively; panel A). Titration with 0.1% or 1% BSA resulted in stiffer effective stiffness measurements ($p < 0.001$ for both comparisons; panel B).

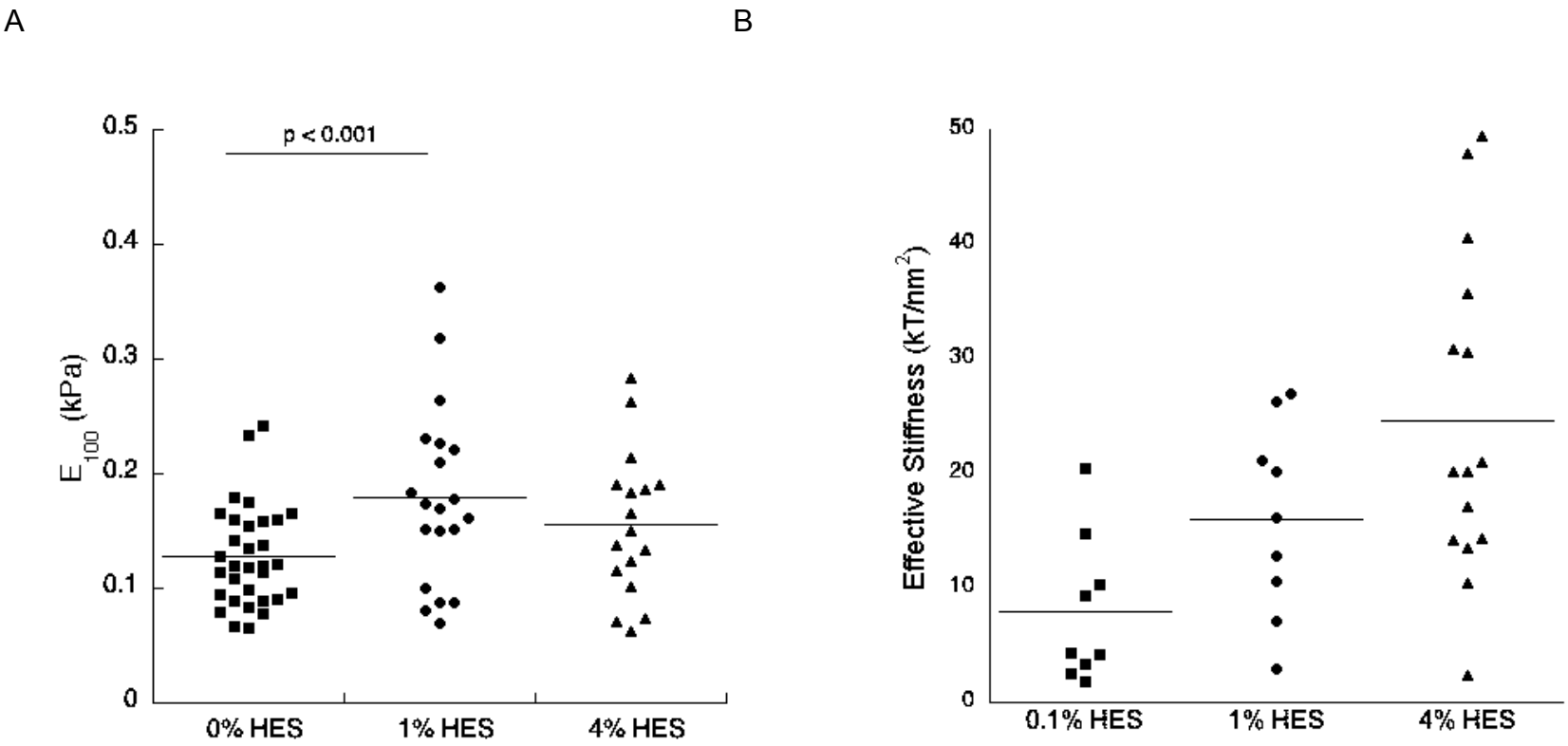

Figure 4.6 Elastic moduli at 100 nm indentation depth (panel A; AFM) and equilibrium constants of the outermost layer (panel B; RICM) for HES supplemented monolayers. Samples were acquired in media III and labeled according to supplement concentration: 0% (■), 1% (●), or 4% (▲) HES. HES titration samples showed a decrease in modulus when all macromolecules were removed (0% HES vs. 1% HES; $p < 0001$; panel A) and a general increase in effective stiffness that was not significant (panel B).

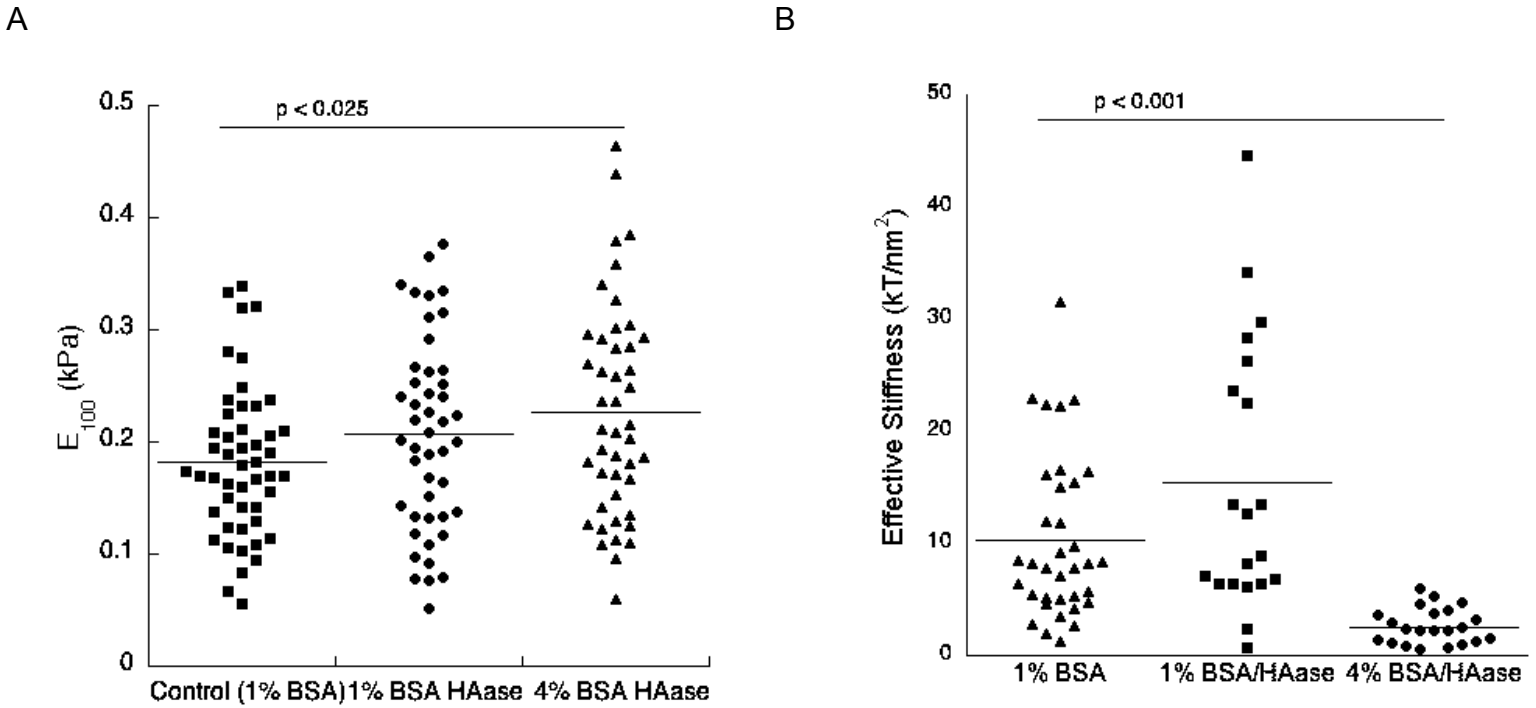

Figure 4.7 Elastic moduli at 100 nm indentation depth (panel A; AFM) and equilibrium constants of the outermost layer (panel B; RICM) for enzymatically degraded, BSA supplemented monolayers. BLMVEC monolayers were pretreated with MII supplemented with 50 U/mL hyaluronidase in MIII; controls (■) were pretreated with unsupplemented MII. Measurements were acquired in media supplemented with 1% or 4% BSA and labeled as 1% BSA/HAase (●) and 4% BSA/HAase (▲), respectively. Supplementation with 4% BSA significantly decreased compliance ($p < 0.025$; panel A) and effective stiffness when compared with the respective 1% BSA controls ($p < 0.001$ panel B).

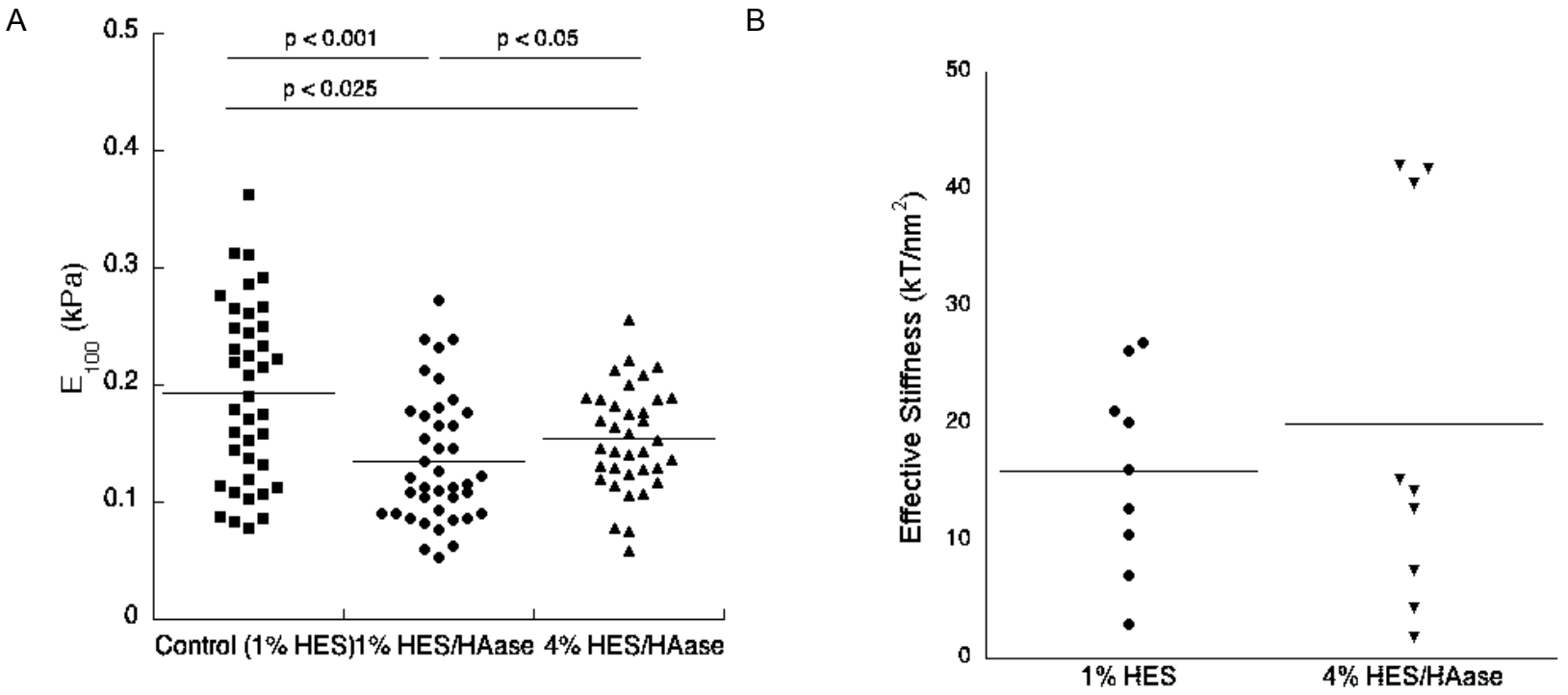

Figure 4.8 Elastic moduli at 100 nm indentation depth (panel A; AFM) and equilibrium constants of the outermost layer (panel B; RICM) for enzymatically degraded, HES supplemented monolayers. BLMVEC monolayers were pretreated with MII supplemented with 50 U/mL hyaluronidase; controls were pretreated with unsupplemented MII. Measurements were acquired in MIII supplemented with 1% or 4% HES, labeled 1% HES/HAase (●) and 4% HES/HAase (▲), respectively. Groups were compared to untreated monolayers measured in 1% HES (■). Enzymatic removal significantly decreased the elastic modulus of HES supplemented monolayers; however, monolayers supplemented with 4% HES were significantly stiffer than monolayers supplemented with 1% HES after enzymatic removal. Significant differences are shown when $p < 0.05$.

effective stiffness of monololayers supplemented with 1% HES (Figure 4.6B) or 1% BSA (Figure 4.5B). While there was a general increase in stiffness observed, these differences were not statistically significant (0.1% HES, 7.9 kT/nm^2 ± 2.1, n = 9; 1% HES, 16.0 kT/nm^2 ± 2.8, n = 9; and 4% HES, 24.5 kT/nm^2 ± 3.6, n = 15).

Figure 4.7A shows E_{100} results for BSA titration after HAase treatment. Measurements were taken in MIII + 1% or 4% BSA and labeled as 1% BSA/HAase (●) and 4% BSA/HAase (▲), respectively; the control (1% BSA, ■) was not treated with HAase. Reconstitution with 4% BSA after HAase treatment significantly increased E_{100} at junctions (1% BSA; $p = 0.025$; Figure 4.7A) and decreased stiffness (Figure 4.7B) compared to control (1% BSA; $p < 0.001$): 1% BSA/HAase, 0.21 kPa ± 0.01, n = 46; 4% BSA/HAase, 0.23 kPa ± 0.01, n = 45; and 1% BSA, 0.18 kPa ± 0.01, n = 49. Effective stiffnesses as measured by RICM (borosilicate glass probe; diameter ~17.3 μm) are shown for BSA in Figure 4.7B: 10.2 kT/nm^2 ± 1.2 (1% BSA, n = 35), 15.4 kT/nm^2 ± 2.7, (1% BSA/HAase, n = 20), and 2.5 kT/nm^2 ± 0.3 (4% BSA/HAase, n = 22).

Figure 4.8 shows the E_{100} and effective stiffness of monolayers with HES supplemented media after pretreatment with HAase. HES groups were labeled 1% HES/HAase (●) and 4% HES/HAase (▼), respectively. Comparison was against untreated monolayers measured in 1% HES (■). The average elastic modulus at an indentation depth of 100 nm is shown in Figure 4.8A (1% HES, 0.19 kPa ± 0.01, n = 39; 1% HES/HAase, 0.14 kPa ± 0.01, n = 40; and 4% HES/HAase, 0.15 kPa ± 0.01, n = 36). Differences were significant between all groups at junctions (1% HES vs. 1% HES/HAase: $p < 0.001$; 1% HES vs. 4%

HES/HAase: $p < 0.05$; and 1% HES/HAase vs. 4% HES/HAase: $p < 0.025$). Effective stiffness as measured by RICM (borosilicate glass probe; diameter ~17.3 μm) are shown for HES addition in Figure 4.8B: 16.0 kT/nm^2 ± 0.3 (1% HES, n = 9) and 20.0 kT/nm^2 ± 5.6 (4% HES/HAase, n = 9). The 1% HES after HAase pretreatment group did not yield a confluent monolayer and therefore is not included in effective stiffness data.

4.4 Discussion

The endothelial glycocalyx has been implicated in barrier function by acting as a primary molecular sieve for plasma proteins and mechanical sensor/transducer. While it is recognized that albumin interacts [14, 37] with glycocalyx, little focus has been given to the glycocalyx interactions of HES beyond Jacob et al. [48] who found that HES 450 was able to induce change in shear stress in the vasculature. Previous explanations of mechanotransduction have focused on the functions of glycosaminoglycan and syndecan components of the glycocalyx while excluding the interactions of albumin, other proteins, and large macromolecules such as HES. These interactions have the potential to alter glycocalyx thickness and glycocalyx overall structure. Herein we utilize two original techniques to evaluate glycocalyx structure as a function of macromolecule concentration.

Our group previously established two complementary techniques to evaluate the soft-layer mechanics of the glycocalyx [95, 116], RICM and AFM, utilizing a 20 μm probe. Reconstitution of glycocalyx functions may be possible with albumin or HES and, therefore, these two techniques were used to measure

the mechanical effects of albumin and HES in conjunction with HA removal. These techniques have been described in detail elsewhere [95, 116]. In the BLMVEC monolayer setup, AFM measures mechanics with progressive indentation in the outer 700 nm region and RICM measures equilibrium mechanics at shallow, very fast indentation rates. These differences in indentation method result in equilibrium measurements that are ~50x larger than elastic modulus measurements at indentation depths of 100 nm.

Previous AFM loading studies of the glycocalyx/endothelial surface have shown that the outer endothelial components/layer(s) are more compliant than deeper intracellular layers and components. Specifically, degradation of actin with Cytochalasin D removed indentation dependent changes in modulus, which were independent of glycocalyx integrity. Based on these results and E(d) profiles, elastic modulus results were compared at 100 nm where stiffness was relatively flat. E_{100} for BLMVEC monolayers increased after glycocalyx degradation with either HAase or 15 mU/mL heparinase III; however, only HAase resulted in increased effective stiffness. This observation suggests that changes in glycocalyx composition can affect glycocalyx ability to transmit signals to stiffer intracellular layers by dampening physical signals.

Two of the most commonly used colloids, 5% albumin and 6% hydroxyethyl starch (HES), were selected for supplementation. Albumin has been studied in the clinical environment, but there have been relatively few studies to explain the interactions with the glycocalyx beyond transient oncotic effects [18, 35, 36, 89, 150]. Reduced albumin has been shown to increase hydraulic

conductivity and 4% albumin has been shown to decrease hydraulic conductivity [36, 89]. Furthermore, albumin has been shown to associate with HA [14] and is clinically relevant as a volume expander. HES has also been shown to be an effective volume expander and to minimize endothelial activation and prevent neutrophil adhesion [151]. It is postulated that there may be a physical interaction with the glycocalyx that leads to changes in signaling capabilities; albumin and HES intercalation with the glycocalyx could act to stiffen or cushion the mechanosensing components of the glycocalyx.

Figure 4.2 compares E(d) of BLMVEC monolayers in the presence of 1% HES and 1% BSA. Both curves are fit to the double-layer model described in the Materials and Methods. Fitting parameters suggest that 1% BSA results in a stiffer and significantly thicker glycocalyx. These results support previously accepted findings that albumin is integral to glycocalyx structure. As shown in both Figure 4.3A and Figure 4.5A, BSA titration resulted in the greatest monolayer stiffness at a BSA concentration of 1%. In Figure 4.5B, RICM results suggest a decrease in stiffness at 4% BSA. In our previous study [116], reduced albumin (0.1% BSA) also resulted in decreased stiffness. While this specific difference may be dependent on glycocalyx-BSA interactions, it is more likely that these results are due to increased sample size in the current experiments.

The BSA titration results may be explained several ways. BSA can bind both hyaluronan and water. Reduced albumin may collapse the glycocalyx while increased albumin may hydrate and swell the glycocalyx. At faster loading rates, the collapsed glycocalyx could be less dependent on hysteretic effects. After

pretreatment with hyaluronidase (Figure 4.7A), addition of 4% BSA had the opposite effect and increased elastic modulus at 100 nm indentation. This increase may be explained by hyaluronidase treatment, which does not completely degrade the glycocalyx. BSA could still bind with remaining hyaluronan; however, the necessary support structure is not available to increase glycocalyx thickness.

Increasing the amount of HES was not as significant as increasing the amount of BSA to apparent moduli at 100 nm (Figure 4.6A vs. Figure 4.5A) and effective stiffness (Figure 4.6B vs. Figure 4.5B). With increasing depth, however, 1% HES resulted in greater stiffness than with unsupplemented or 4% HES (Figure 4.3B). Double-layer model fitting parameters suggest an increase in estimated glycocalyx thickness of ~75 nm at 4% HES compared with 1% HES. While this parameter has a large standard deviation associated with the fitting, an increase in thickness was corroborated visually in RICM experiments with a decrease in the observed fringe profile pattern when supplementation was increased from 1% to 4% HES.

An intact glycocalyx also resulted in greater changes in HES elastic modulus at indentation depths of >200 nm (Figure 4.3B vs 4.4B). When the glycocalyx was compromised by HAase treatment, these differences were ameliorated and moduli decreased for all indentation depths in HES groups, but not significantly for 1% BSA groups (Figure 4.4B). E_{100} of the compromised glycocalyx shows the opposite effect. The greatest change in groups was seen after the compromised glycocalyx was supplemented with HES (Figure 4.8A). In

the intact glycocalyx, addition of HES E_{100} measurements showed a stiffer glycocalyx (Figure 4.6A), whereas in the compromised glycocalyx, HES addition significantly softened the glycocalyx. Hyaluronidase does not completely degrade the glycocalyx [95, 116], suggesting that the glycocalyx can be reconstituted with BSA and HES interactions may be compromised when the glycocalyx is not intact. Whereas there was a general increase in effective stiffness, differences were not significant. HES effective stiffness measurements are complicated by media viscosity differences: water (1 cP), HES (6%, 4 cP), and blood (~4.2 cP) [152]. As the HES concentration was increased, viscosity likely approaches that of the glycocalyx.

The clinical effects of resuscitative fluids on barrier function are not completely understood. While evidence suggests that HES has both anti-inflammatory effects and can alleviate ALI/ARDS after hemorrhagic shock [137, 153-156], the mechanism responsible for these effects is not entirely understood. Colloid-related oncotic effects have been noted in clinical setting [157] and need to be addressed in regards to the experimental setup. Tissue directed fluid flow is counteracted by oncotic pressure component for both natural protein and synthetic starches; however, this fluid redirection is most effective in the short-term [91]. Observations may be due to the change in media; however, both lactate ringers and MCDB-131 are formulated to be physiologic. HEXTEND [151] and all other media was in balanced solutions. This balance was confirmed mathematically from the respective formulation sheets. Oncotic pressure differences are greatest at initial exposure to macromolecules and are

subsequently modified by hydraulic conductivity as well as molecule movement. Over time, filtering of macromolecules by the glycocalyx alters this balance. Additionally, the glycocalyx is an imperfect barrier and will allow macromolecules of all sizes to cross. Thus, any barrier damage increases extravasation. This has been observed with both albumin [89] and HES [158-161]. Zahn et al., [162] modeled fluid and albumin flux across the glycocalyx based on a quasiperiodic fiber array structure [163]. While albumin is transferred into the endothelium, albumin concentration directly underneath the glycocalyx is maintained effectively at 0, thus maintaining oncotic pressure. At high albumin (50 mg/ml) concentration, isotonic conditions, equal extracellular/intracellular albumin concentrations, and minimal hydrostatic pressure (1 cmH2O), both albumin and fluid flux are predicted to approach minimal levels (1.2 mg/ml nm/s and 0.284 nm/s, respectively). When intracellular albumin concentration is dropped to 20 mg/ml, the model predicts albumin flux of -18.30 mg/ml nm/s and hydraulic conductivity of -8.56 nm/s, suggesting an outward flux of protein and fluid. Weinbaum et al. have shown that albumin concentrations equilibrate quickly across the endothelium and that colloidal pressure is zero across the microvascular in vivo [93, 164]. Glycocalyx degradation further speeds up this process. AFM and RICM experiments are on the order of 1 to 2 hours and therefore are likely to occur after colloidal and hydraulic pressure equilibration. Additionally, hydraulic pressure is zero further minimizing hydraulic and osmotic conductivity and suggests that swelling or crenation of the endothelial is minimal. Mechanical changes can therefore be assigned to the glycocalyx. Enzymatic

treatment eliminated or attenuated macromolecule-associated changes in compliance over the nuclei. If swelling or crenation occurred, these differences would be visualized. Even if there was significant endothelial cell crenation and swelling, measurements are unlikely to be effected in the intact glycocalyx. RICM and the outer measurements of AFM should not be significantly affected. With increasing extracellular molecules, endothelial cells are expected to become crenulated, which would stiffen measurements; the opposite was observed. Furthermore, whereas 4% HES is similar to 1% BSA in particle number per volume, AFM indentation depth profiles are different.

Clinical understanding of natural protein and synthetic starch as resuscitative fluids has been compromised by the recent removal of seminal papers by Boldt. This expulsion creates an appropriate time to reevaluate the breadth of research, as a significant portion of knowledge must be reestablished. An aspect that has been overlooked in the past is the role of colloidal interactions with the microvasculature at a basic level. The glycocalyx is described as a protective layer and has been implicated in macromolecule filtration and signal transduction controlling hydraulic permeability. While evidence suggests that albumin interacts and affects the glycocalyx, there is little known about the starch interactions. An understanding of the mechanics of the glycocalyx in association with these components may provide highly controlled models for further physiologic studies.

The results presented herein are the first mechanical measurements of the microvascular endothelium as a function of macromolecule concentration and

provide a new methodology to examine some of the available clinical observations with albumin and HES macromolecule formulations. Specifically, results indicated that both albumin and HES interact with and influence glycocalyx mechanics (see Figure 4.9). Here we used HEXTEND (670 kDa) because it was the most readily available; however, HES molecular weights and structures are also relevant in the discussion of clinical effectiveness. Recently, both an 130/0.4 HES mix [165] and an HES pentastarch [143] have been central in this broad discussion, and are therefore are viable next targets for evaluation.

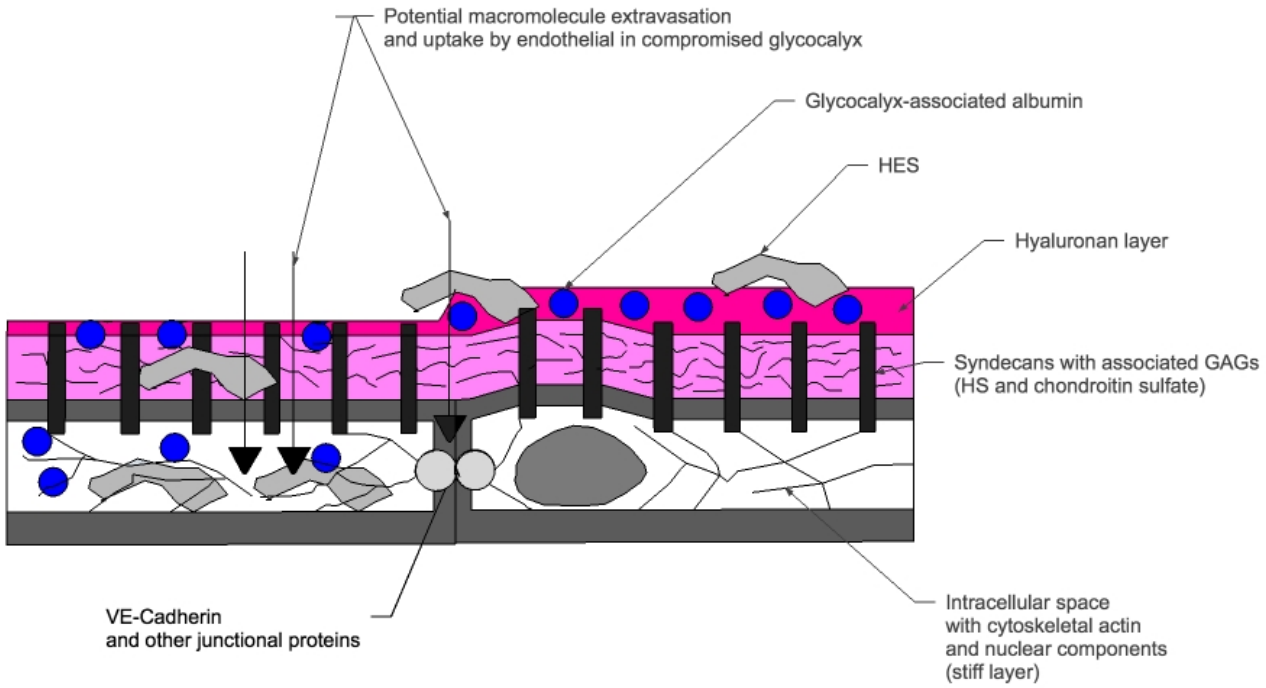

Figure 4.9 Endothelial glycocalyx model showing postulated macromolecule interactions with intact glycocalyx. Albumin has been shown to interact and penetrate into the glycocalyx and associates with hyaluronan. The exact nature of HES interactions is not known. When glycocalyx is compromised, protein extravasation increases.

CHAPTER 5

5.1 SUMMARY, PERSPECTIVES, AND FUTURE DIRECTIONS

The focus on cell mechanics has grown exponentially since the implication of cytoskeleton, ECM, integrin-anchored focal adhesions, cadherins, and other cell structures in both mechanosensing and mechanotransduction. Tools used to measure cell mechanics need to be sensitive to small forces without unintentionally destroying the soft tissue or cell. Tool development is further complicated by the use of live samples. While advances in soft tissue measurements have been made, these techniques must be developed and modified for application-specific, real-time measurements of biologic tissues such as the glycocalyx.

The microvascular endothelial glycocalyx is a hydrated, negatively charged, meshwork layer that lines the luminal surface of blood vessels. The glycocalyx is comprised of proteoglycans, glycoproteins, glycosaminoglycans, glycolipids, and absorbed blood serum proteins. In addition to general barrier functions, this layer has been implicated in mechanosensing functions, including leukocyte adhesion and inflammatory processes as well as blood flow and coagulation. Accurate characterization of glycocalyx including thickness and structural properties is vital to understanding its mechanosensing and physiologic functions.

The mechanical roles of specific components to the glycocalyx have not been explicitly measured with regard to the ability of the glycocalyx to transfer mechanical signals through the cellular architecture. However, it has been postulated that syndecan has a bending rigidity of 700 $pN*nm^2$, which is over 20 times smaller than the bending modulus of an actin filament [2]. These measurements suggest that there is resistance to biologic stress and that a threshold number of syndecans must be deformed in order to transmit signals to cytoskeletal components. Any measurements of this layer must be made using a technique with sufficient sensitivity.

The goal of this research is to measure the mechanical contributions of glycosaminoglycans (heparan sulfate and hyaluronan) and associated macromolecules (albumin and hydroxyethyl starch) to lung glycocalyx mechanical structure and also to incorporate this information into an inclusive mechanical model. Glycocalyx-associated hyaluronan and heparan sulfate have been implicated in vascular endothelial mechanotransduction and macromolecules (particularly albumin) have been found to be critical to lung function and associated with lung glycocalyx mechanical structure.

Two complementary probing techniques have been used to characterize the contribution of heparan sulfate and hyaluronan to the material properties of the glycocalyx: AFM and RICM. Compressive force characteristics of the glycocalyx were measured with AFM with a bead-modified cantilever. Elastic modulus measurements were obtained from discrete regions overlying the monolayer, including 1) intercellular junctions, 2) cell bodies, and 3) nuclear

regions. AFM sensitivity does not extend to the outer 50 nm of the endothelial surface, which potentially is exposed to the most mechanical stimulation. The mechanical information of this outer several nanometer region was therefore examined utilizing RICM, which does not push extensively into the glycocalyx. RICM tracked microfluctuations of bead probes on the glycocalyx, which were associated with the potential energy of the glycocalyx. These two methods were used to measure enzymatically (heparinase or hyaluronidase) treated bovine lung microvascular endothelial cell (BLMVEC) monolayers.

In Chapter 2, mechanical properties of BLMVEC glycocalyx, including modulus and thickness, were assessed by AFM with a modified silica bead indenter (diameter ~18 μm). This modification provided lower compressive pressures on the glycocalyx than the standard sharp cantilever tip, which allowed for determination of the E in a pointwise fashion as a function of the δ. Enzymatic degradation of individual HS and HA GAG components showed a reduction in glycocalyx thickness and that the elastic modulus in the cell junction increased more rapidly at lower indentations than in untreated samples. Furthermore, digestion of a single glycocalyx did not compromise other components, which were able to maintain a similar stiffness in the probe-cell contact area. Interestingly, AFM results demonstrated marked spatial heterogeneity of the glycocalyx composition between cell junctions and nuclear regions. Confocal profiling confirmed these results.

Chapter 3 describes the glycocalyx-specific utilization of RICM technique to detect the subtle changes in the outer several nanometers of the endothelial

glycocalyx stiffness due to removal of GAG components. This technique applied very light loads and small indentations by bead probes (diameter ~18 μm). Results implied that hyaluronan chains act as cushioning elements by organizing the glycocalyx structure. RICM images and results also suggested glycocalyx thickness and compliance are increased at higher BSA concentrations. Overall, this chapter establishes RICM as a sensitive technique that is complementary to the bead-AFM indentation technique described in Chapter 2.

In Chapter 4, AFM and RICM are combined to measure the mechanics of the glycocalyx in the presence of the serum protein albumin and clinically relevant hydroxyethyl starch. Presented results are the first mechanical measurements of the microvascular endothelium as a function of macromolecule concentration and provide a new methodology to examine available clinical observations with albumin and HES macromolecule formulations. Specifically, results indicated that both albumin and HES interact with and influence glycocalyx mechanics.

5.2 Future Directions

5.2.1 AFM and RICM Development

The sensitivity and spatial resolution afforded by both AFM and RICM techniques is ideal for biologic layers with demonstrated heterogeneity like the glycocalyx. These techniques can further be developed to improve mechanical resolution. Specifically, combining RICM and AFM is a viable option, which would combine the benefits of both techniques to a single set of experiments with identical parameters. This combination could also allow for real-time

measurement of inflammatory molecules such as calcium and ROS through the use of fluorescent markers.

The probe-modified AFM technique is particularly appealing because of the precise location of measurements is easily obtained and force application can be modified. Not surprisingly, other groups have concurrently or recently utilized probe-modified AFM techniques similar to the method developed here to investigate the endothelium and glycocalyx [166-169].

5.2.2 Physiologically Relevant Pressures

The response of endothelial cells to hydrostatic pressure and/or flow is postulated to be mechanically transmitted: pressure/flow results in drag on glycocalyx elements; drag leads to deformation (stress/strain); deformation directs in intracellular transmission and signaling pathway activation; activation ultimately leads to permeability changes. Understanding the glycocalyx of lung capillary endothelial cell biomechanical response(s) to local mechanical forces is imperative to forming a strategy for counteracting pathologic, inflammatory phenotypes associated with acute pulmonary inflammation; therefore, characterizing the individual components of the microvascular endothelial glycocalyx is fundamentally important.

The significance of glycocalyx mechanical properties as part of barrier function is ultimately demonstrated by endothelial changes in permeability in response to mechanical stimuli. The majority of inflammatory methods include application of shear or pressure with subsequent measurement of fluid, protein, and/or inflammatory molecule flux. Endothelial cells have previously been shown

to respond to both shear and pressure forces [18, 40, 89]. Hydraulic conductivity, which measures the fluid flux across the vascular wall, was as an indicator of mechanotransduction. Changes in fluid flux have been shown to a function of albumin concentration; this method can therefore be used to measure effects of both albumin and HES concentration.

In Appendix A, hydraulic conductivity is measured as a function of BSA or HES weight to volume concentration. Surprisingly, an increase in concentration resulted in a greater response to pressure. Rat lung microvascular endothelial cell (RLMVEC) monolayers, as viewed after staining, appeared to be intact at the end of experiments. Previously, Dull et al. found that an increase in albumin concentration decreased hydraulic conductivity. These results could be dependent on cell type and show that albumin integration does increase mechanostimulation properties.

5.2.3 Heparan sulfate

Another potential aspect of this research regards sulfation pattern. Heparan sulfate has been identified as the most abundant GAG in the microvascular glycocalyx. In Chapter 2, glycocalyx stiffness was shown to be dependent on subtle changes in glycocalyx concentration. It has been shown that the sulfation pattern affects cell growth and morphology [170, 171]. This has been attributed to specific recognizable chemical patterns. This diversity is also projected to alter vascular permeability [1]. Additionally, the mechanosensing functions of the dynamic glycocalyx are determined by its structure. Subtle differences in physical characteristics of heparan sulfates, and perhaps

chondroitin sulfates, may differentially transmit shear and pressure forces. AFM and RICM are ideal methods to measure subtle experimental modifications in HS or chondroitin sulfate structure. In Appendix B, baseline GAG content of rat lung microvascular endothelial cells was measured and reported. Included is the specific disaccharide content for both heparan and chondroitin sulfates.

APPENDIX A

HYDRAULIC CONDUCTIVITY OF MICROVASCULAR ENDOTHELIAL MONOLAYERS

A.1 Introduction

Transendothelial fluid movement across the endothelium is tightly controlled by both hydrostatic and oncotic forces. The traditional Starling's equations [172, 173] predict that these forces would be linearly related; however, increases in hydrostatic pressure lead to nonlinear changes in hydraulic conductivity (cm/sec/cmH_2O) [40] as shown in Figure A.1. These changes in fluid flux as a function of pressure are a measure of changes in signaling sensitivity.

As discussed in Chapter 4, 5% albumin and 6% hydroxyethyl starch (HES) are two of the most commonly used colloids and were therefore selected for supplementation. Albumin has been studied in the clinical environment, but there have been relatively few studies to explain its interactions with the glycocalyx beyond transient oncotic effects [18, 35, 36, 89, 150]. Reduced albumin has been shown to increase hydraulic conductivity and 4% albumin has been shown to decrease hydraulic conductivity [36, 89]. Furthermore, albumin has been shown to associate with HA [14] and is clinically relevant as a volume expander. HES has also been shown to be an effective volume expander and to minimize endothelial activation and to prevent neutrophil adhesion [151]. It is postulated

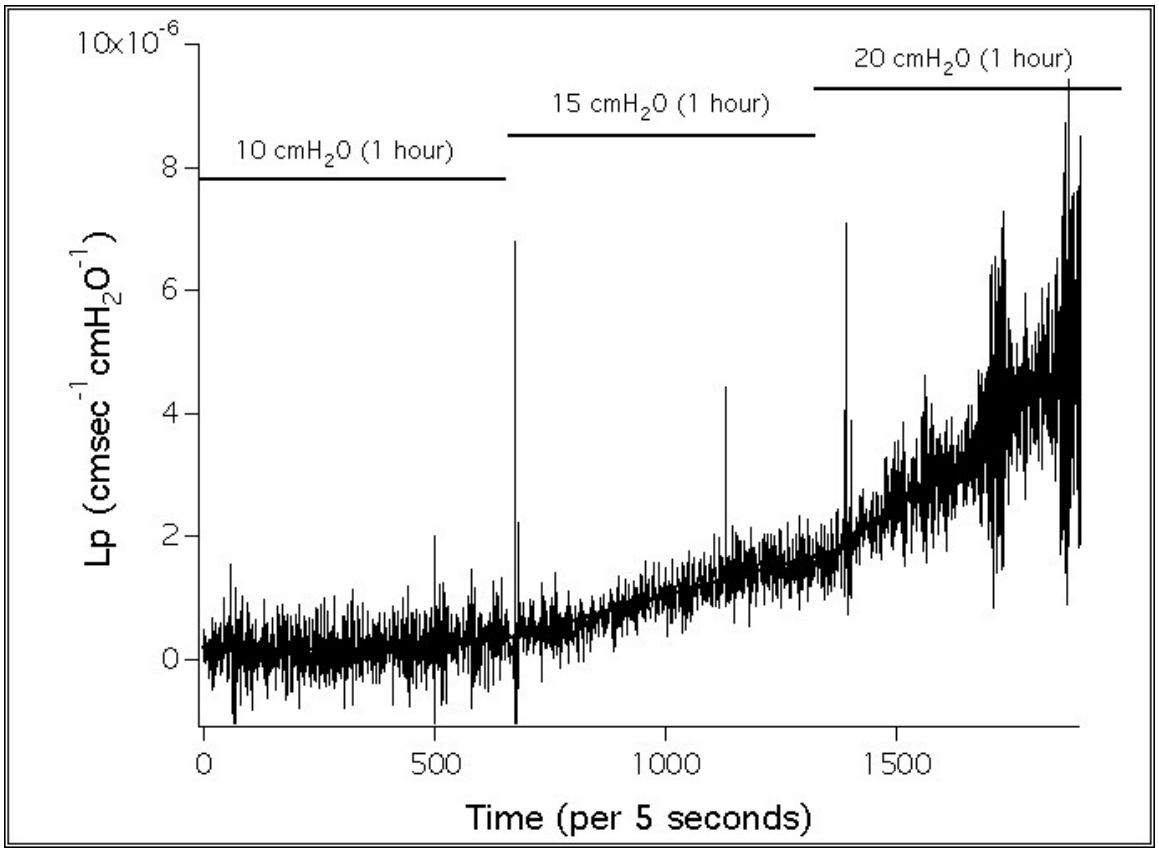

Figure A.1 Hydraulic conductivity across a confluent BLMVEC monolayer as a function of hydraulic pressure and time. Lp rate increases nonlinearly with each step increase in pressure.

that there may be a physical interaction with the glycocalyx that leads to changes in signaling capabilities. Albumin and HES intercalation with the glycocalyx could act to stiffen or cushion the mechanosensing components of the glycocalyx.

A.2 Methods

General methods to measure hydraulic conductivity (Lp; cm/sec/cmH_2O) with endothelial cell monolayers have been described in detail elsewhere [40, 174]. Briefly, BLMVECs or Rat lung microvascular endothelial cell (RLMVECs) were grown to confluency on Snapwell chambers (Costar, polycarbonate membranes, 0.4 μm pore size, 12 mm diameter). Chambers were placed in a modified pressure chamber attached to a hydraulic pressure manifold 7-11 days postplating. The manifold was filled with experimental media (MIII + macromolecule). Monolayers were treated for 1 hour in MII or MII + 50 U/mL HAase then equilibrated in the chambers for 1 hour at 1 cmH_2O prior to experiments with discrete pressure application. Hydraulic flux was measured by monitoring the movement of an introduced airbubble. Lp was defined as flow rate per water pressure (cm/sec/cmH_2O). Measurements were normalized to 10 cmH_2O values, which were considered baseline.

A.3 Results

Lp measured as a function of BSA or HES weight to volume concentration and glycocalyx integrity is shown in Table A.1 and Figure A.2. Sample sizes for each measurement were ~5 confluent monolayers. Surprisingly, an increase in concentration resulted in a greater response to pressure. RLMVEC monolayers appeared to be intact at the end of experiments as viewed after staining.

Table A.1

Hydraulic conductivity (cm/sec/cmH_2O) of confluent monolayers as a function of applied fluid pressure.

Applied fluid Pressure	Hydraulic Conductivity (cm/sec/cmH_2O)				
(cmH_2O)	0.1% BSA	1% BSA	4% BSA	1% HES	4% HES
10	1.15E-06	8.17E-07	7.14E-07	7.23E-07	8.21E-07
15	1.13E-06	1.62E-06	1.70E-06	1.08E-06	1.65E-06
20	2.25E-06	4.06E-06	5.94E-06	2.97E-06	6.39E-06

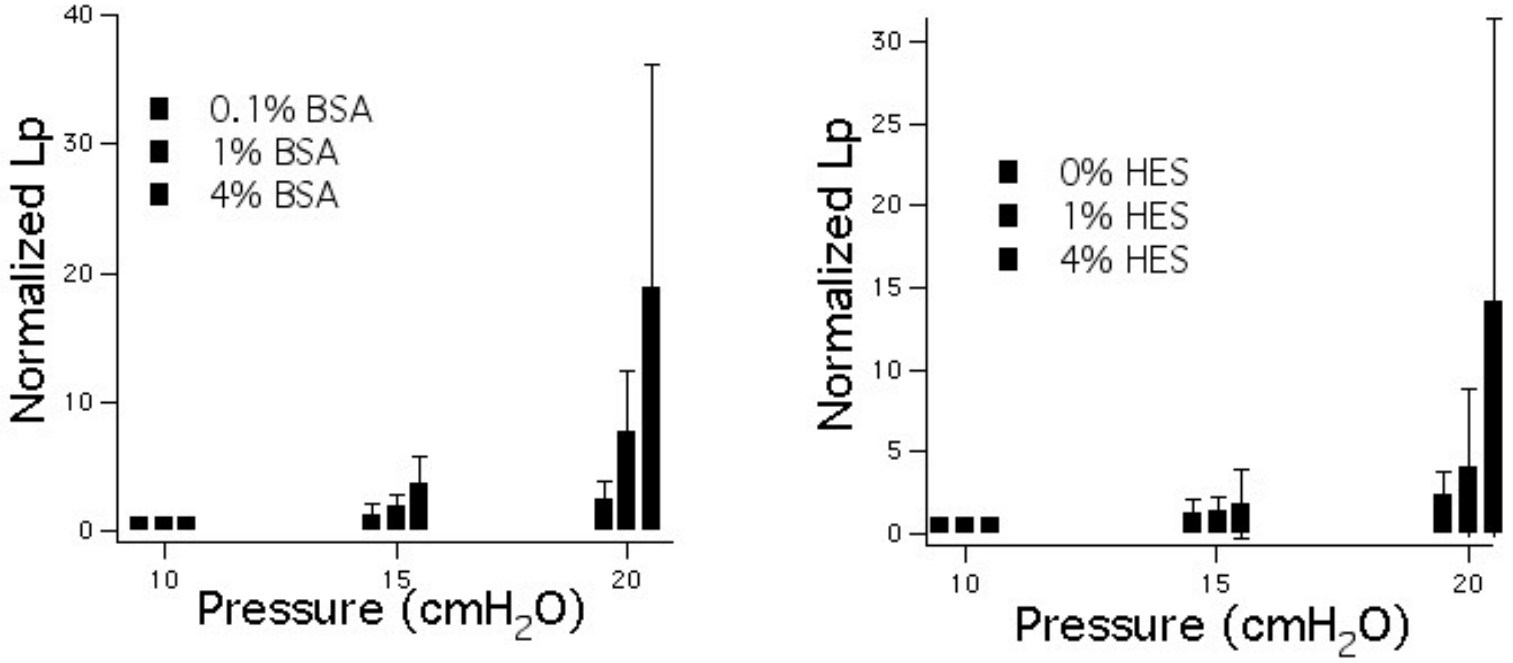

Figure A.2 Normalized hydraulic conductivities (Lp) of RLMVEC as a function of macromolecule concentration and applied fluid pressure. Sample sizes for each measurement were ~5 confluent monolayers. Bars represent mean +/- the standard deviation. Samples were normalized with respect to Lp at 10 cmH_2O.

A.4 Conclusions

The endothelial glycocalyx plays significant roles in the water and solute barrier functions of lung capillaries. It functions as a macromolecular sieve at cell-cell junctions and as a transducer of extracellular mechanical stimuli into intracellular chemical signals. Endothelial cell layer permeability depends upon local protein concentration, which is also controlled by the glycocalyx. In the lungs, these functions are vital to appropriate nutrient exchange and vascular stability. We used a combination of reflectance interference contrast microscopy (RICM) and atomic force microscopy (AFM) to measure compliance of the glycocalyx (Chapter 4), and hydraulic conductivity experiments (Lp) to measure the fluid exchange rate across confluent endothelial cell monolayers. Specifically, 0.1, 1, and 4% w/v of bovine serum albumin (BSA) or hydroxyethyl starch (HES) were applied to lung microvascular endothelial cell monolayers. Baseline hydraulic conductivity was elevated at 0.1% macromolecule concentrations. Pressure-induced changes in hydraulic conductivity increased with increasing macromolecule concentrations. In combination with results from Chapter 4, these results demonstrate the structural importance of albumin in the capillary glycocalyx and a role for HES in the lung capillary environment. The precise role may be elucidated by enzymatically treating monolayers and subsequent macromolecule addition in the future.

APPENDIX B

GLYCOSAMINOGLYCAN CHARACTERIZATION OF MICROVASCULAR ENDOTHELIAL CELLS

The mechanosensing functions of the mesh-like glycocalyx are determined by its structure. This structure is determined by glycocalyx composition, which is a function of cell surface GAG presentation. In this section, GAG content of rat lung microvascular endothelial cells was measured and reported (Table B.1). Included are the specific disaccharide contents, as described in Table B2 and Table B3, for both chondroitin sulfate (Table B4 and Table B5) and heparan sulfate (Table B.6).

RLMVEC monolayers, passage 6 monolayers 11 days postconfluence, were acetone extracted, frozen, and then sent away for separation, digestion, and GAG characterization[6]. GAGs were protease- and RNAse treated, then isolated via weak anionic exchange. GAG aliquots were selectively digested with chondroitinase ABC, chondroitinase AC, a mixture of heparinases I, II, and III, hyaluronidase, and keratanase to selectively digest the different GAGs. Chondroitinase ABC depolymerizes chondroitin sulfate A and C, as well as dermatan sulfate, producing mostly disaccharides. These enzyme combinations

[6] GAG analysis was completed at the Complex Carbohydrate Research Center in Georgia

allow for direct or inferred calculation of disaccharide components. Separation and quantification were attained with a SAX-HPLC on an Agilent system using a 4.6×250 mm Waters Spherisorb analytical column with 5 μm particle size at 25 °C and a Na-phosphate elution buffer.

Overall GAG composition is shown in Table B.1: HS, dermatan sulfate, and chondroitin sulfate comprise the majority of GAGs. Table B.2 shows the 4-character, alphanumeric code used to define the disaccharides [175]. Numbers refer to the sulfation patterns. Table B.2 lists the letter and number combination of the nonreducing end monosaccharide. Table B.3 lists the hexosamine residues. Table B.4, Table B.5, and Table B.6 show samples HS and choindroitin sulfate disaccharide compositions after enzymatic treatment with chondroitinase ABC, chondroitinase AC, and heparinase (I, II, and III), respectively. Approximately 26% of HS by weight is sulfated.

Table B.1

GAG composition of RLMVECs

	Sample 1		Sample 2	
Glycosaminoglycan	μg	% (w/w)	μg	% (w/w)
Chondroitin sulfate	67.5	17.9	60.1	21.1
Dermatan sulfate	134.6	35.7	91.8	32.3
Hyaluronic acid	8.4	2.2	2.0	0.7
Heparan sulfate	161.9	43.0	127.1	44.7
Keratan sulfate	4.4	1.2	3.6	1.3
Total	376.8	100	284.6	100

Table B.2

Disaccharide structure code letters and numbers for nonreducing end residues.

Descriptor		Sulfation	
U	undesignated uronic acid	0	no sulfates
D	$\Delta^{4,5}$-unsaturated uronic acid	2	2-O-sulfation
G	glucuronic acid	3	3-O-sulfation
I	iduronic acid	6	6-O-sulfation
g	galactose		

Table B.3

Disaccharide structure code letters and numbers for hexosamine residue.

Descriptor		Sulfation	
A	N-acetylglucosamine	0	no sulfates
a	N-acetylgalactosamine	3	3-O-sulfation
S	N-sulfoglucosamine	4	4-O-sulfation
		6	6-O-sulfation
		9	3,6-O-disulfation
		10	4,6-O-disulfation

Table B.4

Chondroitin sulfate disaccharides after chondroitinase ABC digestion.

	Sample 1		Sample 2	
Disaccharide	μg	% (w/w)	μg	% (w/w)
D0a0 (CS, DS, HA)	7.8	3.7	4.5	2.9
D0a6	22.3	10.6	13.8	8.9
D0a4	158.0	75.0	120.6	78.4
D0a10	9.0	4.3	6.4	4.2
D2a4	13.4	6.4	8.6	5.6
Total	210.5	100	153.9	100

Table B.5

Chondroitin sulfate disaccharides after chondroitinase AC digestion

	Sample 1		Sample 2	
Disaccharide	μg	% (w/w)	μg	% (w/w)
D0a0 (CS, HA)	13.6	18.0	7.79	12.6
D0a6	19.0	25.1	11.85	19.1
D0a4	40.2	52.9	40.40	65.1
D0a10	3.0	4.0	2.02	3.3
D2a4	n.d.	n.d	n.d	n.d
Total	75.9	100.0	62.1	100.0

Table B.6

Heparan sulfate disaccharides after heparinase I, II, and III digestion.

	Sample 1		Sample 2	
Disaccharide	μg	% (w/w)	μg	% (w/w)
D0A0	68.2	42.1	53.3	42.0
D0S0	38.4	23.7	27.5	21.7
D0A6	13.2	8.2	8.4	6.6
D2A0	8.7	5.4	4.7	3.7
D0S6	8.7	5.4	10.0	7.8
D2S0	14.3	8.8	10.1	8.0
D2S6	10.4	6.4	13.1	10.3
Total	161.9	100	127.1	100

REFERENCES

[1] Reitsma S, Slaaf DW, Vink H, van Zandvoort MAMJ, oude Egbrink MGA. The endothelial glycocalyx: composition, functions, and visualization. Pflugers Arch. 2007;454:345-59.

[2] Weinbaum S, Zhang X, Han Y, Vink H, Cowin SC. Mechanotransduction and flow across the endothelial glycocalyx. Proc Natl Acad Sci USA. 2003;100:7988-95.

[3] Kamm R, Lammerding J, Mofrad M. Cellular Nanomechanics. In: B. Bhushan, editor. Springer Handbook of Nanotechnology. 3rd ed: Springer; 2010. p. 1171-200.

[4] Luft JH. Fine structures of capillary and endocapillary layer as revealed by ruthenium red. Fed Proc. 1966;25:1773-83.

[5] Rostgaard J, Qvortrup K. Electron microscopic demonstrations of filamentous molecular sieve plugs in capillary fenestrae. Microvasc Res. 1997;53:1-13.

[6] Squire JM, Chew M, Nneji G, Neal C, Barry J, Michel C. Quasi-periodic substructure in the microvessel endothelial glycocalyx: a possible explanation for molecular filtering? J Struct Biol. 2001;136:239-55.

[7] Klitzman B, Duling BR. Microvascular hematocrit and red cell flow in resting and contracting striated muscle. Am J Physiol. 1979;237:H481-90.

[8] Pries AR, Secomb TW, Gessner T, Sperandio MB, Gross JF, Gaehtgens P. Resistance to blood flow in microvessels in vivo. Circ Res. 1994;75:904-15.

[9] Weinbaum S, Tarbell JM, Damiano ER. The structure and function of the endothelial glycocalyx layer. Annu Rev Biomed Eng. 2007;9:121-67.

[10] Vink H, Wieringa PA, Spaan JA. Evidence that cell surface charge reduction modifes capillary red cell velocity-flux relationships in hamster cremaster muscle. The Journal of Physiology. 1995;489 (Pt 1):193-201.

[11] Vink H, Duling BR. Identification of distinct luminal domains for macromolecules, erythrocytes, and leukocytes within mammalian capillaries. Circ Res. 1996;79:581-9.

[12] Smith ML, Long DS, Damiano ER, Ley K. Near-wall micro-PIV reveals a hydrodynamically relevant endothelial surface layer in venules in vivo. Biophys J. 2003;85:637-45.

[13] Zeng Y, Ebong EE, Fu BM, Tarbell JM. The structural stability of the endothelial glycocalyx after enzymatic removal of glycosaminoglycans. PLoS ONE. 2012;7:e43168.

[14] Stevens AP, Hlady V, Dull RO. Fluorescence correlation spectroscopy can probe albumin dynamics inside lung endothelial glycocalyx. American journal of physiology Lung cellular and molecular physiology. 2007;293:L328-35.

[15] Pries AR, Secomb TW, Gaehtgens P. The endothelial surface layer. Pflugers Arch. 2000;440:653-66.

[16] David G, Bernfield M. The emerging roles of cell surface heparan sulfate proteoglycans. Matrix Biol. 1998;17:461-3.

[17] Desjardins C, Duling BR. Heparinase treatment suggests a role for the endothelial cell glycocalyx in regulation of capillary hematocrit. Am J Physiol. 1990;258:H647-54.

[18] Florian JA, Kosky JR, Ainslie K, Pang Z, Dull RO, Tarbell JM. Heparan sulfate proteoglycan is a mechanosensor on endothelial cells. Circ Res. 2003;93:e136-42.

[19] Dull RO, Dinavahi R, Schwartz L, Humphries DE, Berry D, Sasisekharan R, et al. Lung endothelial heparan sulfates mediate cationic peptide-induced barrier dysfunction: a new role for the glycocalyx. American journal of physiology Lung cellular and molecular physiology. 2003;285:L986-95.

[20] Davies PF. Flow-mediated endothelial mechanotransduction. Physiol Rev. 1995;75:519-60.

[21] Henry CBS, Duling BR. Permeation of the luminal capillary glycocalyx is determined by hyaluronan. Am J Physiol-Heart C. 1999;277:H508-H14.

[22] Bernfield M, Götte M, Park PW, Reizes O, Fitzgerald ML, Lincecum J, et al. Functions of cell surface heparan sulfate proteoglycans. Annu Rev Biochem. 1999;68:729-77.

[23] Lennon FE, Singleton PA. Hyaluronan regulation of vascular integrity. Am J Cardiovasc Dis. 2011;1:200-13.

[24] Cabrales P, Vázquez BYS, Tsai AG, Intaglietta M. Microvascular and capillary perfusion following glycocalyx degradation. J Appl Physiol. 2007;102:2251-9.

[25] Genasetti A, Vigetti D, Viola M, Karousou E, Moretto P, Rizzi M, et al. Hyaluronan and human endothelial cell behavior. Connect Tissue Res. 2008;49:120-3.

[26] Singleton PA, Bourguignon LYW. CD44 interaction with ankyrin and IP3 receptor in lipid rafts promotes hyaluronan-mediated Ca2+ signaling leading to nitric oxide production and endothelial cell adhesion and proliferation. Exp Cell Res. 2004;295:102-18.

[27] Scott JE, Heatley F. Hyaluronan forms specific stable tertiary structures in aqueous solution: a 13C NMR study. Proc Natl Acad Sci U S A. 1999;96:4850-5.

[28] Scott JE, Thomlinson AM, Prehm P. Supramolecular organization in streptococcal pericellular capsules is based on hyaluronan tertiary structures. Exp Cell Res. 2003;285:1-8.

[29] Tarbell JM, Pahakis MY. Mechanotransduction and the glycocalyx. Journal of internal medicine. 2006;259:339-50.

[30] Schnitzer J. Specific albumin binding to microvascular endothelium in culture. American Journal of Physiology - Heart and Circulatory Physiology. 1988;254.

[31] Schneeberger EE, Lynch RD, Neary BA. Interaction of native and chemically modified albumin with pulmonary microvascular endothelium. Am J Physiol. 1990;258:L89-98.

[32] McCandless BK, Powers MR, Cooper JA, Malik AB. Effect of albumin on hydraulic conductivity of pulmonary artery endothelial monolayers. Am J Physiol. 1991;260:L571-6.

[33] Schneeberger EE, Hamelin M. Interaction of serum proteins with lung endothelial glycocalyx: its effect on endothelial permeability. Am J Physiol. 1984;247:H206-17.

[34] Mehta D, Malik AB. Signaling mechanisms regulating endothelial permeability. Physiological Reviews. 2006;86:279-367.

[35] Huxley VH, Curry FE. Effect of superfusate albumin on single capillary hydraulic conductivity. Am J Physiol. 1987;252:H395-401.

[36] Huxley VH, Curry FE. Albumin modulation of capillary permeability: test of an adsorption mechanism. Am J Physiol. 1985;248:H264-73.

[37] Jacob M, Paul O, Mehringer L, Chappell D, Rehm M, Welsch U, et al. Albumin augmentation improves condition of guinea pig hearts after 4 hr of cold ischemia. Transplantation. 2009;87:956-65.

[38] Adamson RH, Clough G. Plasma proteins modify the endothelial cell glycocalyx of frog mesenteric microvessels. The Journal of Physiology. 1992;445:473-86.

[39] Kozar RA, Peng Z, Zhang R, Holcomb JB, Pati S, Park P, et al. Plasma restoration of endothelial glycocalyx in a rodent model of hemorrhagic shock. Anesth Analg. 2011;112:1289-95.

[40] Dull RO, Mecham I, McJames S. Heparan sulfates mediate pressure-induced increase in lung endothelial hydraulic conductivity via nitric oxide/reactive oxygen species. American journal of physiology Lung cellular and molecular physiology. 2007;292:L1452-8.

[41] Pahakis MY, Kosky JR, Dull RO, Tarbell JM. The role of endothelial glycocalyx components in mechanotransduction of fluid shear stress. Biochem Biophys Res Commun. 2007;355:228-33.

[42] Dewey CF. Effects of fluid flow on living vascular cells. Journal of biomechanical engineering. 1984;106:31-5.

[43] Bai K, Wang W. Shear stress-induced redistribution of the glycocalyx on endothelial cells in vitro. Biomechanics and modeling in mechanobiology. 2013.

[44] Giantsos-Adams KM, Koo AJ-A, Song S, Sakai J, Sankaran J, Shin JH, et al. Heparan Sulfate Regrowth Profiles Under Laminar Shear Flow Following Enzymatic Degradation. Cellular and Molecular Bioengineering. 2013;6:160-74.

[45] Mochizuki S, Vink H, Hiramatsu O, Kajita T, Shigeto F, Spaan JA, et al. Role of hyaluronic acid glycosaminoglycans in shear-induced endothelium-derived nitric oxide release. American journal of physiology Heart and circulatory physiology. 2003;285:H722-6.

[46] Vink H, Duling BR. Capillary endothelial surface layer selectively reduces plasma solute distribution volume. American journal of physiology Heart and circulatory physiology. 2000;278:H285-9.

[47] Ichimura H, Parthasarathi K, Quadri S, Issekutz AC, Bhattacharya J. Mechano-oxidative coupling by mitochondria induces proinflammatory responses in lung venular capillaries. J Clin Invest. 2003;111:691-9.

[48] Jacob M, Rehm M, Loetsch M, Paul JO, Bruegger D, Welsch U, et al. The endothelial glycocalyx prefers albumin for evoking shear stress-induced, nitric oxide-mediated coronary dilatation. J Vasc Res. 2007;44:435-43.

[49] Orr AW, Helmke BP, Blackman BR, Schwartz MA. Mechanisms of mechanotransduction. Developmental cell. 2006;10:11-20.

[50] Yao Y, Rabodzey A, Dewey CF. Glycocalyx modulates the motility and proliferative response of vascular endothelium to fluid shear stress. Am J Physiol Heart Circ Physiol. 2007;293:H1023-30.

[51] Thi MM, Tarbell JM, Weinbaum S, Spray DC. The role of the glycocalyx in reorganization of the actin cytoskeleton under fluid shear stress: a "bumper-car" model. Proc Natl Acad Sci USA2004. p. 16483-8.

[52] Kuebler WM, Ying X, Bhattacharya J. Pressure-induced endothelial Ca(2+) oscillations in lung capillaries. Am J Physiol Lung Cell Mol Physiol. 2002;282:L917-23.

[53] Kiefmann R, Rifkind JM, Nagababu E, Bhattacharya J. Red blood cells induce hypoxic lung inflammation. Blood. 2008;111:5205-14.

[54] Ichimura H, Parthasarathi K, Issekutz AC, Bhattacharya J. Pressure-induced leukocyte margination in lung postcapillary venules. Am J Physiol Lung Cell Mol Physiol. 2005;289:L407-12.

[55] Constantinescu AA, Vink H, Spaan JAE. Endothelial cell glycocalyx modulates immobilization of leukocytes at the endothelial surface. Arterioscl Throm Vas. 2003;23:1541-7.

[56] Adamson RH. Permeability of frog mesenteric capillaries after partial pronase digestion of the endothelial glycocalyx. J Physiol. 1990;428:1-13.

[57] Jacob M, Bruegger D, Rehm M, Stoeckelhuber M, Welsch U, Conzen P, et al. The endothelial glycocalyx affords compatibility of Starling's principle and high cardiac interstitial albumin levels. Cardiovasc Res. 2007;73:575-86.

[58] Pries AR, Secomb TW. Microvascular adaptation--regulation, coordination and function. Zeitschrift für Kardiologie. 2000;89 Suppl 9:IX/117-20.

[59] Townsley MI, Lim EH, Sahawneh TM, Song W. Interaction of chemical and high vascular pressure injury in isolated canine lung. J Appl Physiol1990. p. 1657-64.

[60] Maron MB. A canine model of neurogenic pulmonary edema. J Appl Physiol. 1985;59:1019-25.

[61] Maggiorini M, Mélot C, Pierre S, Pfeiffer F, Greve I, Sartori C, et al. High-altitude pulmonary edema is initially caused by an increase in capillary pressure. Circulation. 2001;103:2078-83.

[62] Parker JC, Hernandez LA, Peevy KJ. Mechanisms of ventilator-induced lung injury. Crit Care Med. 1993;21:131-43.

[63] Rippe B, Townsley M, Thigpen J, Parker JC, Korthuis RJ, Taylor AE. Effects of vascular pressure on the pulmonary microvasculature in isolated dog lungs. J Appl Physiol. 1984;57:233-9.

[64] Parker RE, Roselli RJ, Harris TR, Brigham KL. Effects of graded increases in pulmonary vascular pressures on lung fluid balance in unanesthetized sheep. Circ Res. 1981;49:1164-72.

[65] Moon JJ, Matsumoto M, Patel S, Lee L, Guan J-L, Li S. Role of cell surface heparan sulfate proteoglycans in endothelial cell migration and mechanotransduction. J Cell Physiol. 2005;203:166-76.

[66] Hoffman BD, Crocker JC. Cell mechanics: dissecting the physical responses of cells to force. Annu Rev Biomed Eng. 2009;11:259-88.

[67] Satcher RL, Dewey CF. Theoretical estimates of mechanical properties of the endothelial cell cytoskeleton. Biophys J. 1996;71:109-18.

[68] Janmey PA, McCulloch CA. Cell mechanics: integrating cell responses to mechanical stimuli. Annu Rev Biomed Eng. 2007;9:1-34.

[69] Chen CS, Tan J, Tien J. Mechanotransduction at cell-matrix and cell-cell contacts. Annu Rev Biomed Eng. 2004;6:275-302.

[70] Addae-Mensah KA, Wikswo JP. Measurement techniques for cellular biomechanics in vitro. Exp Biol Med (Maywood). 2008;233:792-809.

[71] Costa KD. Imaging and probing cell mechanical properties with the atomic force microscope. Methods Mol Biol. 2006;319:331-61.

[72] Costa KD, Yin FC. Analysis of indentation: implications for measuring mechanical properties with atomic force microscopy. Journal of biomechanical engineering. 1999;121:462-71.

[73] Mathur AB, Truskey GA, Reichert WM. Atomic force and total internal reflection fluorescence microscopy for the study of force transmission in endothelial cells. Biophys J. 2000;78:1725-35.

[74] Ohashi T, Ishii Y, Ishikawa Y, Matsumoto T, Sato M. Experimental and numerical analyses of local mechanical properties measured by atomic force microscopy for sheared endothelial cells. Bio-medical materials and engineering. 2002;12:319-27.

[75] Sato H, Kataoka N, Kajiya F, Katano M, Takigawa T, Masuda T. Kinetic study on the elastic change of vascular endothelial cells on collagen matrices by atomic force microscopy. Colloids and surfaces B, Biointerfaces. 2004;34:141-6.

[76] Pesen D, Hoh JH. Micromechanical architecture of the endothelial cell cortex. Biophys J. 2005;88:670-9.

[77] Costa KD, Sim AJ, Yin FC-P. Non-Hertzian approach to analyzing mechanical properties of endothelial cells probed by atomic force microscopy. Journal of biomechanical engineering. 2006;128:176-84.

[78] Tarbell JM, Weinbaum S, Kamm RD. Cellular fluid mechanics and mechanotransduction. Ann Biomed Eng. 2005;33:1719-23.

[79] Curtis AS. The mechanism of adhesion of cells to glass. A study by interference reflection microscopy. J Cell Biol. 1964;20:199-215.

[80] Zilker A, Ziegler M, Sackmann E. Spectral analysis of erythrocyte flickering in the 0.3-4- microm-1 regime by microinterferometry combined with fast image processing. Phys Rev, A. 1992;46:7998-8001.

[81] Simson R, Wallraff E, Faix J, Niewöhner J, Gerisch G, Sackmann E. Membrane bending modulus and adhesion energy of wild-type and mutant cells of Dictyostelium lacking talin or cortexillins. Biophys J. 1998;74:514-22.

[82] Bruinsma R, Behrisch A, Sackmann E. Adhesive switching of membranes: experiment and theory. Physical review E, Statistical physics, plasmas, fluids, and related interdisciplinary topics. 2000;61:4253-67.

[83] Neumaier KR, Elender G, Sackmann E, Merkel R. Ellipsometric microscopy. Europhys Lett. 2000;49:14-9.

[84] Schilling J, Sengupta K, Goennenwein S, Bausch AR, Sackmann E. Absolute interfacial distance measurements by dual-wavelength reflection interference contrast microscopy. Physical review E, Statistical, nonlinear, and soft matter physics. 2004;69:021901.

[85] Sackmann E. Supported membranes: scientific and practical applications. Science. 1996;271:43-8.

[86] Kühner M, Sackmann E. Ultrathin hydrated dextran films grafted on glass: preparation and characterization of structural, viscous, and elastic properties by quantitative microinterferometry. Langmuir. 1996;12:4866-76.

[87] Wiegand G, Neumaier KR, Sackmann E. Microinterferometry: Three-Dimensional Reconstruction of Surface Microtopography for Thin-Film and Wetting Studies by Reflection Interference Contrast Microscopy (RICM). Applied optics. 1998;37:6892-905.

[88] Rädler J, Sackmann E. On the measurement of weak repulsive and frictional colloidal forces by reflection interference contrast microscopy. Langmuir. 1992;8:848-53.

[89] Dull RO, Jo H, Sill H, Hollis TM, Tarbell JM. The effect of varying albumin concentration and hydrostatic pressure on hydraulic conductivity and albumin permeability of cultured endothelial monolayers. Microvasc Res. 1991;41:390-407.

[90] Tatara T, Itani M, Sugi T, Fujita K. Physical plugging does not account for attenuation of capillary leakage by hydroxyethyl starch 130/0.4: A synthetic gel layer model. J Biomed Mater Res Part B Appl Biomater. 2013;101(1):85-90.

[91] Tatara T, Tashiro C. Analysis using a linear viscoelastic model of the in vitro osmotic kinetics of polydisperse synthetic colloids. Biomacromolecules. 2005;6:1732-8.

[92] Henry CB, Durán WN, DeFouw DO. Permselectivity of angiogenic microvessels following alteration of the endothelial fiber matrix by oligosaccharides. Microvasc Res. 1997;53:150-5.

[93] Dubniks M, Persson J, Grände P-O. Plasma volume expansion of 5% albumin, 4% gelatin, 6% HES 130/0.4, and normal saline under increased microvascular permeability in the rat. Intensive Care Med. 2007;33:293-9.

[94] Toner A. Fluid physiology, tissue compliance, and colloids. Br J Anaesth. 2012;108:1035; author reply -6.

[95] O'Callaghan R, Job KM, Dull RO, Hlady V. Stiffness and heterogeneity of the pulmonary endothelial glycocalyx measured by atomic force microscopy. Am J Physiol Lung Cell Mol Physiol. 2011;301:L353-60.

[96] LeBoeuf RD, Raja RH, Fuller GM, Weigel PH. Human fibrinogen specifically binds hyaluronic acid. The Journal of biological chemistry. 1986;261:12586-92.

[97] Adamson RH, Lenz JF, Zhang X, Adamson GN, Weinbaum S, Curry FE. Oncotic pressures opposing filtration across non-fenestrated rat microvessels. J Physiol. 2004;557:889-907.

[98] Vink H, Constantinescu AA, Spaan JA. Oxidized lipoproteins degrade the endothelial surface layer : implications for platelet-endothelial cell adhesion. Circulation. 2000;101:1500-2.

[99] Henry CB, Duling BR. TNF-alpha increases entry of macromolecules into luminal endothelial cell glycocalyx. Am J Physiol Heart Circ Physiol. 2000;279:H2815-23.

[100] Lipowsky HH. Microvascular rheology and hemodynamics. Microcirculation. 2005;12:5-15.

[101] Zuurbier CJ, Demirci C, Koeman A, Vink H, Ince C. Short-term hyperglycemia increases endothelial glycocalyx permeability and acutely

decreases lineal density of capillaries with flowing red blood cells. J Appl Physiol. 2005;99:1471-6.

[102] Henry CB, Duling BR. Permeation of the luminal capillary glycocalyx is determined by hyaluronan. Am J Physiol. 1999;277:H508-14.

[103] VanTeeffelen JW, Brands J, Jansen C, Spaan JA, Vink H. Heparin impairs glycocalyx barrier properties and attenuates shear dependent vasodilation in mice. Hypertension. 2007;50:261-7.

[104] Lopez-Quintero SV, Amaya R, Pahakis M, Tarbell JM. The endothelial glycocalyx mediates shear-induced changes in hydraulic conductivity. Am J Physiol Heart Circ Physiol. 2009;296:H1451-6.

[105] Beatty MF, Usmani SA. On the indentation of a highly elastic half-space. The Quarterly Journal of Mechanics and Applied Mathematics. 1975;28:47-62.

[106] Doerner MF, Nix WD. A method for interpreting the data from depth-sensing indentation instruments. Journal of Materials Research. 1986;1:601-9.

[107] Kovalev A, Shulha H, Lemieux M, Myshkin N, Tsukruk VV. Nanomechanical probing of layered nanoscale polymer films with atomic force microscopy. Journal of Materials Research. 2004;19:716-28.

[108] Ito S, Suki B, Kume H, Numaguchi Y, Ishii M, Iwaki M, et al. Actin cytoskeleton regulates stretch-activated Ca2+ influx in human pulmonary microvascular endothelial cells. American journal of respiratory cell and molecular biology. 2010;43:26-34.

[109] Duling BR, Berne RM. Propagated vasodilation in the microcirculation of the hamster cheek pouch. Circ Res. 1970;26:163-70.

[110] Boal D. Mechanics of the Cell. Cambridge, UK: Cambridge University Press; 2002.

[111] Takai E, Costa KD, Shaheen A, Hung CT, Guo XE. Osteoblast elastic modulus measured by atomic force microscopy is substrate dependent. Ann Biomed Eng. 2005;33:963-71.

[112] Brouland JP, Gilbert MA, Bonneau M, Pignaud G, Bal Dit Solier C, Drouet L. Macro and microheterogeneity in normal endothelial cells: differential composition of luminal glycocalyx and functional implications. Endothelium : journal of endothelial cell research. 1999;6:251-62.

[113] Haldenby KA, Chappell DC, Winlove CP, Parker KH, Firth JA. Focal and regional variations in the composition of the glycocalyx of large vessel endothelium. J Vasc Res. 1994;31:2-9.

[114] Giantsos KM, Kopeckova P, Dull RO. The use of an endothelium-targeted cationic copolymer to enhance the barrier function of lung capillary endothelial monolayers. Biomaterials. 2009;30:5885-91.

[115] Chang YS, Munn LL, Hillsley MV, Dull RO, Yuan J, Lakshminarayanan S, et al. Effect of vascular endothelial growth factor on cultured endothelial cell monolayer transport properties. Microvasc Res. 2000;59:265-77.

[116] Job KM, Dull RO, Hlady V. Use of reflectance interference contrast microscopy to characterize the endothelial glycocalyx stiffness. American journal of physiology Lung cellular and molecular physiology. 2012;302:L1242-9.

[117] Vogel V, Sheetz M. Local force and geometry sensing regulate cell functions. Nat Rev Mol Cell. 2006;7:265-75.

[118] Bao G, Suresh S. Cell and molecular mechanics of biological materials. Nature Mater. 2003;2:715-25.

[119] Lo CM, Wang HB, Dembo M, Wang YL. Cell movement is guided by the rigidity of the substrate. Biophys J. 2000;79:144-52.

[120] Georges PC, Miller WJ, Meaney DF, Sawyer ES, Janmey PA. Matrices with compliance comparable to that of brain tissue select neuronal over glial growth in mixed cortical cultures. Biophys J. 2006;90:3012-8.

[121] Iwaki M, Ito S, Morioka M, Iwata S, Numaguchi Y, Ishii M, et al. Mechanical stretch enhances IL-8 production in pulmonary microvascular endothelial cells. Biochemical and biophysical research communications. 2009;389:531-6.

[122] Suresh S, Spatz J, Mills JP, Micoulet A, Dao M, Lim CT, et al. Connections between single-cell biomechanics and human disease states: gastrointestinal cancer and malaria. Acta Biomaterialia. 2005;1:15-30.

[123] Helmke BP, Thakker DB, Goldman RD, Davies PF. Spatiotemporal analysis of flow-induced intermediate filament displacement in living endothelial cells. Biophys J. 2001;80:184-94.

[124] Ebong EE, Macaluso FP, Spray DC, Tarbell JM. Imaging the endothelial glycocalyx in vitro by rapid freezing/freeze substitution transmission electron microscopy. Arteriosclerosis, thrombosis, and vascular biology. 2011;31:1908-15.

[125] Gao L, Lipowsky HH. Composition of the endothelial glycocalyx and its relation to its thickness and diffusion of small solutes. Microvasc Res. 2010;80:394-401.

[126] Cooper JA. Effects of cytochalasin and phalloidin on actin. J Cell Biol. 1987;105:1473-8.

[127] Davies PF. Flow-mediated endothelial mechanotransduction. Physiological Reviews. 1995;75:519-60.

[128] Lemons DS, Gythiel A. Paul Langevin's 1908 paper "On the Theory of Brownian Motion"["Sur la théorie du mouvement brownien," CR Acad. Sci.(Paris)[bold 146], 530–533 (1908)]. Am J Phys. 1997;65:1079.

[129] Rädler J, Sackmann E. Imaging optical thicknesses and separation distances of phospholipid vesicles at solid surfaces. Journal de Physique II. 1993;3:727-48.

[130] Gingell D, Todd I. Interference reflection microscopy. A quantitative theory for image interpretation and its application to cell-substratum separation measurement. Biophys J. 1979;26:507-26.

[131] Zidovska A, Sackmann E. Brownian motion of nucleated cell envelopes impedes adhesion. Phys Rev Lett. 2006;96:048103.

[132] Gönnenwein S. Generic and Specific Cell Adhesion: Investigations of a Model System by Micro-Interferometry [PhD Dissertation]. Munchen: Technischen Universitat Munchen; 2003.

[133] Prieve D. Measurement of colloidal forces with TIRM. Advances in Colloid and Interface Science. 1999;82:93-125.

[134] Oberleithner H, Peters W, Kusche-Vihrog K, Korte S, Schillers H, Kliche K, et al. Salt overload damages the glycocalyx sodium barrier of vascular endothelium. Pflugers Arch. 2011;462:519-28.

[135] Zwanzig R, Bixon M. Compressibility effects in the hydrodynamic theory of Brownian motion. J Fluid Mech. 1975;69:21-5.

[136] Banerjee SD, Toole BP. Hyaluronan-binding protein in endothelial cell morphogenesis. J Cell Biol. 1992;119:643-52.

[137] Balkamou X, Xanthos T, Stroumpoulis K, Moutzouris DA, Rokas G, Agrogiannis G, et al. Hydroxyethyl starch 6% (130/0.4) ameliorates acute lung injury in swine hemorrhagic shock. Anesthesiology. 2010;113:1092-8.

[138] Wang J, Oppenheimer L, Fata P, Pintin J, Stimpson R, Mantsch HH. Spectroscopic approach to capillary-alveolar membrane damage induced acute lung injury. Can Respir J. 1999;6:499-506.

[139] Costa ELV, Amato MBP. The new definition for acute lung injury and acute respiratory distress syndrome: is there room for improvement? Curr Opin Crit Care. 2013;19:16-23.

[140] Levick JR, Michel CC. Microvascular fluid exchange and the revised Starling principle. Cardiovascular Research. 2010;87:198-210.

[141] Assaad S, Popescu W, Perrino A. Fluid management in thoracic surgery. Curr Opin Anaesthesiol. 2013;26:31-9.

[142] Jacob M, Bruegger D, Rehm M, Welsch U, Conzen P, Becker BF. Contrasting effects of colloid and crystalloid resuscitation fluids on cardiac vascular permeability. Anesthesiology. 2006;104:1223-31.

[143] Huang C-C, Kao K-C, Hsu K-H, Ko H-W, Li L-F, Hsieh M-J, et al. Effects of hydroxyethyl starch resuscitation on extravascular lung water and pulmonary permeability in sepsis-related acute respiratory distress syndrome. Crit Care Med. 2009;37:1948-55.

[144] Mitra S, Khandelwal P. Are all colloids same? How to select the right colloid? Indian J Anaesth. 2009;53:592-607.

[145] Vincent J-L. The pros and cons of hydroxyethyl starch solutions. Anesth Analg. 2007;104:484-6.

[146] Rehm M, Zahler S, Lötsch M, Welsch U, Conzen P, Jacob M, et al. Endothelial glycocalyx as an additional barrier determining extravasation of 6% hydroxyethyl starch or 5% albumin solutions in the coronary vascular bed. Anesthesiology. 2004;100:1211-23.

[147] Strunden MS, Bornscheuer A, Schuster A, Kiefmann R, Goetz AE, Heckel K. Glycocalyx degradation causes microvascular perfusion failure in the ex vivo perfused mouse lung: hydroxyethyl starch 130/0.4 pretreatment attenuates this response. Shock. 2012;38:559-66.

[148] Woodcock TE, Woodcock TM. Revised Starling equation and the glycocalyx model of transvascular fluid exchange: an improved paradigm for prescribing intravenous fluid therapy. Br J Anaesth. 2012;108:384-94.

[149] Michel CC, Curry FE. Microvascular permeability. Physiol Rev. 1999;79:703-61.

[150] Osterloh K, Ewert U, Pries AR. Interaction of albumin with the endothelial cell surface. Am J Physiol Heart Circ Physiol. 2002;283:H398-405.

[151] Wilkes NJ, Woolf RL, Powanda MC, Gan TJ, Machin SJ, Webb A, et al. Hydroxyethyl starch in balanced electrolyte solution (Hextend)--pharmacokinetic and pharmacodynamic profiles in healthy volunteers. Anesth Analg. 2002;94:538-44; table of contents.

[152] Pries AR, Secomb TW. Microvascular blood viscosity in vivo and the endothelial surface layer. Am J Physiol Heart Circ Physiol. 2005;289:H2657-64.

[153] Di Filippo A, Ciapetti M, Prencipe D, Tini L, Casucci A, Ciuti R, et al. Experimentally-induced acute lung injury: the protective effect of hydroxyethyl starch. Ann Clin Lab Sci. 2006;36:345-52.

[154] Feng X, Yan W, Wang Z, Liu J, Yu M, Zhu S, et al. Hydroxyethyl starch, but not modified fluid gelatin, affects inflammatory response in a rat model of polymicrobial sepsis with capillary leakage. Anesth Analg. 2007;104:624-30.

[155] Feng X, Liu J, Yu M, Zhu S, Xu J. Protective roles of hydroxyethyl starch 130/0.4 in intestinal inflammatory response and survival in rats challenged with polymicrobial sepsis. Clin Chim Acta. 2007;376:60-7.

[156] Feng X, Ren B, Xie W, Huang Z, Liu J, Guan R, et al. Influence of hydroxyethyl starch 130/0.4 in pulmonary neutrophil recruitment and acute lung injury during polymicrobial sepsis in rats. Acta Anaesthesiol Scand. 2006;50:1081-8.

[157] Ali MA, Saleh M. Selection of optimal quantity of hydroxyethyl starch in the cardiopulmonary bypass prime. Perfusion. 2004;19:41-5.

[158] Bruegger D, Jacob M, Rehm M, Loetsch M, Welsch U, Conzen P, et al. Atrial natriuretic peptide induces shedding of endothelial glycocalyx in coronary vascular bed of guinea pig hearts. American journal of physiology Heart and circulatory physiology. 2005;289:H1993-9.

[159] Chappell D, Hofmann-Kiefer K, Jacob M, Rehm M, Briegel J, Welsch U, et al. TNF-alpha induced shedding of the endothelial glycocalyx is prevented by hydrocortisone and antithrombin. Basic Res Cardiol. 2009;104:78-89.

[160] Chappell D, Jacob M, Hofmann-Kiefer K, Bruegger D, Rehm M, Conzen P, et al. Hydrocortisone preserves the vascular barrier by protecting the endothelial glycocalyx. Anesthesiology. 2007;107:776-84.

[161] Chappell D, Jacob M, Hofmann-Kiefer K, Rehm M, Welsch U, Conzen P, et al. Antithrombin reduces shedding of the endothelial glycocalyx following ischaemia/reperfusion. Cardiovascular research. 2009;83:388-96.

[162] Zhang X, Adamson RH, Curry F-RE, Weinbaum S. A 1-D model to explore the effects of tissue loading and tissue concentration gradients in the revised Starling principle. Am J Physiol Heart Circ Physiol. 2006;291:H2950-64.

[163] Zhang X, Curry F-R, Weinbaum S. Mechanism of osmotic flow in a periodic fiber array. American journal of physiology Heart and circulatory physiology. 2006;290:H844-52.

[164] Rippe B, Haraldsson B. Transport of macromolecules across microvascular walls: the two-pore theory. Physiological Reviews. 1994;74:163-219.

[165] Van Der Linden P, James M, Mythen M, Weiskopf RB. Safety of modern starches used during surgery. Anesth Analg. 2013;116:35-48.

[166] Marsh G, Waugh RE. Quantifying the mechanical properties of the endothelial glycocalyx with atomic force microscopy. J Vis Exp. 2013:e50163.

[167] Callies C, Fels J, Liashkovich I, Kliche K, Jeggle P, Kusche-Vihrog K, et al. Membrane potential depolarization decreases the stiffness of vascular endothelial cells. Journal of Cell Science. 2011;124:1936-42.

[168] Callies C, Schön P, Liashkovich I, Stock C, Kusche-Vihrog K, Fels J, et al. Simultaneous mechanical stiffness and electrical potential measurements of living vascular endothelial cells using combined atomic force and epifluorescence microscopy. Nanotechnology. 2009;20:175104.

[169] Oberleithner H, Callies C, Kusche-Vihrog K, Schillers H, Shahin V, Riethmüller C, et al. Potassium softens vascular endothelium and increases nitric oxide release. Proc Natl Acad Sci USA. 2009;106:2829-34.

[170] Selleck SB. Signaling from across the way: transactivation of VEGF receptors by HSPGs. Mol Cell. 2006;22:431-2.

[171] Little PJ, Ballinger ML, Osman N. Vascular wall proteoglycan synthesis and structure as a target for the prevention of atherosclerosis. Vasc Health Risk Manag. 2007;3:117-24.

[172] Starling EH. On the Absorption of Fluids from the Connective Tissue Spaces. J Physiol (Lond). 1896;19:312-26.

[173] Jacob M, Chappell D. Reappraising Starling: the physiology of the microcirculation. Curr Opin Crit Care. 2013;19(4):282-9.

[174] Hubert CG, McJames SW, Mecham I, Dull RO. Digital imaging system and virtual instrument platform for measuring hydraulic conductivity of vascular endothelial monolayers. Microvasc Res. 2006;71:135-40.

[175] Lawrence R, Lu H, Rosenberg RD, Esko JD, Zhang L. Disaccharide structure code for the easy representation of constituent oligosaccharides from glycosaminoglycans. Nature methods. 2008;5:291-2.